UNIVERSITÉ DE MONTRÉAL

DESIGN AND IMPLEMENTATION OF APODIZED AND UNAPODIZED FREQUENCY
CONVERTERS IN BULK APERIODICALLY POLED NONLINEAR MATERIALS

AMENEH BOSTANI

DÉPARTEMENT DE GÉNIE PHYSIQUE

ÉCOLE POLYTECHNIQUE DE MONTRÉAL

THÈSE PRÉSENTÉE EN VUE DE L'OBTENTION

DU DIPLÔME DE PHILOSOPHIAE DOCTOR

(GÉNIE PHYSIQUE)

JUIN 2016

UNIVERSITÉ DE MONTRÉAL

ÉCOLE POLYTECHNIQUE DE MONTRÉAL

Cette thèse intitulée :

DESIGN AND IMPLEMENTATION OF APODIZED AND UNAPODIZED FREQUENCY
CONVERTERS IN BULK APERIODICALLY POLED NONLINEAR MATERIALS

présentée par: BOSTANI Ameneh

en vue de l'obtention du diplôme de : Philosophiae Doctor

a été dûment acceptée par le jury d'examen constitué de :

M. LEBLOND Frédéric, Ph. D., président

M. KASHYAP Raman, Ph. D., membre et directeur de recherche

M. KÉNA-COHEN Stéphane, Ph. D., membre

M. LÉGARÉ François , Ph. D., membre

DEDICATION

Dedicated to my parents,

for all their love, endless supports and accepting my decisions in life

in memory of

my uncle Abbas Ahmad Bostani

ACKNOWLEDGEMENTS

RÉSUMÉ

Cette thèse porte sur l'étude, la conception et la fabrication de convertisseurs de fréquences à large bande pour la génération efficace de seconde harmonique (SHG) et de somme de fréquences (SFG) sur des dispositifs non-linéaires en quasi-accord de phase (QPM). Les dispositifs de QPM comprennent des réseaux de domaines inversés, qui fournissent un accord de phase non critique pour la conversion de fréquences dans les matériaux non-linéaires. Pour créer des cristaux à QPM, le coefficient non-linéaire de second ordre est périodiquement inversé à l'aide d'une méthode de polarisation périodique. Avec d'excellentes propriétés telle sa non-linéarité, le cristal de niobate de lithium (LN), utilisé pour les simulations et la fabrication de ces travaux de recherche, est un des meilleurs candidats pour les dispositifs à QPM. Les matériaux périodiquement polarisés uniformément tel le niobate de lithium périodiquement polarisé (PPLN), possèdent une largeur de bande d'acceptation spectrale et thermique étroite. La largeur de bande étroite limite la conversion de fréquences pour une longueur d'onde spécifique d'un laser pompe et nécessite l'utilisation d'un contrôleur de température pour maximiser l'efficacité de conversion. En addition, les conversions de fréquences pour plusieurs longueurs d'onde simultanément ainsi que le réglage de la longueur d'onde de pompe sans réglage de température sont restreints par les PPLN uniformes. Les réseaux à pas variable (*chirped*) et *step-chirped* dans le LN ont été récemment proposés pour pallier la limitation de la bande passante des doubleurs de fréquences basés sur la SHG. Les réseaux *chirped* peuvent être conçus pour obtenir une largeur de bande souhaitée et enlever la nécessité de l'installation du régulateur de température dans le montage expérimental. Cependant, ces dispositifs souffrent d'ondulations et de fluctuations dans leurs réponses spectrales. L'application d'apodisation sur les réseaux *chirped* est proposée pour diminuer les ondulations dans la réponse de ces dispositifs, dans lesquels les changements de coefficient non linéaire effectif en fonction de la longueur converge vers zéro au niveau des rebords du réseau. Dans cette thèse, les méthodes d'ingénieries non linéaires effectives appropriées pour supprimer des ondulations des convertisseurs à large bande sont explorées.

La mise en œuvre d'une fonction d'apodisation souhaitée sur les convertisseurs à large bande basés sur la variation du rapport cyclique est examinée en profondeur. La dépendance de la phase du champ electrique sur la génération de seconde harmonique à l'endroit de la région polarisée dans un réseau apériodique est explorée théoriquement. Il a été démontré pour la première fois

que la bande spectrale de conversion de doubleurs de fréquences *chirped* apodisés dépend du lieu de la région polarisée dans la période de réseaux. La conception adéquate pour minimiser les ondulations et pour réaliser une fonction de non-linéarité souhaitée pour un réseau *chirped* apodisé a été proposée, ce qui améliore la tolérance aux erreurs de fabrication.

Il a été également démontré qu'une autre approche alternative pour adapter et contrôler efficacement la non-linéaire dans les convertisseurs à large bande est de focaliser le faisceau gaussien dans un réseau *chirped* non-apodisé. Il a été démontré théoriquement et expérimentalement pour la première fois que le changement spectral de l'intensité lumineuse en focalisant un faisceau gaussien peut être traduit en une fonction d'apodisation et supprime l'ondulation (*ripple*) dans la réponse à large bande de convertisseurs *chirped*. Pour démontrer cette approche, un réseau *chirped* dans un morceau de LN a été fabriqué pour fonctionner dans une bande de SH de 30 nm pour la bande de communication (*C-band*), en utilisant un design de réseau *step-chirped*. Il a été vérifié qu'en augmentant la focalisation, une réponse sans ondulation est progressivement réalisée sur une bande passante de 6 dB de >5nm, avec une taille de faisceau de 20 μm. L'augmentation de la focalisation rétrécit également la bande passante des réseaux, car elle réduit l'intensité de la lumière rapidement loin du point focal. Cependant, le réglage en continu est également démontré en déplaçant le point focal dans le réseau *step-chirped*.

En outre, il a été prouvé que les PPLN *chirped* apodisés spécialement conçus, basés sur le positionnement particulier des régions polarisées dans les périodes, présentent une réponse réciproque dans les spectres de SHG, pour les directions de *chirped* vers l'avant et vers l'arrière. Les résultats de simulations sont comparés à un autre PPLN *chirped* apodisé pour lequel le placement des régions polarisées est dévié de la position optimale. Expérimentalement, pour la première fois, la conversion de fréquence des dispositifs fabriqués est obtenue sur une largeur de bande de 30 nm dans les deux sens pour montrer la réciprocité de la conception.

Enfin, le convertisseur de bande indépendant de la température est utilisé, pour la première fois, pour la génération de SHG et SFG d'un puissant laser à fibre à onde continue (CW laser) avec une largeur de bande de quelques nanomètres centrée autour de 1550 nm, sans l'aide d'un régulateur de température. Il a été démontré que ce dispositif est insensible à la dérive de fréquences du laser et des variations spectrales lorsque la puissance intégrée augmente. De plus, la puissance quadratique de SHG par rapport à la puissance de pompe est obtenue en utilisant un

PPLN *step-chirped* avec la source de puissance élevée. Il a été également démontré que ce dispositif est entièrement en accord de phase simultanément pour les deux processus de conversion non-linéaire de second ordre : SHG et SFG. Il a été démontré que l'ensemble du spectre d'un laser pompe peut être converti en onde de SFG par l'ingénierie d'une fonction de transfert appropriée pour un réseau. À l'aide d'un laser monochromatique accordable comme signal de contrôle et en réglant à plus de 30 nm dans la bande de communication, une conversion de fréquences à large bande super-accordable du puissant laser CW dans la gamme de 770-778 nm est réalisée. L'effet de focalisation a également été pris en compte dans l'élaboration de la théorie de la conversion de faisceau laser pour un maximum d'efficacité de conversion non-linéaire.

ABSTRACT

This thesis focuses on research study, design and fabrication of broadband frequency converters based on second harmonic generation (SHG) and sum frequency generation (SFG) in nonlinear quasi-phase-matched (QPM) devices. QPM devices based on domain-inverted gratings provide noncritical phase matching for frequency conversion in nonlinear media. For creating QPM crystals, the second-order nonlinear coefficient is periodically reversed by periodic poling method. Lithium niobate (LN) crystal with excellent properties such as high nonlinearity is one of the best candidates for QPM devices, which has been used for the simulations and fabrication in this research work. Conventional uniform periodically poled materials such as periodically poled lithium niobate (PPLN) crystals possess a narrow spectral and thermal acceptance bandwidth. The narrow bandwidth limits the frequency conversion for a specified pump wavelength and necessitates the use of a temperature controller to maximize the efficiency. In addition, uniform gratings restrict simultaneous frequency conversion for several wavelengths and tunability of the pump wavelength without temperature tuning. Therefore, chirped and step-chirped gratings in LN were recently proposed to overcome the bandwidth limitation of frequency doublers based on SHG. Chirped gratings can be engineered to obtain the desired bandwidth and remove the necessity of controlling the temperature in the experimental set-up. However, these devices suffer from ripples and fluctuations in their spectral responses. Applying apodization in chirped grating is suggested to diminish the ripples in the response of these devices, in which the effective nonlinear coefficient changes, as a function of length, smoothly to zero at the edges of the grating. In this dissertation, methods for engineering proper effective nonlinearity are explored to suppress ripples of broadband converters.

Implementation of a desired apodization function on broadband converters based on duty ratio variation is deeply examined. The dependence of SH electrical field phase on the place of poled region in an apreriodic grating is explored theoretically. It has been demonstrated for the first time that the spectral conversion bandwidth of apodized chirped frequency doublers depends on the place of the poled region within the period of gratings. The proper design to minimize the ripples and achieve a desired nonlinearity function for an apodized chirped grating has been proposed which improves the tolerance to fabrication errors.

It has been also shown that another alternative approach for shaping effective nonlinearity in broadband converters is focusing the Gaussian beam in a un-apodized chirped grating. It has been demonstrated theoretically and experimentally for the first time that the spatial change of light intensity by focusing of a Gaussian beam can be translated to apodization and suppresses the ripple in the wideband response of a chirped grating. For demonstration of this approach, a chirped grating in bulk LN has been fabricated to operate in a 30-nm SH bandwidth for the communication band, using a step-chirped grating (SCG) design. It has been verified that by increasing the focusing, a ripple-free response is progressively achieved over a 6-dB bandwidth of >5nm, with a beam waist of 20 µm. Increasing the focusing also shrinks the bandwidth of gratings as it reduces the intensity of light rapidly far from the focal point. However, continuous tuning is also demonstrated by changing the focal point within the SCG.

Also, it has been proved that a specially-designed apodized chirped PPLN based on the particular positioning of poled regions within the periods exhibits a reciprocal response in the SHG, for up-chirp and down-chirp directions. The simulation results are compared with another apodized chirped PPLN in which the placement of poled regions deviates from optimum positions. Experimentally the frequency conversion is obtained over a 30-nm bandwidth of fabricated device in both directions to show the reciprocity of the design.

Finally, the temperature-independent broadband converter is used for the first time to generate SH and SF of a CW high power fiber laser with a few nm bandwidth centered at 1550 nm without using temperature controller. It has been shown that this device is insensitive to laser frequency drift and spectral variations as the integrated power raises. In addition, quadratic SH power with respect to the pump power is obtained using step-chirped (SC)-PPLN for the high power source. It has been also demonstrated that this device is fully phased-matched simultaneously for both second-order nonlinear up-conversion processes, SHG and SFG. It has been shown the entire BW of a pump laser can be converted to an SF wave by engineering a proper transfer function for a grating. Utilizing a tunable monochromatic laser as a control signal and tuning over 30 nm in the communication band, a super-tunable broadband frequency up conversion of the high power CW laser in the range of 770-778 nm is realized. The effect of focusing is also has been considered in developing the theory of laser beam conversion for maximum up-conversion efficiency.

TABLE OF CONTENTS

LIST OF TABLES

LIST OF FIGURES

LIST OF SYMBOLS AND ABBREVIATIONS

AC   Apodized Chirped

AC-PPLN   Apodized Chirped Periodically Poled Lithium Niobate

APE   Annealed Proton Exchange

APPLN   Aperiodically Poled Lithium Niobate

BW   Bandwidth

CPS   Center-Poled Structure

C-band   Conventional Band

CW   Continuous Wave

DAC   Data Acquisition Card

DFG   Difference Frequency Generation

DI   Deionized

EDFA   Erbium-Doped Fiber Amplifier

EFP   Electric Field Poling

FH   Fundamental Harmonic

FWHM   Full-Width Half Maximum

FWM   Four-Wave Mixing

GaAs   Gallium Arsenide

HF   Hydrofluoric

HWP   Half Wave Plate

HV   High Voltage

IPA   Isopropyl Alcohol

KTP   Potassium Titanyl Phosphate

LCG   Linearly Chirped Grating

Li   Lithium

LiCL   Lithium Chloride

LiNbO$_3$ Lithium Niobate

LN   Lithium Niobate (LiNbO$_3$)

M   Mirror

MgO   Magnesium Oxide

Nb   Niobium

NLO   Nonlinear Optic

OCPS   Off-Center-Poled Structure

OR   Optical Rectification

OSA   Optical Spectrum Analyzer

PBS   Polarization Beam Splitter

PC   Polarization Controller

PPLN	Periodically Poled Lithium Niobate
QPM	Quasi Phase Matching
SC	Step-Chirped
SAC	Step-Apodized Chirped
SFG	Sum Frequency Generation
SH	Second Harmonic
SHG	Second Harmonic Generation
UV	Ultra-Visible
WC	Wavelength Converter
WDM	Wavelength Division Multiplexing

LIST OF APPENDICES

CHAPTER 1   INTRODUCTION

1.1   Motivation

In photonics, producing broadband light at high frequencies such as green and blue light has been of great interest in recent years. High-frequency broadband light has numerous applications in optical communications, optical information processing, and optical sensing in the past decades [1], [2]. One common way to produce such light is based on nonlinear frequency conversion, specially quasi-phase-matching (QPM) technique in which the nonlinear coefficient of crystal is reversed in specific periods [3], [4]. QPM in the form of uniform gratings has been investigated in many studies for up and down frequency conversions. However, uniform gratings have a small conversion bandwidth and are sensitive to temperature variation as well as angular rotation. Broadband wavelength converters in the form of spatially-modulated gratings, chirped and step-chirped periodically poled material have already been suggested to solve these limitations [5], [6]. Although utilizing chirped grating allows us to obtain a wider bandwidth but it introduces many ripples in the output response and significantly decreases the efficiency. Imposing some apodization has been suggested in chirped gratings [7] to decrease the fluctuations and ripples in second harmonic generation (SHG) responses. Increasing SH power is still a real problem as well as applying apodization on chirped gratings for realization. The broadband frequency conversion device requires a special design to be suitable for fabrication while decreasing the ripples. The ripple in the conversion efficiency is a function of wavelength in chirped gratings and depends strongly on apodization. All of these necessitate studying and realizing of a different kind of apodization in aperiodically poled material to achieve ultra-wide bandwidth devices, which fulfill the requirements by compromising between different criteria such as flatness, bandwidth, intensity and practicability of fabrication. In this dissertation, our aim is the realization of an apodized broadband wavelength up-converter (for high-power lasers with an output power in the order of 10's-1000s of watts) based on SHG and sum frequency generation (SFG) in bulk lithium niobate (LN) using engineered step-chirped grating as a feasible fabrication approach.

1.1   Literature review

Second harmonic generation (SHG) was first demonstrated by Franken et al. in 1961 [8] by focusing a ruby laser beam at 694 nm in a plate of crystalline quartz shortly after demonstration of the first laser. The equations for SHG and other nonlinear interactions for monochromatic light are formulated by Armstrong and his colleague in a nonlinear medium using quantum-mechanical perturbation theory [9]. They derived coupled equations and solved it in phased matched velocities and imperfect phase matching. These nonlinear interactions require phase matching between fundamental and second harmonic wave vectors to compensate phase drift coming from the difference in their phase velocities due to material dispersion. Earliest approach to satisfy phase matching condition was using the birefringent material, in which two waves with orthogonal polarization can keep the same phase velocity for one wavelength due to different dispersion [10], [11]. As the refractive index is dependent on the temperature, phase matching for the wavelength of interest can be achieved by temperature tuning, named noncritical phase matching in which all polarization directions are along the two different crystal axes. Another technique for birefringence phase matching is tuning the angle of crystal or beams to adjust the phase velocities of propagation to fulfill the phase matching condition [12], [13]. In birefringence phase matching, the propagation directions and polarizations are severely constrained. The frequency converted light should be perpendicular to one or two polarized inputs named as the type II and type I phase matching, respectively. For SHG at a desired wavelength, the combination of temperature and angle tuning should be considered in proper crystal. In addition, the birefringence phase matching suffers from the birefringent walk-off in a critical phase matching (angle tuning). The SHG efficiency is a function of crystal's properties and its length. Many theoretical and experimental works have been done on SHG for plane waves and focused beams [11], [12], [14]–[18]. Kleinman and his colleagues were the first to have examined the effect of a focused Gaussian laser beam on the SHG efficiency in nonlinear crystals. In their investigation, the birefringent walk-off in which intensity distribution drifts away from initial wave vector, with different beam tightness and focusing position, has been considered [17], [19], [20]. When light is focused into the crystal, the light is diffracted more rapidly when the spot size diminishes and leads to a reduction in the effective interaction length. Therefore, there is a tradeoff between the spot size and interaction length to get the maximum efficiency.

In a dispersive material, the fundamental and second harmonic waves have different phase velocities, and they shift π out of phase relative to each other over a distance called the coherence length (l_c). If the sign of the nonlinear coefficient reverses in every other coherence length, it can locally transfer power to the second harmonic wave. This compensation of phase velocity dispersion in frequency conversion by the modulation of nonlinearity is called quasi phase matching (QPM). QPM provides non-critical phase matching at a specific temperature in the entire transmission band of the material and consequently does not suffer from the spatial walk-off. This technique also provides usage of materials with low birefringence for frequency conversion which was not efficient before QPM were introduced. Also, the largest nonlinear coefficient can be exploited [21], [22] and [23]. In addition to the type I and type II phase matching, type 0 phase matching, with the same polarization of input and output waves, is also possible using QPM. The quasi phase matched structure and mechanism of field accumulation in QPM are shown in Fig.1.1 and they are compared with a non-phase matched crystal.
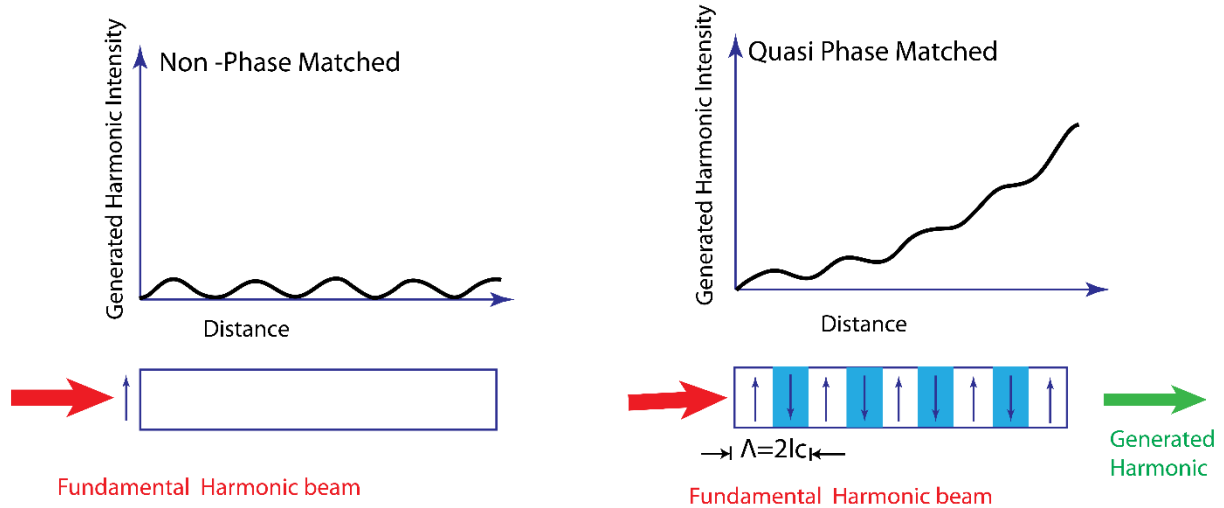
Figure 1.1: Non-phase-matched crystal compared to quasi phased-matched structure and its generated harmonic intensity. l_c represents the coherence length.

The QPM technique was proposed first time by Armstrong *et al.* in 1962 [9] for correction of the mismatch in nonlinear material. In 1972, Somekh and Yariv investigated the periodic modulation

in the boundaries of a thin film waveguide [21]. Experimentally, making QPM structures was first done based on stacking polished plates of nonlinear material together while alternating the sign of susceptibility in successive plates of GaAs at a Brewster angle [22]. The QPM is possible in a medium in which the nonlinear susceptibility can be patterned on a microscopic scale. Ferroelectrics and semiconductors are the best candidates for this purpose. While semiconductors such as GaAs are suitable for long-wavelength operation in the mid-IR, ferroelectrics have been widely used in the near IR and visible regions since the beginning of QPM devices. By enhancing the manufacturing ability on microscopic scale, many methods and experiments were undertaken to make QPM structures in ferroelectrics including electron beam writing [23], inversion during crystal growth [24], thermal inversion [25], surface impurity diffusion [26], ion exchange through a lithographic mask [27] and electric field poling [28]. Electric field poling in which the electric fields higher than the coercive field of ferroelectric material are applied to a periodic electrode pattern on the surface of a millimeter-thick wafer, is applied for both bulk materials and waveguides [29]. Nowadays, periodic domain inversion or poling by applying a high voltage at room temperature is the most common technique [30], [31]. The electrode pattern, which is an insulating grating pattern is made by lithography on the crystal which is then immersed into a liquid electrolyte. A high voltage is applied to create the electric field [32]. In the present work, electric field poling at room temperature was used for the fabrication of QPM devices in the form of chirped periodically poled lithium niobate (PPLN).

The most widely exploited ferroelectric for periodic domain inversion is lithium niobate ($LiNbO_3$, LN) due to its largest nonlinear coefficient d_{33}, among all other popular ferroelectrics such as lithium tantalate ($LiTaO_3$, LT) and Potassium titanyl phosphate ($KTiOPO_4$, KTP). It benefits from wide transparency from mid-IR into the near UV with an absorption edge at 320 nm. It is commercially available in three- and four-inch diameter substrates, convenient for lithographic patterning, processing and providing long interaction length. On the other hand, lithium niobate suffers from photorefractive damage in which the refractive index variation is induced by the generation of charges due to photo-ionization at relatively low intensities [33]. Photorefractive damage results in beam distortion within the PPLN and consequently affects the phase matching condition and particularly is severe for visible light [34]. In order to increase photorefractive damage threshold heating the crystal above the annealing temperature has been

suggested [35]. Also, magnesium oxide (MgO) doping can improve the LN resistant to photorefractive effect [36]–[38].

PPLN is used for frequency conversion in bulk and waveguide form. The first periodic poling based on the lithographic technique was only possible in waveguide geometries as it was based on the in-diffusion of titanium under the lithographic pattern and the domain gradually penetrated only a few microns below the surface of the substrate [26], [39]. However, by the emergence of electric-field poling techniques, the waveguide-usage limitation was overcome and the fabrication of PPLN was made also possible in the bulk form. Nowadays, annealed proton-exchanged and titanium in-diffusion after and before domain patterning (uniform grating) is a common way to fabricate PPLN waveguides [40], [41]. Waveguide PPLN has the advantage of having several times higher efficiency over bulk PPLN due to the high intensity from the beam confinement in the waveguide length. However, waveguides in PPLN can suffer from photorefractive damage at about 100 kW/cm^2 [42] even with a small input power of around 100 mW [43], [44]. Therefore, for high power and ultra-short pulse laser pump with a high peak power, bulk PPLN is preferred. Bulk PPLN can tolerate several average kW input power and can avoid reaching the optical damage threshold. Also as long as the output power is the main concern, bulk QPM with higher input power can be utilized to compensate for lower efficiency. Further, the conversion efficiency in bulk configuration can be improved by optimum laser beam focusing using QPM. The conditions of focused light through the PPLN have been investigated theoretically and experimentally [45]–[47]. Focusing the light inside the quasi phase matched structure induces a central wavelength shift which can be fixed by modifying the period of QPM device [48].

The bandwidth of uniform poled structures is about few nanometers and similar to the birefringence phase matched converters, is inversely proportional to the length of a converter. The narrow bandwidth is not acceptable for many applications. There are many works on optical frequency converters to raise their bandwidths. In some schemes, multi-crystal design with the possibility of small angular detuning is used to satisfy the phase matching condition in crystals for different spectral components of input pulse [49], [50]. Segmenting the crystal and reversing the temporal or spatial walk-off in alternating segment of a multi-crystal is another approach to increase acceptance bandwidths in optical frequency converters [51]. Also, angular dispersion provided by a system of diffraction gratings and lenses or several prisms is exploited to guide

light at their phase matched angle and results in wider acceptance bandwidth [52], [53]. This method can also be applicable in QPM grating structures [54]. All of above approaches need very precise alignment and in the two last cases also need additional optical components. Another way to make a broader bandwidth device in a QPM grating is the use of segmented QPM waveguide [55]. Two fabrication techniques have been suggested for segmented grating structures. In one of them, several uniform structures with small period change are placed beside each other with a gap. In the second technique, the variation of waveguide width in a uniform grating is used to control the effective refractive index and consequently to satisfy phase matching condition for neighboring phase matched wavelengths. Also, the effect of using a constant-temperature gradient imposed along the bulk nonlinear crystal [56], [57] and uniform grating [6] have been studied to improve the tuning of the spectral bandwidth for a fixed crystal orientation. In 1990, Suhara offered a chirped grating structure to increase the SH bandwidth at the cost of reduced efficiency. In his proposed approach, instead of the identical periods, the period changes linearly within the crystal [5]. Chirped gratings not only have application in bandwidth broadening but also in compressing and stretching the second harmonic generated pulse relative to the input pulse [58].

Linearly chirped grating has two problems; Firstly, continuous change in the linear-chirped grating periods which is typically around 100 picometers makes it difficult for the fabrication [59]. Second problem is the noticeable ripples in the SHG conversion efficiency response [60]. Proposing step-chirped grating in which the change of period increases in steps and also applying some apodization to smooth ripples in the SHG efficiency response of the chirped PPLN waveguide have assisted to overcome the mentioned problems [7]. Apodization is the removal of the sharp edges in the spatial profile of nonlinearity in which the maximum of nonlinearity is brought down smoothly to zero at the grating edges. This leads to a reduction in ripples in chirped grating and diminishes the side-lobes of the sinc response of a uniform grating. Several schemes have been suggested for apodization in a uniform grating such as deleting domain reversal in some parts of the grating; waveguide tapering by placing grating into and out of the waveguide or integrating two directional couplers with a QPM grating; and by altering the duty cycle [59] ,[60]. An efficient method for apodization of step-chirped grating in waveguides was proposed theoretically by Tehranchi and Kashyap [7], which facilitates the process of fabrication and employs the variation in the duty cycle on the two edges of step-chirped grating. To

compensate for the efficiency reduction in the step-chirped gratings, a high-power laser with an average power in the order of several Watts to kWs can be used.

1.2   Objectives

As mentioned before, the development of apodized temperature-insensitive broadband QPM in bulk lithium niobate for high power application is the motivation of this work. In details, the purpose of this thesis is specified in the following objectives:

1. Development of the theory and design of engineered apodization in chirped gratings in poled crystals, e.g., lithium niobate for second harmonic generation

2. Spectral SHG response evaluation of the proposed apodized chirped grating devices

3. Investigation of a new approach to control the spectral SH response of a chirped grating instead of fabricating an apodized chirped grating

4. Fabrication of apodized and un-apodized step-chirped gratings

5. Characterization of the device using SHG and sum frequency generation with a high power laser

6. Removing the temperature controller as a result of the device temperature-insensitivity.

1.3   Overview

In Chapter 1, after explaining the motivation for this dissertation, the literature behind this work is reviewed. The objectives and an overview of this dissertation explaining the general organization of the work are presented.

Chapter 2 introduces the basics of nonlinear optics relevant to frequency up-conversion. The theory of nonlinear optics and wave equations in nonlinear media is described. The concepts of phase matching and applicable techniques to satisfy it are presented. Continuous- and step-chirped grating, and apodization with different functions and ratios are introduced. Moreover, apodization using a Gaussian beam is explained.

In Chapter 3, the properties of lithium niobate as our working material are discussed and our fabrication approach for making PPLN devices based on electric field poling at room temperature is described in details.

Chapters 4 to 7 present four articles, addressing the objectives of this dissertation. Chapter 4 contains the first paper entitled "Engineering of effective second-order nonlinearity in uniform and chirped gratings". This article addresses the first objective. This paper proposes the proper design to apply apodization in uniform and chirped gratings. It has been shown that when applying a desired apodization function, not only is the duty ratio but also the location of the poled region within the pitch is important. This is due to the amplitude and phase of the SH electric field being function of the duty cycles and position of the poled regions, respectively. The effect of displacement of the poled region position in the pitch on the SH conversion efficiency spectrum is investigated theoretically and numerically in the absence and the presence of domain errors. It is shown that our approach is robustly resistant to fabrication errors.

In Chapter 5, which is the second article entitled "Tailoring and tuning of the broadband spectrum of a step-chirped grating based frequency doubler using tightly focused Gaussian beams", we propose the use of Gaussian beam to control the SH response of a step-chirped grating device. In this paper, SHG response characterization of the fabricated un-apodized device is obtained by the use of a tunable monochromatic laser. We address objective 3 and part of objective 4 for successful fabrication of step-chirped gratings.

Chapter 6 presents the design and fabrication of an apodized chirped grating while considering a proper position for a poled region within a pitch which is theoretically described in Chapter 4. This paper shows the reciprocal SH response as is expected from the theory and simulation in Chapter 4. This paper which is entitled "Design, fabrication, and characterization of a specially apodized chirped grating for reciprocal second harmonic generation" addresses the second objective and the part of the fourth objective, only the fabrication of an apodized grating.

In Chapter 7, a high power laser is used to pump the specially designed step-chirped grating to address the objectives five and six, which are the characterization of our chirped device with a high power laser considering the temperature insensitivity of the device. The temperature controller is removed in the experimental set-up as the device has a broad temperature acceptance bandwidth. The article entitled "Super-tunable, broadband up-conversion of a high-power CW laser based on $\chi^{(2)}$ processes in an engineered nonlinear photonic crystal" in this chapter can be divided into two experimental parts. In the primary part, we used a high power laser in addition to a tunable laser with neighboring frequencies around the pump as a control signal to be able to

tune the output wavelength of a chirped grating in the sum-frequency band. In secondary part the SHG of a broadband high power pump laser using the chirped grating is examined for different pump powers.

Chapter 8 provides a general discussion on the aspects of the four articles and a summary of technical points in this work. Finally, we conclude the work in Chapter 9 and it is followed with a view on future work and recommendations.

CHAPTER 2   INTRODUCTION TO NONLINEAR OPTICS AND FREQUENCY CONVERTERS

2.1   Basics in nonlinear optics

When an electromagnetic wave enters a dielectric material, it interacts with the medium, causing a displacement of negative and positive charge centers in the constituent atoms and consequently creates dipoles. The dipole moment per unit volume is named the polarization ($\vec{P}$). The induced polarization in materials depends on the strength of input electric field and medium crystal structure. At low intensities, the polarization depends linearly on input electric field. This linear dependence is proportional to the linear susceptibility $\chi^{(1)}$ of material and determines the refractive index of the material. In this case, charges radiate their own electromagnetic wave with the same frequency as the input wave but with a phase delay, which results in a slower propagating output light compared to the original one due to its interference with the input wave. At high intensities, depending on the material structure, the dipoles do not oscillate sinusoidal for an applied sinusoidal electric field: in other words the generated polarization by dipoles is not equal for an applied electric field of $+E_0$ compared to applied field of magnitude $-E_0$. This nonlinear response leads to the creation of other frequency components than the input one. The relation between the polarization and electric field can be described mathematically by means of the Taylor expansion

$$\vec{P} = \varepsilon_0 \left(\chi^{(1)} \vec{E} + \chi^{(2)} \vec{E}\vec{E} + \chi^{(3)} \vec{E}\vec{E}\vec{E} + \cdots \right) = \vec{P}_L + \vec{P}_{NL}, \qquad 2.1$$

where $\vec{P}_L = \varepsilon_0 \chi^{(1)} \vec{E}$ presents the linear part of the polarisation , and ε_0 is the permittivity of free space [61]. The linear part of polarization contributes to linear phenomenon causing by produced phase delay in the material such as refraction, diffraction, reflection and dispersion. $\vec{P}_{NL}$ denotes the nonlinear part of polarization. The quantities $\chi^{(2)}$ and $\chi^{(3)}$ are known as the second- and third-order nonlinear optical susceptibilities, respectively. The second term, proportional to the square of the electric field, is responsible for different kinds of frequency conversion, parametric fluorescence, and optical rectification. The second-order nonlinear interactions can occur only in non-centrosymmetric crystals that do not display inversion symmetry. On the other hand, third-

order nonlinear optical interactions can occur both in centrosymmetric and non-centrosymmetric media and give rise effects such as third harmonic generation (THG), the Kerr effect, Brillouin scattering, Raman scattering, self-phase modulation (SPM), soliton formation, cross-phase modulation (XPM) and four-wave mixing (FWM).

In order to understand different second-order nonlinear interactions which our focus in this dissertation is on, we consider an optical field strength $\tilde{E}$ (which consists of two distinct frequency components as

$$\tilde{E}(t) = E_1 e^{-\omega_1 t} + E_2 e^{-\omega_2 t} + c.c.,$$

2.2

where *c.c.* is the complex conjugate. The second order contribution to the nonlinear polarization strength in Eq. (2.1) can be written in the following form

$$\tilde{P}^{(2)}(t) = \varepsilon_0 \chi^{(2)} \tilde{E}(t)^2.$$

2.3

By substituting (2.2) in (2.3), the second order polarization is given by

$$\tilde{P}^{(2)}(t) = \varepsilon_0 \chi^{(2)} [E_1^2 e^{-2i\omega_1 t} + E_2^2 e^{-2i\omega_2 t} + 2E_1 E_2 e^{-i(\omega_1 + \omega_2)t} + 2E_1 E_2^* e^{-i(\omega_1 - \omega_2)t} + c.c.]$$
$$+ \varepsilon_0 \chi^{(2)} [E_1 E_1^* + E_2 E_2^*]$$

2.4

If the polarization is expanded for different positive and negative frequency ω_n, then:

$$\tilde{P}^{(2)}(t) = \sum_n P(\omega_n) e^{-i\omega_n t}.$$

2.5

The complex amplitudes of different frequency components are given by

$$P(2\omega_1) = \varepsilon_0 \chi^{(2)}_{(2\omega_1)} E_1^2$$
$$P(2\omega_2) = \varepsilon_0 \chi^{(2)}_{(2\omega_2)} E_2^2$$
$$P(\omega_1 + \omega_2) = 2\varepsilon_0 \chi^{(2)}_{(\omega_1 + \omega_2)} E_1 E_2$$
$$P(\omega_1 - \omega_2) = 2\varepsilon_0 \chi^{(2)}_{(\omega_1 - \omega_2)} E_1 E_2^*$$
$$P(0) = 2\varepsilon_0 \chi^{(2)}_{(0)} (E_1 E_1^* + E_2 E_2^*)$$

2.6

The two first relations in Eqs. (2.6) describe second harmonic generation (SHG) of two pumps, the third and fourth one indicate on sum frequency generation (SFG) and different frequency generation (DFG). The last expression denotes on optical rectification (OR). For all frequency conversion equations (nonzero frequencies), also there is a response at negative frequency of each equation in (2.6) coming from the conjugation form of electric field which is not distinguishable. In practice, from these four different nonzero frequency conversions, typically, just one interaction occurs with a high-intensity input as the phase matching condition (This shall be explained in section 2.4) should be satisfied for frequency conversion which is not always easy to satisfy. Also, the interacting susceptibility ($\chi_{int}^{(2)}$) for the selected polarization should be nonzero.

The susceptibility coefficient $\chi^{(m)}$ for each allowed interaction is a ($m+1$) tensor and it consists of 3^{m+1} elements. For instance, $\chi^{(2)}$ can be represented by a matrix of $3\times3\times3$ and consists of 27 elements. Considering all kind of symmetries such as intrinsic permutation, lossless media symmetries and the Kleinman symmetry (the $\chi_{ijk}^{(2)}$ are not strongly dependent on frequency, if all the frequencies contribute to the interaction are far enough from any resonance frequencies of the nonlinear material) [62], the second-order susceptibility tensor can be simplified into a more convenient form called d-tensor, with components determined by

$$\begin{aligned} 2d_{il}(-\omega_3;\omega_1,\omega_2) &= \chi_{ijk}^{(2)}(-\omega_3;\omega_1,\omega_2) \\ &= \chi_{ikj}^{(2)}(-\omega_3;\omega_2,\omega_1) = \chi_{ijk}^{(2)}(-\omega_3;\omega_2,\omega_1) \end{aligned}$$
  2.7

The indices *i, j, and k* indicate the field polarization directions of different axes *x*, *y*, and *z*. The indices *j* and *k* can be replaced by the index *m,* using the Voigt contraction. The contracted *d*-tensor has a more convenient form with 18 independent elements for nonlinear material with minimum symmetry. Therefore, the induced second-order nonlinear polarization for sum frequency generation in different directions is proportional to various components of applied electric field as

$$
\begin{bmatrix} \tilde{P}_x^{(\omega_1+\omega_2)} \\ \tilde{P}_y^{(\omega_1+\omega_2)} \\ \tilde{P}_z^{(\omega_1+\omega_2)} \end{bmatrix} = 4\varepsilon_0 \begin{bmatrix} d_{11} & d_{12} & d_{13} & d_{14} & d_{15} & d_{16} \\ d_{21} & d_{22} & d_{23} & d_{24} & d_{25} & d_{26} \\ d_{31} & d_{32} & d_{33} & d_{34} & d_{35} & d_{36} \end{bmatrix} \begin{bmatrix} \tilde{E}_x^{(\omega_1)}\tilde{E}_x^{(\omega_2)} \\ \tilde{E}_y^{(\omega_1)}\tilde{E}_y^{(\omega_2)} \\ \tilde{E}_z^{(\omega_1)}\tilde{E}_z^{(\omega_2)} \\ \tilde{E}_y^{(\omega_1)}\tilde{E}_z^{(\omega_2)} + \tilde{E}_z^{(\omega_1)}\tilde{E}_y^{(\omega_2)} \\ \tilde{E}_x^{(\omega_1)}\tilde{E}_z^{(\omega_2)} + \tilde{E}_z^{(\omega_1)}\tilde{E}_x^{(\omega_2)} \\ \tilde{E}_x^{(\omega_1)}\tilde{E}_y^{(\omega_2)} + \tilde{E}_y^{(\omega_1)}\tilde{E}_x^{(\omega_2)} \end{bmatrix}.
$$

2.8

 In the case of SHG, the two frequencies are equal, and a coefficient of ½ is multiplied in the second term due to the use of one source.

Based on different classes of crystals, holding symmetries, the *d*-tensor elements can be reduced. For example for lithium niobate crystal which places in the 3m point group class, the *d*-tensor just has three nonzero elements; d_{31}, d_{22} and d_{33} and in the form of tensor can be given by:

$$
\begin{bmatrix} 0 & 0 & 0 & 0 & d_{31} & -d_{22} \\ -d_{22} & d_{22} & 0 & d_{31} & 0 & 0 \\ d_{31} & d_{31} & d_{33} & 0 & 0 & 0 \end{bmatrix}.
$$

2.9

The quantity of nonzero elements and their places in the tensor are important in designing parametric devices as it can benefit from a maximum of the *d*-tensor element to maximize the conversion efficiency and the selection of proper polarizations.

2.2   Wave Equations

In order to understand and obtain wave equation describing propagation of light through a nonlinear optical medium, we begin with the Maxwell's equations

$$\vec{\nabla} \cdot \vec{D} = \rho_{ext}, \qquad 2.10$$

$$\vec{\nabla} \cdot \vec{B} = 0, \qquad 2.11$$

$$\vec{\nabla} \times \vec{E} = -\frac{\partial \vec{B}}{\partial t}, \qquad 2.12$$

$$\vec{\nabla} \times \vec{H} = \vec{J}_{ext} + \frac{\partial \vec{D}}{\partial t}. \qquad 2.13$$

We are interested in the solutions of these equations in regions of space that contain no free charges, so that

$$\rho_{ext} = 0. \qquad 2.14$$

Also, the region does not contain any free currents, therefore

$$\vec{J}_{ext} = 0. \qquad 2.15$$

With the assumption of solving equation in nonmagnetic material, we have

$$\vec{B} = \mu_0 \vec{H}, \qquad 2.16$$

however, in nonlinear material experiencing induced polarization, the fields $\vec{D}$ and $\vec{E}$ are related by

$$\vec{D} = \varepsilon_0 \vec{E} + \vec{P}, \qquad 2.17$$

and in general, the polarization vector $\vec{P}$ depends on the local electric field $\vec{E}$.

To derive the optical wave equation in the usual manner, we take the *curl* of the 3rd Maxwell's Eq. (2.12), and interchange the order of space and time derivatives on the right-hand side of the resulting equation. Using Eq. (2.13), (2.15), and (2.16) to replace $\vec{\nabla} \times \vec{B}$ by $\mu_0 \frac{\partial \vec{D}}{\partial t}$, we obtain

$$\nabla \times \nabla \times \vec{E} + \mu_0 \frac{\partial^2 \vec{D}}{\partial t^2} = 0.$$

2.18

Substituting Eq. (2.17) in the above equation, to eliminate $\vec{D}$, results in

$$\nabla \times \nabla \times \vec{E} + \frac{1}{c^2} \frac{\partial^2 \vec{E}}{\partial t^2} = - \mu_0 \frac{\partial^2 \vec{P}}{\partial t^2}.$$

2.19

This is the most general form of the wave equation in nonlinear optics [61]. This equation can be simplified under certain conditions. Using a vector calculus identity, the first term on the left-hand side of Eq. (2.19) can be rewritten as

$$\nabla \times \nabla \times \vec{E} = \nabla(\nabla \cdot \vec{E}) - \nabla^2 \vec{E}.$$

2.20

In linear optics, for an isotropic and homogeneous media with no charge, the first term on the right-hand side of this equation wiped out as the Maxwell's equation $\vec{\nabla} \cdot \vec{D} = 0$ results in $\vec{\nabla} \cdot \vec{E} = 0$. However, in nonlinear optics, this term cannot generally vanish even for isotropic materials, because of the general relation between $\vec{D}$ and $\vec{E}$ described in Eq. (2.17). Nevertheless, for transverse $\vec{E}$ field and infinite plane wave, this term can be dropped from the equation in nonlinear optics. Also, for slowly varying amplitude due to smallness compared to the second phrase in the right hand side of Eq. (2.20) can be ignored. Therefore, we can have this equation in the following form

$$\nabla^2 \vec{E} - \frac{1}{c^2} \frac{\partial^2 \vec{E}}{\partial t^2} = \mu_0 \frac{\partial^2 \vec{P}}{\partial t^2}.$$

2.21

By separating linear and nonlinear part of polarization as

$$\vec{P} = \vec{P}^{(1)} + \vec{P}_{NL},$$

2.22

where $\vec{P}^{(1)}$ and P_{NL} are the linear and nonlinear part of $\vec{P}$, respectively. The displacement field $\vec{D}$ can be decomposed into two parts of linear and nonlinear.

$$\vec{D} = \vec{D}^{(1)} + \vec{P}_{NL},$$

<div align="right">2.23.a</div>

where the linear part is given by

$$\vec{D}^{(1)} = \varepsilon_0 \vec{E} + \vec{P}_L .$$

<div align="right">2.23.b</div>

Considering all of these quantities, the wave Eq. (2.21) becomes

$$\nabla^2 \vec{E} + \mu_0 \frac{\partial^2 \vec{D}^{(1)}}{\partial t^2} = -\mu_0 \frac{\partial^2 \vec{P}_{NL}}{\partial t^2} .$$

<div align="right">2.24</div>

In the case of a lossless, non-dispersive medium, the relation between $\vec{D}^{(1)}$ and $\vec{E}$ is real and the frequency-independent dielectric tensor $\vec{\varepsilon}^{(1)}$ can be expressed as

$$\vec{D}^{(1)} = \vec{\varepsilon}^{(1)} \cdot \vec{E} .$$

<div align="right">2.25.a</div>

For isotropic materials, this relation simplifies to

$$\vec{D}^{(1)} = \varepsilon^{(1)} \vec{E} ,$$

<div align="right">2.25.b</div>

where $\varepsilon^{(1)}$ is now a scalar quantity, then wave Eq. (2.24) for an isotropic and dispersion-less material becomes

$$-\nabla^2 \vec{E} + \frac{n^2}{c^2} \frac{\partial^2 \vec{E}}{\partial t^2} = -\mu_0 \frac{\partial^2 \vec{P}^{NL}}{\partial t^2}$$

<div align="right">2.26</div>

Eq. 2.26 is the inhomogeneous wave equation in the presence of a source. Actually, the nonlinear response of the medium acts like a source term, which appears on the right-hand side of this equation. In the absence of this source term, Eq. (2.26) converts to the form of wave propagation in a dielectric with the phase velocity of c/n, where $\mu_0 \varepsilon^{(1)} = \mu_0 \varepsilon_0 \frac{\varepsilon^{(1)}}{\varepsilon_0} = \frac{n^2}{c^2}$ and n is the (linear) refractive index.

2.3 Nonlinear Coupled Wave Equations for SFG and SHG

For a dispersive medium, each frequency component of the optical field must be considered separately. In general, the total electric field and polarization are considered as a superposition of all different frequency components as

$$
\begin{aligned}
\vec{E}(\mathbf{r},t) &= \frac{1}{2}\sum_n \hat{e}_n E_n(\mathbf{r},\omega)\exp(-i\omega_n t) + c.c. \\
&= \frac{1}{2}\sum_n \hat{e}_n A_n(\mathbf{r})\exp[i(\mathbf{k}_n \cdot \mathbf{r} - \omega_n t)] + c.c.
\end{aligned}
\qquad 2.27
$$

$$
\vec{P}_{NL}(\mathbf{r},t) = \frac{1}{2}\sum_n \hat{e}_n P_n(\mathbf{r},\omega)\exp(-i\omega_n t) + c.c..
\qquad 2.28
$$

For each frequency component, Eq. (2.26) is valid, therefore

$$
-\nabla^2 \vec{E}_n + \frac{\varepsilon(\omega)}{c^2}\frac{\partial^2 \vec{E}_n}{\partial t^2} = -\mu_0 \frac{\partial^2 \vec{P}_n^{NL}}{\partial t^2}.
\qquad 2.29
$$

Consider plane waves propagating in the z-direction, combining the two input waves at ω_1 and ω_2, the sum frequency is generated at ω_3. The present waves in the medium can be expressed by:

$$
\vec{E}_1(z,t) = \frac{1}{2}A_1(z)\exp[i(k_1 z - \omega t)] + c.c.
\qquad 2.30.a
$$

$$
\vec{E}_2(z,t) = \frac{1}{2}A_2(z)\exp[i(k_2 z - 2\omega t)] + c.c.
\qquad 2.30.b
$$

$$
\vec{E}_3(z,t) = \frac{1}{2}A_3(z)\exp[i(k_3 z - \omega t)] + c.c.
\qquad 2.30.c
$$

where $k_i = \omega n_i/c$ and $i = 1, 2$ and 3 denotes the pump 1, pump 2, and generated SF wave, respectively. A_i is the slowly varying amplitude of the electric fields for the waves. The appropriate nonlinear polarization components for all contributing frequencies, according to Eq. (2.8), can be written as

$$P_3 = \frac{1}{2}\varepsilon_0 \chi^{(2)}(\omega_1+\omega_2;\omega_1,\omega_2)\,\mathrm{E}_1\,E_2 = 4\varepsilon_0 d_{e\!f\!f}\,\mathrm{E}_1\,E_2 \quad,$$

2.31.a

$$P_1 = \frac{1}{2}\varepsilon_0 \chi^{(2)}(\omega_3-\omega_2;\omega_3,\omega_2)\,\mathrm{E}_3\,E_2^* = 4\varepsilon_0 d_{e\!f\!f}\,E_3 E_2^*,$$

2.32.b

$$P_2 = \frac{1}{2}\varepsilon_0 \chi^{(2)}(\omega_3-\omega_1;\omega_3,\omega_1)\,\mathrm{E}_3\,E_1^* = 4\varepsilon_0 d_{e\!f\!f}\,E_3 E_1^*.$$

2.31.c

For a negative uniaxial crystal of class 3m , the effective value of d for type I, II and zero phase matching can be given by $d_{e\!f\!f} = d_{31}\sin\theta - \mathrm{d}_{22}\cos\theta\sin3\phi$, $d_{e\!f\!f} = \mathrm{d}_{22}\cos^2\theta\sin3\phi$ and $d_{e\!f\!f} = \mathrm{d}_{33}$, respectively. Here, for SFG in type I phase matching, pump 1 and pump 2 have a different polarizations and the polarization of one field is perpendicular to the polarization of generated SF wave. In type II phase matching, two pumps have the same polarization and their polarization are perpendicular to the generated SF wave and in type zero phase matching, the pumps and generated output have the same polarization.

We assumed that the Kleinman's symmetry holds. Therefore, the same $d_{e\!f\!f}$ appears in all of three equations. Substituting Eqs. (2.30) and (2.31) into the wave Eq. (2.29) for example for SFG, and replacing ∇^2 by d^2/dz^2 as the field is just dependent on the z axis, we find:

$$\left[\frac{d^2 A_3}{dz^2} + 2ik_3\frac{dA_3}{dz} - k_3^2 A_3 + \frac{\varepsilon^{(1)}(\omega_3)\omega_3^2 A_3}{c^2}\right]e^{i(k_3 z - \omega_3 t)} + c.c.$$
$$= \frac{-4d_{e\!f\!f}\,\omega_3^2}{c^2}A_1 A_2 e^{i[(k_1+k_2)z-\omega_3 t]} + c.c.$$

2.33

The third and fourth term in brackets on the left-hand side of this equation, cancel each other. Also using the slowly-varying envelope approximation,

$$\left|\frac{d^2 A}{dz^2}\right| << k\left|\frac{dA}{dz}\right|,$$

2.34

we end up with the well-known coupled wave equations for SFG

$$\frac{dA_3}{dz} = 2i\frac{\omega_3^2 d_{eff}}{k_3 c^2} A_1 A_2 \exp(i\Delta kz) \quad , \tag{2.35}$$

where $\Delta k = k_1 + k_2 - k_3$ is called the phase mismatch. Using the same approach for the two pumps, other coupled equations can be obtained as

$$\frac{dA_1}{dz} = 2i\frac{\omega_1^2 d_{eff}}{k_1 c^2} A_2^* A_3 \exp(-i\Delta kz)$$

$$\frac{dA_2}{dz} = 2i\frac{\omega_2^2 d_{eff}}{k_2 c^2} A_1^* A_3 \exp(-i\Delta kz) . \tag{2.36}$$

This equation for SHG with the pump at frequency of ω_1 and second harmonic at ω_2 reduces to two equations as

$$\frac{dA_2}{dz} = i\frac{\omega_2^2 d_{eff}}{k_2 c^2} A_1^2 \exp(i\Delta kz) \quad \text{(up-conversion process)}, \tag{2.37.a}$$

$$\frac{dA_1}{dz} = 2i\frac{\omega_1^2 d_{eff}}{k_1 c^2} A_2 A_1^* \exp(-i\Delta kz) \quad \text{(down-conversion process)}, \tag{2.3.b}$$

where $i = 1, 2$ denotes the fundamental harmonic (FH) and the second harmonic (SH), respectively. Eqs. (2.36.a) and (2.36.b) represent the frequency up-conversion ($\omega + \omega \to 2\omega$) and down-conversion process ($2\omega - \omega \to \omega$), respectively.

The phase mismatch Δk for SHG of light in frequency of λ defined as

$$\Delta k = k_2 - 2k_1 = \frac{4\pi}{\lambda}(n_2 - n_1) . \tag{2.38}$$

Under the non-depleted condition in which the pump power stays constant ($A_1 \sim$ constant) Eq. (2.36) can be solved by direct integration to give the amplitude of the SH,

$$A_2 = 2\frac{\omega_2^2}{k_2}\frac{d}{c^2}\frac{A_1^2(0)}{\Delta k}\left(e^{i\Delta kL}-1\right).$$

This assumption is valid whenever the conversion efficiency is not too large (around 10%) [63]. $A_1(0)$ is the input FH amplitude, and L is the length. The intensity of a light wave with the amplitude A can be written as

$$I = \frac{1}{2}c\varepsilon_o n|A|^2.$$

Using (2.39) and Eq. (2.38), results in calculating SH intensity

$$I_2 = \frac{2\omega_2^2 d_{eff}^2}{\varepsilon_o c^3 n_1^2 n_2}L^2 I_1^2(0)\frac{\sin^2\left(\frac{\Delta kL}{2}\right)}{\left(\frac{\Delta kL}{2}\right)^2} \propto \mathrm{sinc}^2\left(\frac{\Delta kL}{2}\right)$$

where we define $\mathrm{sinc}\, x = \dfrac{\sin x}{x}$.

Normalized SH intensity versus wave vector mismatch is plotted in Figure 2.1. The maximum SH intensity occurs when the mismatch is zero and decreases by increasing phase mismatch. For this reason, phase matching is very critical for having an effective conversion. In the next section, condition for phase-matching is explained in more details.
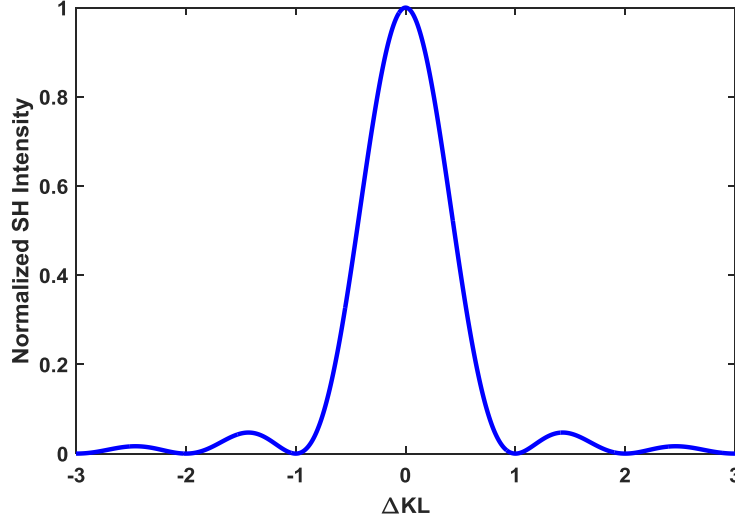
Figure 2.1. Normalized SH intensity vs. phase mismatch.

However, for the high conversion efficiency (more than 10%) the FH power depletion cannot be neglected. The pair of coupled Eqs. (2.36) should be solved simultaneously.

For the phase matching case ($\Delta kL = 0$), the solution exactly reduces to the well-known result (only when $I_2(0) = 0$) as follows

$$I_2(z) = I_1(0)\tanh^2(\Gamma z) , \qquad \qquad \text{2.42.a}$$

$$I_1(z) = I_1(0)\operatorname{sech}^2(\Gamma z), \qquad \qquad \text{2.42.b}$$

where Γ is a normalized nonlinear coefficient defined as

$$\Gamma = \frac{\omega d_{eff}}{cn_1}\sqrt{\frac{2I_1(0)}{\varepsilon_0 cn_2}} . \qquad \qquad \text{2.43}$$

For low conversion efficiencies, $\tanh^2(\Gamma L) \approx (\Gamma L)^2$ and Eq. (2.41) reduces to maximum the SH intensity in Eq. (2.41) for phase matched one in the case of undepleted pump. The normalized SH efficiency $I_{1,2}/I_1$ given by Eqs. (2.42) are shown in Figure 2.2
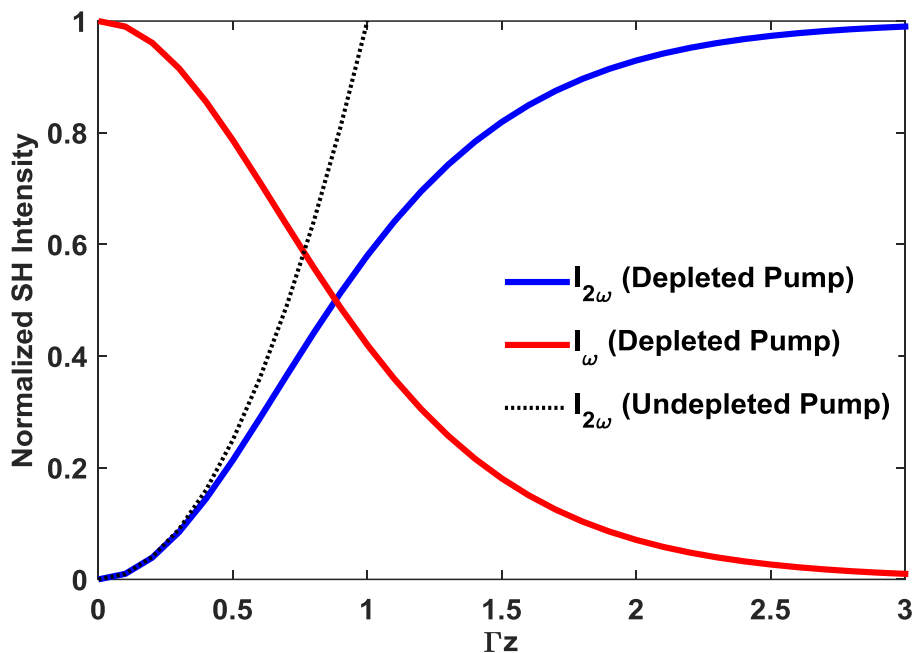
Figure 2.2 Normalized FH amplitude and SH efficiency in depleted case are in comparison with SH efficiency in un-depleted case.

The FH intensity is depleted, approaching to zero while the SH intensity approaches up to one and does not violate the conservation energy. In addition, In order to compare the SH conversion efficiency for an un-depleted case with a depleted case, the un-depleted approximation is plotted in the same figure. Clearly, it can be seen that for efficiencies lower that 10% two graphs are coincident. Therefore, for a conversion with the efficiency of less than 10% we are allowed to use the un-depleted approximation.

2.4   Phase matching

Phase matching is of vital importance in many nonlinear processes that are phase sensitive, such as SHG, SFG, DFG and FWM. The phase matching condition ensures that the harmonic waves add up constructively in the propagating direction. In the microscopic point of view, for example for SHG, at every place in the non-centrosymmetric crystal, fundamental harmonic induces a dipole emitting light at the double frequency of fundamental harmonic as shown in Figure 2.3. The overall effect of this process is obtained by the summation of all the fields emitted from different positions with their respective phases. In order to calculate the phase difference between

two emitted waves, we consider a second harmonic light that is generated in place z_1 and another one generated in the z_2. The second wave bears a phase dictated by fundamental wave equal to $(2k_1)z_2$ while the first SH light had the initial phase of $(2k_1)z_1$ plus the phase that gains by traveling through the crystal $(k_2)\Delta z$. Therefore, the phase-difference between two dipoles can be calculated by $2k_1z_2 - \left[2k_1z_1 + k_2(z_2 - z_1)\right] = (2k_1 - k_2)\Delta z$. The $\Delta k = 2k_1 - k_2$ is called phase mismatch vector as has been derived mathematically in Eq. (2.37). Δk should be equal to zero to ensure that the contributions to SH wave generated at different points in the crystal build up in phase and lead to efficient SHG. In the other word $n_1 = n_2$ and it means the phase velocity for two waves should be the same. Meeting this condition is a common problem as nonlinear optical materials usually have a normal dispersion in which higher frequencies have larger refractive incidence compared to lower frequencies $n_2 > n_1$. The dispersion commonly produces a non-zero phase mismatch $[\Delta k = k_{2\omega} - 2k_\omega \neq 0]$ if no special arrangement is taken. To overcome this difficulty two different techniques have been mostly utilized; birefringent phase matching and quasi-phase matching.
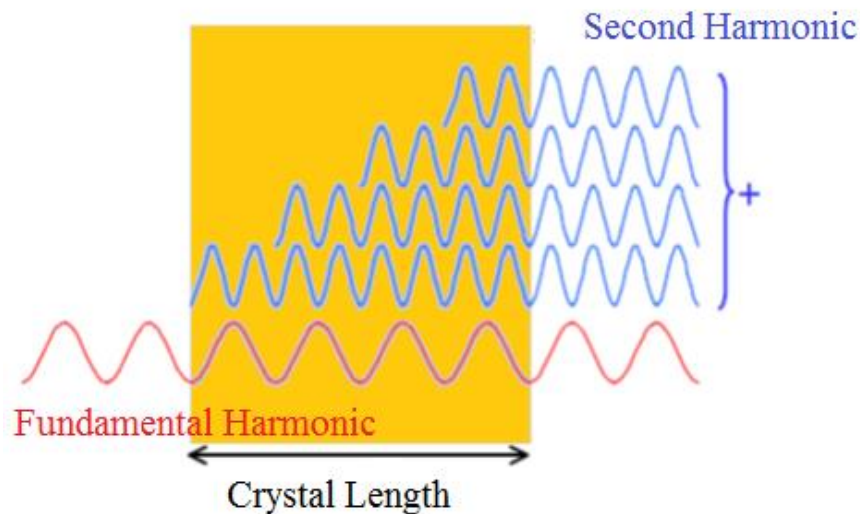
Figure 2.3: Sketch of phase matching concept when all dipoles radiate in phase to build up the SHG. The fundamental wave is plotted in red color and has a well-defined phase, propagating in the crystal. The induced dipoles all emit light at the double frequency of fundamental harmonic with a phase determined by the fundamental wave [64].

2.4.1 Birefringence phase matching

In birefringent material, the refractive index depends on the polarization of the wave and propagation direction. Therefore, the speed of light in these mediums can be governed by selecting the proper wave polarization depending on their wavelengths. Between birefringent material, uniaxial crystals are the most common type in which a single direction governs the optical anisotropy whereas all directions perpendicular to it are optically equivalent. This special direction is known as the optic axis of the crystal. Light with polarization perpendicular to the optic axis experiences ordinary refractive index n_o while the light whose polarization is in the direction of the optic axis experiences an extraordinary refractive index n_e. If the polarization of generated harmonic waves is constrained to lie along the axis with lower refractive index while the fundamental harmonics polarization is constrained to lie along higher refractive index, their corresponding phase velocities can be equalized using birefringence for a specified wavelength. Thus, phase matching condition can be achieved. In Figure 2.4 the arrangement for birefringent phase matching for lithium niobate which is a negative uniaxial crystal has been shown. *a, b*, and *c* are three orthogonal axes of the crystal. In addition, the extraordinary and normal refractive indices versus wavelength are plotted in Figure 2.4.

(a)   (b)
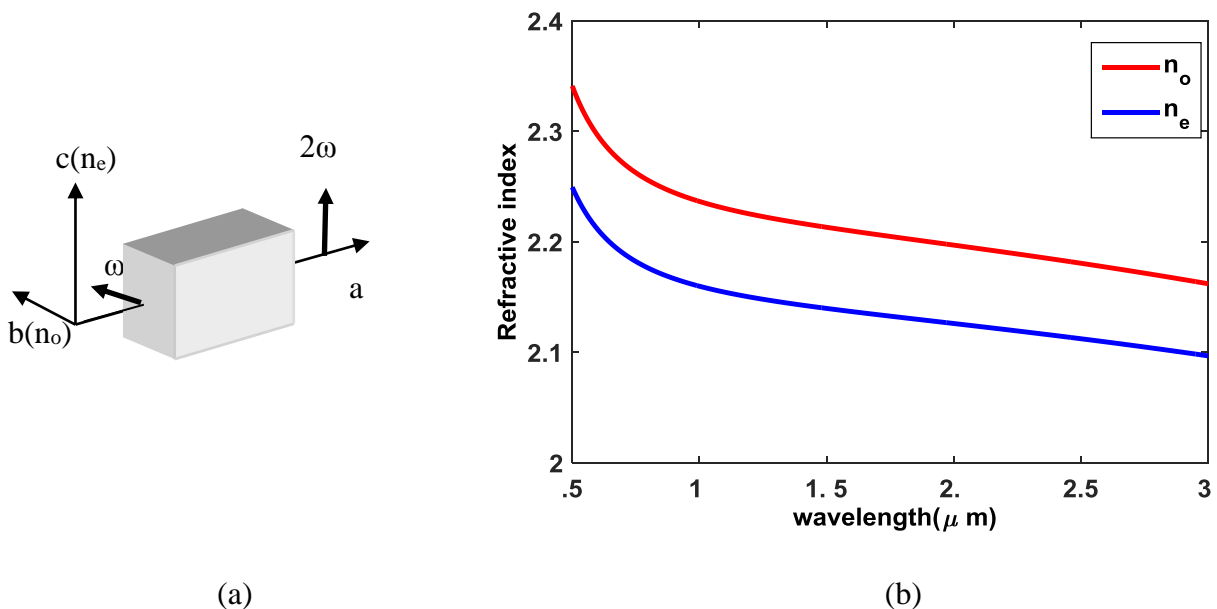
Figure 2.4: a) Configuration for achieving phase matching in a birefringent $LiNbO_3$ ($n_o > n_e$). b) ordinary and extraordinary refractive indices for lithium niobate vs. wavelength.

Phase matching condition can be satisfied just for one specified wavelength at each time, as it can be observed from the plot (b). In order to get conversion frequency in other wavelengths, two methods are utilized including temperature tuning and angle tuning. Temperature tuning is based on the dependence of refractive index on the temperature so that the wavelength at which $\Delta k = 0$ changes with the temperature. In another alternative approach, angle tuning, the direction of propagation changes instead of the temperature to satisfy phase matching. The polarization of fundamental harmonic lies in an angle θ relative to a-axis and in the a-b plane in Figure 2.4 a. In this case, the effective refractive index for fundamental beam can be calculated from the following equation

$$n_\theta(\omega)^2 = \left[\frac{\sin^2(\theta)}{\tilde{n}_e(2\omega)^2} + \frac{\cos^2(\theta)}{\tilde{n}_o(2\omega)^2} \right]^{-1/2}.$$

2.44

In the angle tuning or critical phase matching technique, as optical waves do not propagate collinearly with each other, there is a loss of efficiency due to walk-off. The reason is that the extraordinary wave propagating through a birefringent crystal possesses a Poynting vector that is not parallel to the propagation vector.

Although birefringent nonlinear materials provide phase matching, there is no guarantee for efficient generation of SH. Because the nonlinear d-tensor must contain appropriate elements that couple a linear polarized fundamental harmonic in ordinary axis to a polarized second harmonic in extraordinary one to obtain an efficient SHG.

2.4.2 Quasi-phase matching

In general, in a dispersive material, the phase mismatch leads to SH intensity oscillation within material length if the phase velocities of the FH and SH are different. The SH intensity oscillates in the period of $2l_c = 2\pi/(k_{2\omega} - 2k_\omega)$ as shown in Figure 2.5 when there is no phase matching (Non-PM). If the sign of driving nonlinear susceptibility is reversed in the distance of $l_c = \pi/(k_{2\omega} - 2k_\omega)$ called coherence length, the phase difference is "reset" to zero. This creates a step-wise growth in the output power along the crystal length known as quasi-phase matching (QPM) and can be seen in Figure 2.5. Such a spatial modulation of nonlinear susceptibility can be obtained in

ferroelectric crystals by periodically altering the crystal orientation so that the effective nonlinearity changes according to the orientation.
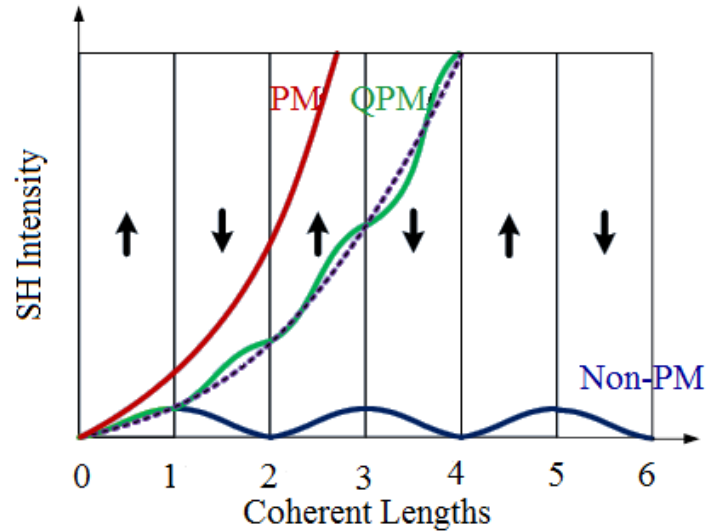
Figure 2.5. Second harmonic intensity as a function of propagating distance for quasi-phase matching (QPM) by flipping the sign of the spontaneous polarization in every other coherence length compared to perfect phase-matched (PM) and non-phase-matched interaction (Non-PM).

Although QPM has lower conversion efficiency for the same nonlinear coefficient compared to the perfect phase matching (the effective nonlinearity d_{eff} is reduced by a factor of $2/\pi$), it brings useful flexibility into optical parametric processes. Among the advantages of QPM, the use of any convenient combination of polarizations in the nonlinear interaction can be mentioned. In this case, in addition to Type I and Type II phase matching, Type 0 in which all interacting waves have the same polarization is allowed and this often corresponds to use of the strongest element of the nonlinear tensor. In addition, QPM makes the noncritical phase matching possible for all frequencies in the transparency region of the nonlinear material. Therefore, the spatial walk-off is eliminated. In order to have a more precise look at QPM, mathematically description of QPM, can be considered. The nonlinearity modulation $d(z)$ (known as QPM grating) changes like a rectangular wave in the space domain with the period of $\Lambda = 2l_c$ as shown in

Figure 2.6.b

<div align="center">(a)　　　　　　　　　　　　　　(b)</div>
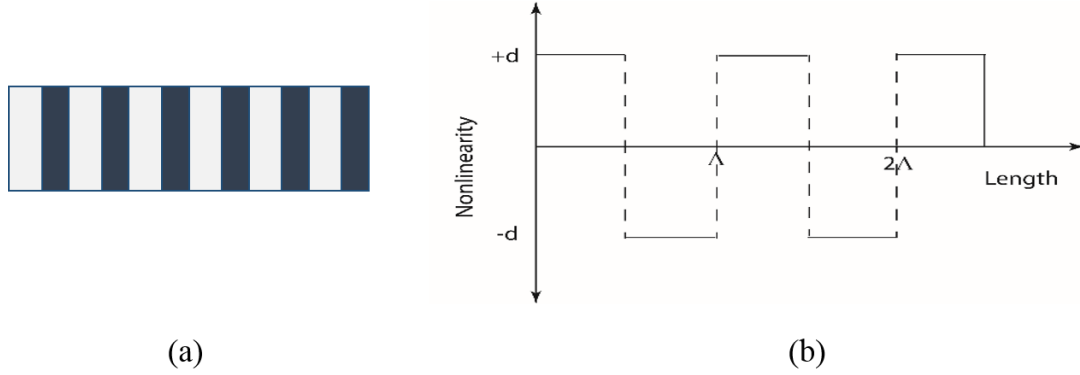
Figure 2.6: a) Uniform grating. b) nonlinearity function in space.

This function can be written in the form of the Fourier transform of spatial frequency ($k = 2\pi / \Lambda$) including all frequency components at fundamental harmonics

$$d(z) = d_{eff} \sum_{m=-\infty}^{\infty} G_m \exp(ik_m z) ,$$

<div align="right">2.45</div>

where d_{eff} is the effective nonlinear coefficient of the material, $K_m = 2\pi m/\Lambda$ is the grating vector of the mth Fourier component, and Λ is the period of the modulated structure. The Fourier coefficients G_m for the duty ratio D is given by:

$$G_m = \frac{2}{\pi m} \sin(m\pi D)$$

<div align="right">2.46</div>

In order to achieve strongest nonlinear interaction, the first order of grating harmonic $m = 1$ and duty cycle of $D = 1$ should be selected. Therefore, the phase matching condition for the first-order QPM in Eq. (2.37) can be written as:

$$\Delta k_Q = \Delta k \pm K = k_2 - 2k_1 \pm \frac{\pi}{l_c}$$

<div align="right">2.47</div>

where $\varDelta k$, k_1 and k_2 are same as in Eq. (2.37), and $l_c = \dfrac{\lambda}{4(n_2 - n_1)} = \dfrac{\varLambda}{2}$ is the coherent length of

SHG for a specific fundamental wavelength λ. For periodically poled lithium niobate (PPLN), exploiting the biggest nonlinear coefficient d_{33} via type 0 phase matching is possible.

The spectral shape of QPM is similar to birefringent phase matching. It still obeys the Eq. (2.30) with different effective nonlinearity but the similar sinc function as shown in Figure 2.1. The maximum of efficiency is correlated with the wavelength λ for which spatial modulation is designed.

2.5   Chirped grating

QPM in the form of periodically poled material has been discussed in the previous section. These devices are designed to be phase matched for a specific wavelength and nonlinearity changes uniformly in the crystal length as shown in

Figure 2.6.a with a constant period. These devices have a narrow spectral and thermal bandwidth. In order to increase the bandwidth of uniform gratings and satisfy phase matching for a wider range of wavelengths, the QPM in the form of chirped grating has been introduced. In the price of losing efficiency, the bandwidth can be enlarged. In chirped QPM the spatial period changes linearly in the crystal length. In Figure 2.7, a chirped grating has been shown.

Figure 2.7: Chirped grating.

Mathematically, $d(z)$ can be written as

$$d(z) = d_{eff} \sum_{m=-\infty}^{\infty} G_m \exp\left(-i k_m (z + rz^2 / 2)\right),$$

2.48

where all parameters are similar to Eq.(2.44) and r is the chirp ratio of the grating. In the chirped structure, the period and wave number of grating change with respect to the distance. They can be described by following equations:

$$\Lambda(z) = \Lambda_0 / (1 + rz)$$
$$K(z) = K_0 (1 + rz)$$

2.49

where Λ_0 is the length of the first period and r is the chirp rate per unit length and can possess the positive or negative quantity. The bandwidth broadening can be managed by changing the chirp rate. The sign of chirp rate influences the bandwidth broadening in the higher or lower frequencies as the positive sign enhances the broadness at shorter wavelengths and negative chirp rate increases the broadening toward higher wavelengths.

As the period variation in linearly chirped gratings is too small, (typically around 100 picometers) the step-chirped grating are suggested to overcome fabrication difficulties [7]. In step-chirped gratings, the total length is divided to p sections as shown in Figure 2.8 and each section consists of n constant period Λ_i. The period of each section is calculated to be

$$\Lambda_i = \Lambda_1 + \Delta\Lambda(i-1),$$

2.50

where Λ_1 is the period of the first section, and $\Delta\Lambda$ is the step in the chirp period or the constant chirp period change between two adjacent sections. Also length of each segment is $L_i = n\Lambda_i$, $i=1,2,...,p$. Here, n represents the number of periods in each section.
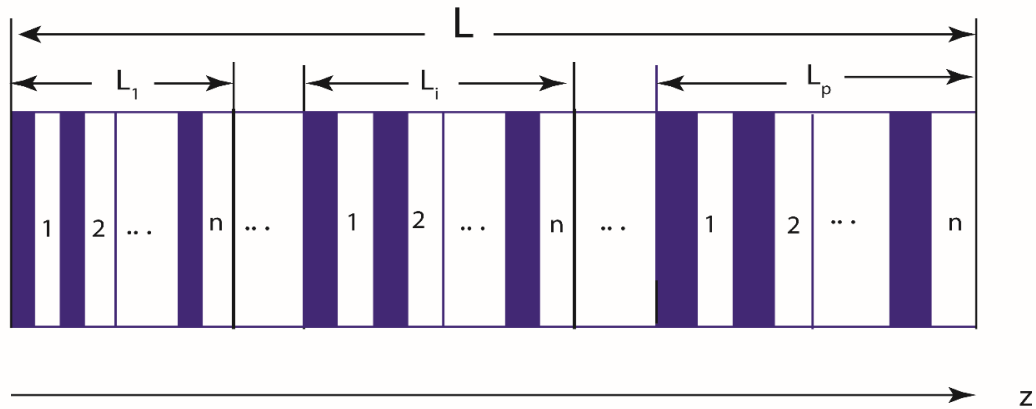
Figure 2.8: Schematic of step-chirped grating.

Chirped grating can be designed to have desired spectral bandwidth. As the phase mismatch depends on temperature through the refractive index, expansion of spectral bandwidth naturally leads to increase of thermal acceptance. Here, to compare spectral and thermal bandwidths of uniform and chirped grating, the SH efficiency of a 2-cm-long uniform PPLN has been compared to the same length of chirped PPLN with 10 sections and $\Delta\Lambda = 0.1$ µm for the central bandwidth at 1.55µm in Figure 2.9 and Figure 2.10. The SH response of chirped grating has some fluctuations (ripples) as it can be clearly seen in these two figures.
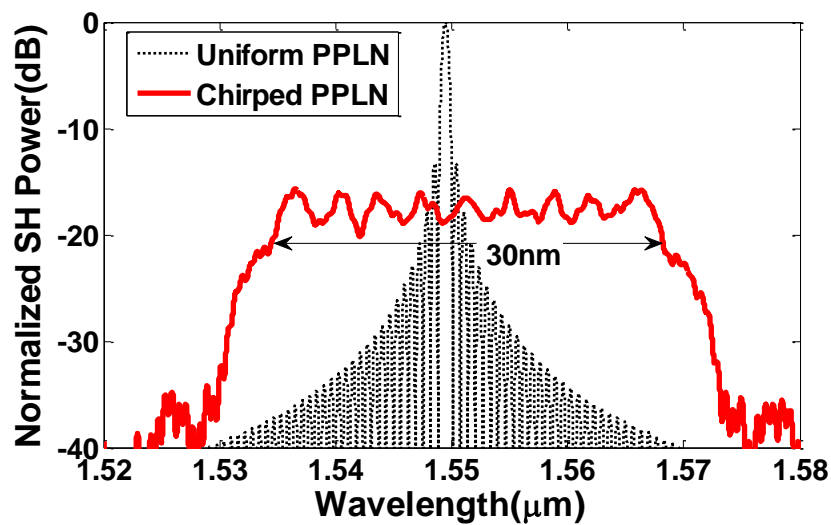
Figure 2.9: Bandwidth of chirped PPLN compared to uniform PPLN.
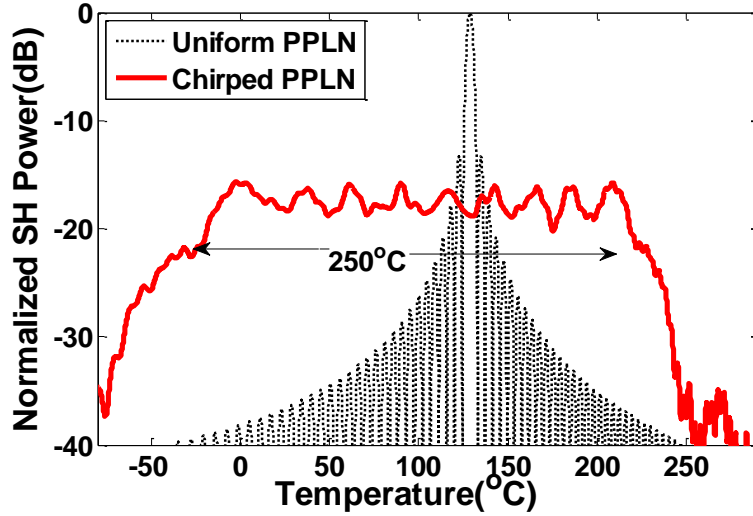
Figure 2.10: Thermal acceptance of chirped PPLN compared to uniform PPLN.

2.6 Apodization

Apodization is utilized as a solution to reduce the fluctuations in the generated harmonic efficiency in chirped grating or to eliminate side lobes in the response of uniform grating. Apodization is a function, which is used to smoothly bring the maximum of nonlinearity down to zero at the edges of the grating. Mathematically for a chirped grating it can be described by multiplication of the apodization function to a chirped nonlinear grating function, therefore, $d(z)$ for an apodized chirped grating changes as

$$d(z) = f_{ap}(z)d_{eff} \sum_{m=-\infty}^{\infty} G_m \exp\left(-i\,k_m(z+rz^2/2)\right), \qquad 2.51$$

where f_{ap} is the apodization function, r is the chirp ratio and d_{eff} is the effective nonlinearity. The other parameters are same as Eq. (2.47).

Apodization function can affect the response of generated harmonics based on the function shape and the ratio of applied function in a grating. Several common apodization functions are as follow:

Sine	$f(z) = \sin z,$	2.52
Raised sine	$f(z) = \sin^2 z$,	2.53
Tanh	$f(z) = \dfrac{e^z - e^{-z}}{e^z + e^{-z}},$	2.54
Gaussian	$f(z) = a \exp(-\alpha \dfrac{z^2}{\omega_0^2})$,	2.55
Cauchy	$f(z) = \dfrac{1 - (z/L)^2}{1 - (Cz/L)^2},$	2.56
Blackman	$f(z) = \dfrac{(1+B)\sin(z) + B\cos(2z)}{2 + 2B}.$	2.57

These functions can be applied on the whole length of grating or on the part of that. For example, for a sine-apodized chirped grating the percentage of unaffected chirped grating in the center can be variable and can be described by the following equations:

$$f(z) = \sin(a\pi z / L), \qquad 0 < z < L/2a, \qquad\qquad 2.58$$

$$f(z) = \sin(a\pi(L - z)/L, \qquad L(1 - 1/2a) < z < L,$$

where *a* is an apodization ratio parameter to adjust the amount of apodization and *L* is the total length of the device. The profiles of apodization for different ratios on the structure are plotted in Figure 2.11
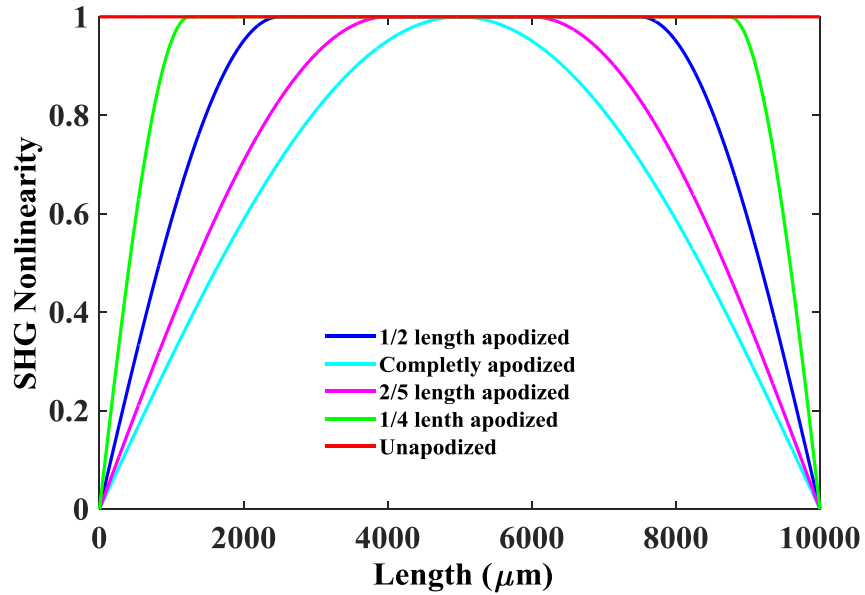
Figure 2.11: SHG nonlinearity versus length for apodization ratios.

Also, profiles of different functions such as sine, hyperbolic tangent, Gaussian, Blackman and Cauchy on half of the grating are depicted in Figure 2.12. For the Gaussian function, $\alpha = 0.3 \times 10^{-6}$, which is sharp enough to reach near zero at the ends of the device. For the Cauchy function, the constant *C* is 0.9. This amount has been chosen to result in a smooth efficiency response. For the Blackman function, the constant *B* is equal to 0.9.
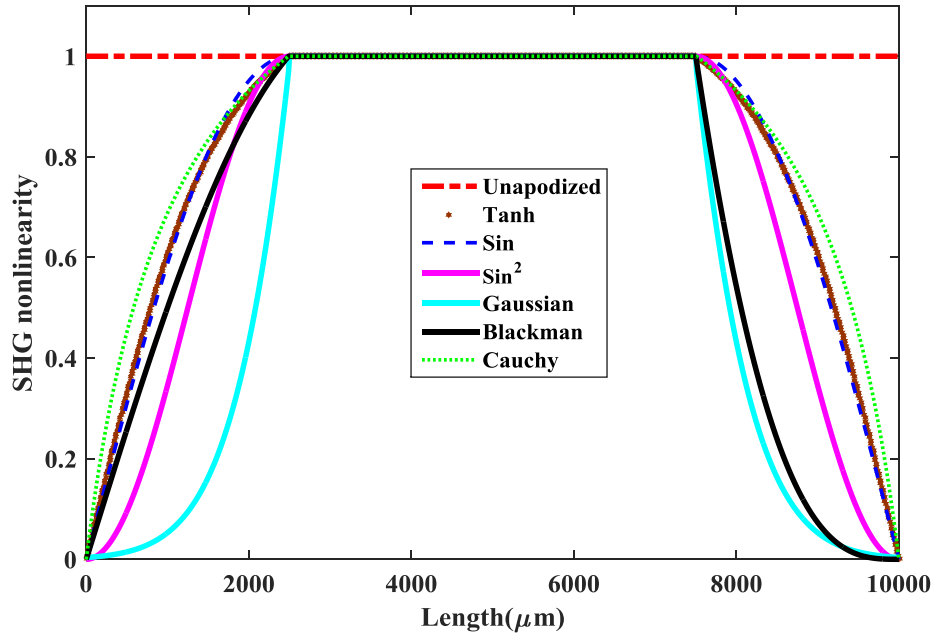
Figure 2.12: SHG nonlinearity versus length for various functions.

The effect of apodization on a grating is shown for the conversion of broadband fundamental harmonic centered at a wavelength of 1570 nm to achieve a 30-nm bandwidth at the output. To obtain this result the chirped ratio, r in Eq. (2.50) for a 1-cm-long aperiodically poled lithium niobate (APPLN) is chosen to be 4×10^{-6}. Therefore, the first-period length is 20 microns and the last one ends with 19.23 microns. The bandwidth in the unapodized chirped grating is around 30 nm and efficiency variation is 53% of maximum efficiency which can be reduced by applying apodization. For different ratios of apodization which is plotted in Figure 2.11, the normalized SHG efficiencies are shown in Figure 2.13. With complete apodization, when $a = 2$ in Eq. (2.57), the nonlinearity grows with a shallow slope and then diminishes abruptly. In this case, ripples are removed, but the bandwidth is reduced to less than 50%. By decreasing the ratio of apodization, bandwidth and ripple increase. In the ½ length apodization, the bandwidth reduced to 66% and the maximum of efficiency change falls to 7%. This case which gives a compromise between bandwidth and flatness is used for examination of other functions profile.
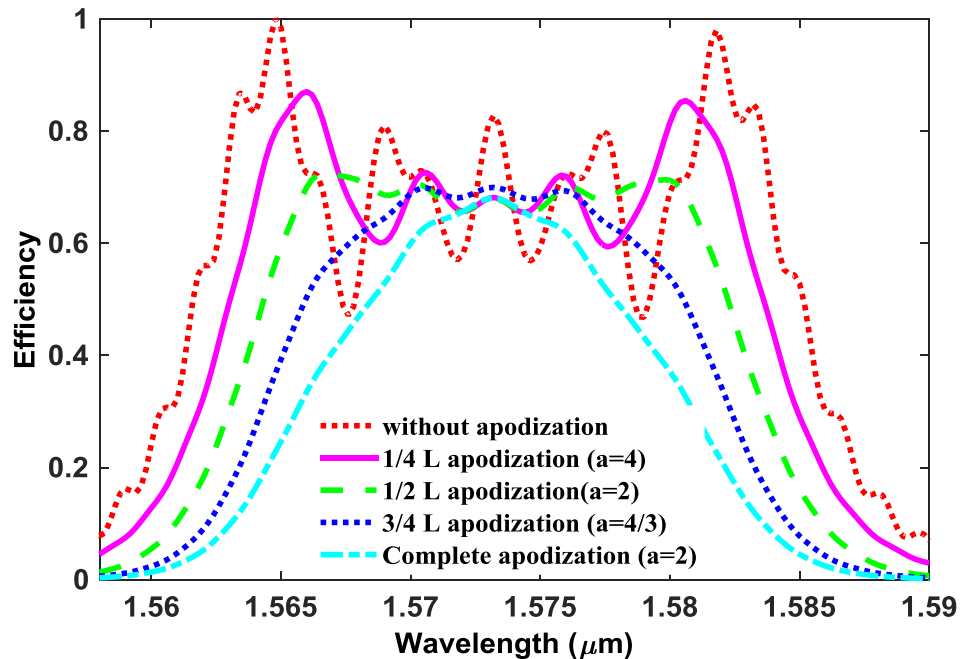
Figure 2.13: Normalized efficiency of SHG for different ratios of sine function appodization.

The normalized simulated results of above apodization functions are shown in Figure 2.14 which are corresponding to plotted functions in Figure 2.12. Since Blackman function is not symmetric, the response is also not symmetric. By diminishing the quantity *B*, the difference between maximum and minimum of ripple reduces but these changes are not large (2%) in comparison with the ripple of this function (18%). The Gaussian function reduces the bandwidth more than other functions (56%) while the ripples are still large (30%). The hyperbolic function gives less intensity change (5%) in comparison with the sine (7%) or Cauchy function (8%) while the bandwidth of *tanh* and sine is almost the same. The raised sine gives the 10% intensity changes but the fluctuations of efficiency with wavelength are the smallest.
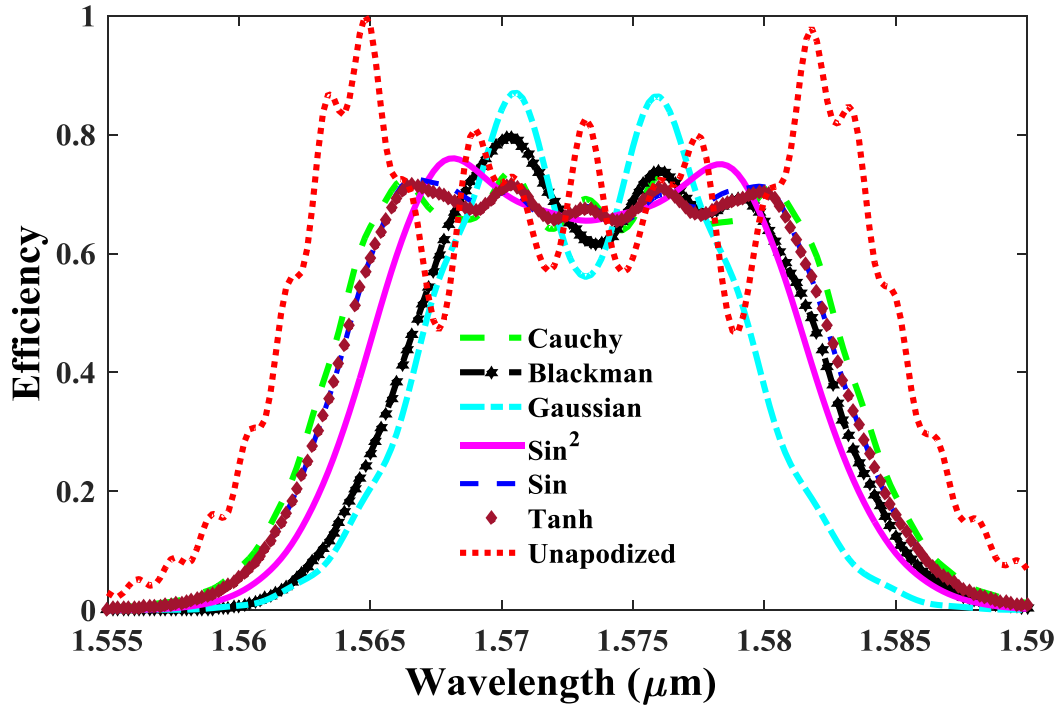
Figure 2.14: Normalized efficiency of SHG for various functions

In practice, apodization in chirped PPLN can be achieved by changing the duty ratio in every period of the chirped structure [8, 9]. Unlike refractive index apodization, it is impossible to have the desired nonlinearity coefficient as it can have just two states: positive and negative. Thus, by changing the duty ratio in each period at both ends of the device, the behavior of nonlinearity coefficient can be controlled. A schematic of the initial part of an apodized chirped grating is shown in Figure 2.15.
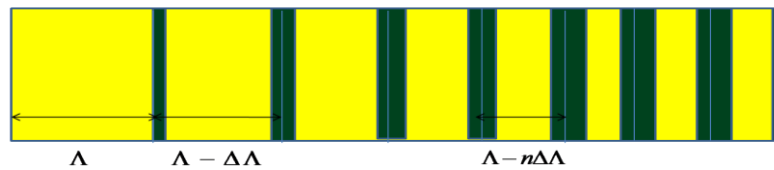
Figure 2.15: Schematic of the apodized chirped grating.

2.7 Gaussian beam

In practice, the incident laser beam is focused in the crystal in order to increase the optical parametric efficiencies. In this case, paraxial wave equation can be used. Therefore, wave equation (2.29) for each frequency component, is given by

$$\nabla^2 \vec{E}_n - \frac{\varepsilon(\omega)}{c^2}\frac{\partial^2 \vec{E}_n}{\partial t^2} = \mu_0 \frac{\partial^2 \vec{P}_n^{NL}}{\partial t^2}$$

2.59

The electric field and polarization field are given by

$$\vec{E}_n(r,t) = A_n(r)e^{i(k_n z - \omega_n t)} + c.c,$$
$$\vec{P}_n(r,t) = p_n(r)e^{i(k_n' z - \omega_n t)} + c.c,$$

2.60

E_n represents the non-plane wave by defining complex amplitudes A_n and p_n is dependent on radial direction. $\vec{P}_n$ is considered different from $\vec{E}_n$ to allow the phase mismatch possibility. By substituting Eq. (2.60) in Eq. (2.59), considering z-axis as the propagation direction and separating Laplacian to transverse and parallel to propagation axis, Eq. (2.59) using slowly varying amplitude results in

$$2ik_n \frac{\partial A_n}{\partial z} + \nabla_2^T A_n = -\frac{\omega_n^2}{c^2} p_n e^{i\Delta k z}$$

2.61

where $\Delta k = k_n' - k_n$ and $\nabla_T^2 = \partial^2/\partial x^2 + \partial^2/\partial y^2$. This derivation is known as the paraxial wave equation due to neglecting $\partial^2/\partial z^2$ on the left-hand side. For a laser beam with a Gaussian form the amplitude A can be written as:

$$A(r,z) = \frac{A_0}{1+i\zeta}e^{-r^2/w_0^2(1+i\zeta)}.$$

2.62

Here $r = \sqrt{x^2 + y^2}$, w_0 is beam waist radius and $\zeta = 2z/b$ is a dimensionless longitudinal coordinate defined in terms of confocal parameter b as

$$b = 2\pi w_0^2 / \lambda = 2z_R, \qquad\qquad 2.63$$

where w_0 is the focal radius and λ is the wavelength of light. The beam converges towards the focal point and expands in a symmetrical manner in the propagation direction. The spot size of the beam changes with z while propagating. It can be calculated from the focus point by

$$w(z) = w_0 \sqrt{1 + \left(\frac{z}{z_R}\right)^2} \ . \qquad\qquad 2.64$$

In the vicinity of the focus point, the beam exhibits approximately parallel behavior between roughly $z = \pm z_R$. The field strength on-axis ($r = 0$) can be obtained from the first term in Eq. (2.62) which can be written as:

$$A(0, z) = (\frac{A_0}{\sqrt{1 + \zeta^2}}) \exp(i\phi_{Gouy}) , \qquad\qquad 2.65$$

where the phase term in Eq. (2.65) is the Gouy phase given by

$$\phi_{Gouy} = \tan^{-1}\zeta \ . \qquad\qquad 2.66$$

The Gaussian beam width as a function of distance (z) along the beam (w_0) and intensity profile in two different places of propagation distance are shown in Figure 2.16.
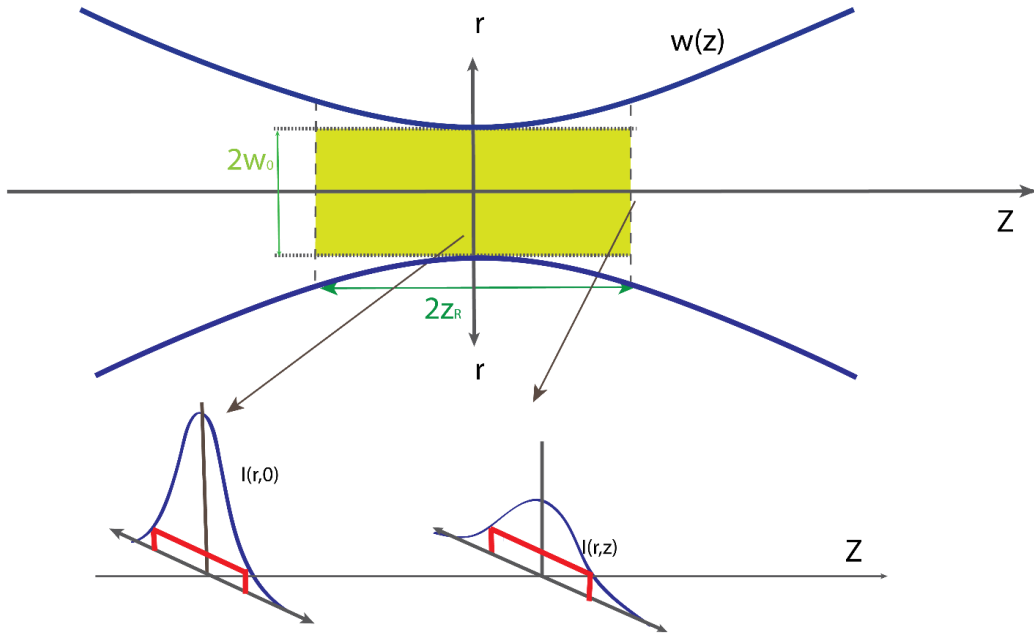
Figure 2.16: Field amplitude of a Gaussian beam.

In order to solve the second harmonic excited by a Gaussian fundamental beam, Eq. (2.60) is used for SHG by substituting $p_2 = 2\varepsilon_0 d_{eff} A_1^2$, resulting in

$$2ik_2 \frac{\partial A_n}{\partial z} + \nabla_2^T A_2 = -\frac{2\omega_2^2 \varepsilon_0}{c^2} d_{eff} A_1^2 e^{i\Delta kz}.$$

2.67

For undepleted pump the fundamental beam is

$$A_1(r,z) = \frac{A_1(0)}{1+i\zeta} e^{-r^2/w_0^2(1+i\zeta)},$$

2.68

and the solution of Eq. (2.67) supposed to have the form of

$$A_2(r,z) = \frac{A_2(z)}{1+i\zeta} e^{-2r^2/w_0^2(1+i\zeta)}.$$

2.69

The amplitude of the second harmonic depends on the *z*-axis and radial dependence is similar to the fundamental pump. If Eq. (2.69) is substituted in Eq. (2.68) then $A_2(z)$ obeys the following differential equation

$$\frac{\partial A_2}{\partial z} = -\frac{4i\omega_2\varepsilon_0}{nc} d_{eff} A_1^2 \frac{e^{i\Delta kz}}{(1+i\zeta)}.$$ 2.70

By direct integration of Eq. (2.70) we obtain

$$A_2 = -\frac{i\omega_2\varepsilon_0}{nc} d_{eff} A_1^2 \int \frac{e^{i\Delta kz}}{(1+i\zeta)} dz.$$ 2.71

The Eq. (2.70) in plane wave approximation ($b \gg |z|$, $|z_0|$) reduces to Eq. (2.37.a)

$$A_2(r,z) = \frac{A_2(z)}{1+i\zeta} e^{-2r^2/w_0^2(1+i\zeta)}.$$ 2.72

The field strength on-axis($r=0$) is plotted versus z direction for different confocal parameter in Figure 2.17.

Figure 2.17. The field strength (A_1) changes on-axis ($r = 0$) for different focusing parameters b

CHAPTER 3   FABRICATION OF PERIODICALLY POLED LITHIUM NIOBATE

Ferroelectric materials with nonzero spontaneous electric polarization are proper candidates for poling. The polarization can be reversed by applying a strong external electric field in opposite direction. The polarization in ferroelectric material exhibits hysteresis loops and depends on the electric field and its history. In periodic poling of lithium niobate, nonlinear coefficient d_{33} along the optic axis of the crystal is reversed in the periodic domains. The dimension of these periods is around several microns and requires high precise fabrication techniques. There are several techniques for reversing the spontaneous polarization in lithium niobate including direct electron beam writing, electric field poling (EFP), and UV assisted electric field poling [65]. Among these techniques, electric field poling at room temperature is accepted as the most convenient method because of its simplicity and poling rapidity. The devices used in this thesis were fabricated using the room temperature EFP technique based on photolithographically-defined liquid electrodes. In this chapter, we first introduce a brief summary of the physical properties and structure of LiNbO$_3$. Then we describe our approach to fabricate PPLNs in details.

3.1   Lithium niobate

Lithium niobate is a human-made dielectric material that does not exist in nature. It was grown from a melt solution, the first time by Matthias and Remeika in 1949 [66]. After, it was synthesized in a single crystal form and examined in Bell Laboratories. Its growth conditions, the crystal structure and the elctro-physical properties were investigated precisely [67]–[72]. Lithium niobate which is now widely used in electro-optic devices exhibits several important properties such as ferroelectricity, pyroelectricity, piezoelectricity, negative uniaxial birefringence and nonlinear optical polarizability. Lithium niobate is classified as the 3m point group and shows three-fold rotation symmetry about its optical c axis [73]. The structure of LiNbO$_3$ crystal is shown in Figure 3.1. Its molecular structure consists of a planar layer of oxygen atoms in the form of distorted hexagonal closed packing. The two third of spaced between these layers filled by Nb atom and Li atoms equally and one third of the lattice is vacant. Below its ferroelectric Curie temperature (~1210 $^o C$), Nb atoms are located just below the average oxygen layers and Li atoms are placed just above the oxygen layer. The spontaneous polarization of LiNbO$_3$ crystal is in a positive direction as it is shown in Figure 3.1.a.

Figure 3.1.LiNbO$_3$ structure in (a) as-grown state and (b) domain inverted state, where P_s and E represent the polarization and electric field direction respectively [74].

If an electric field over the coercive field is applied in the direction of c-axis to the crystal, the locations of Li and Nb atoms changes. Lithium and niobium atoms move a little in the direction of electric field and lithium atoms locate below the oxygen layer and niobium place just above the oxygen layers. Consequently, the spontaneous polarization of LiNbO$_3$ crystal is reversed. The c axis is defined as the axis that the crystal exhibits three-fold rotation symmetry. The direction of the c-axis can be recognized by compressing or heating the crystal and checking the electric charge on the surface of the crystal. The surface with accumulated negative charge is then $+c$. Because the lithium and niobium ions in the oxygen octahedral move closer to the oxygen plane centers, and consequently, reduce the net polarization and exceed the negative charges on $+c$ [75].

Lithium niobate crystal is a negative uniaxial crystal, which holds two refractive indices; the ordinary refractive index (n_o) and the extraordinary refractive index (n_e). The refractive indices are variable for different optical frequencies and depend on temperature. The dependence of refractive index on frequency is known as dispersion. The dispersion comes from the phase difference between natural oscillators in the material and electromagnetic radiation through

oscillation of bound electrons induced by input light [76]. Far from the medium resonance, the refractive index $n(\omega)$ is given by the Sellmeier's equation

$$n^2(\omega) = A + \sum_{j=1}^{m} \frac{B_j\,\omega_j^2}{\omega_j^2 - \omega^2}, \qquad 3.1$$

where ω_j is the resonance frequency and B_j is the oscillator strength of the jth oscillation. Here, $n(\omega)$ stands for n_o or n_e, depending on the light polarization with respect to the crystal axis, and A is a constant. If the summation in Eq.3.1 is extended for all material resonances frequencies that contribute in the required frequency range, it can be derived in an easier form. For the case of LN crystal, the Sellmeier's equations are reported as [77]

$$n_o^2 = a_1 + \frac{a_2 + b_1\,f}{(10^3\lambda)^2 - (a_3 + b_2\,f)^2} + b_3\,f - a_4\,(10^3\lambda)^2, \qquad 3.2$$

$$n_e^2 = a_1 + b_1\,f + \frac{a_2 + b_2\,f}{\lambda^2 - (a_3 + b_3\,f)^2} + \frac{a_4 + b_4\,f}{\lambda^2 - a_5^2} - a_6\,\lambda^2, \qquad 3.3$$

where $f = (T - 24.5)(T + 570.82)$, λ is the wavelength in µm, and T is the temperature in $^{\circ}C$. The parameters in Eqs. (3.1) and (3.2) are shown in Table 3.1. At 25 $^{\circ}C$, the refractive index of lithium niobate versus wavelength is already plotted in Figure 2.4.

	n_o	n_e
a_1	4.9048	5.35583
a_2	1.178×10^5	0.100473
a_3	2.1802×10^2	0.20692
a_4	2.7153×10^{-8}	100
a_5	-	11.34927
a_6	-	1.5334×10^{-2}
b_1	2.2314×10^{-3}	4.629×10^{-7}
b_2	2.9671×10^{-5}	3.862×10^{-8}
b_3	2.1429×10^{-8}	-0.89×10^{-8}
b_4	-	2.657×10^{-5}

Table 3.1. Parameters for Eqs. (3.2) and (3.3).

3.2   Fabrication process

Our designed chirped PPLN is fabricated on the 0.5 mm thick optical grade LN wafers from Crystal Technology. Different steps are involved in the fabrication of PPLNs, which is described in details as follow; making mask based on our design, photolithographic printing of the mask, preparing poling set-up and employing high voltage pulse shape, in-situ optical monitoring of the poling process using crossed-polarizers, and wet-etching of the surface of the poled lithium niobate to reveal the pattern [78].

a. Mask fabrication

Based on the design, length, period, and duty ratio of different sections of the grating are determined. Then typically, five or six channels with the width of 2 mm of the grating are drawn by the Auto Sketch software. We have used a smaller duty ratio (open area to covered area) than

what we finally desire to obtain in final step due to the expansion of open-area widths during UV exposure in photolithography and poling process. The electric field and UV usually penetrate through open windows and increase the width of exposed area undesirably. For example, in order to achieve a final 50:50 duty ratio on the periodically poled sample, we obtained an optimized initial duty ratio of 25:75. Then the designed pattern is fabricated as a positive mask in a 5-inch glass using chrome deposition and laser machining facility in the Polygrames research center at Polytechnique Montreal. Part of the fabricated mask under the microscope is shown in Figure 3.2. In this picture, two different duty ratios are clearly observable.
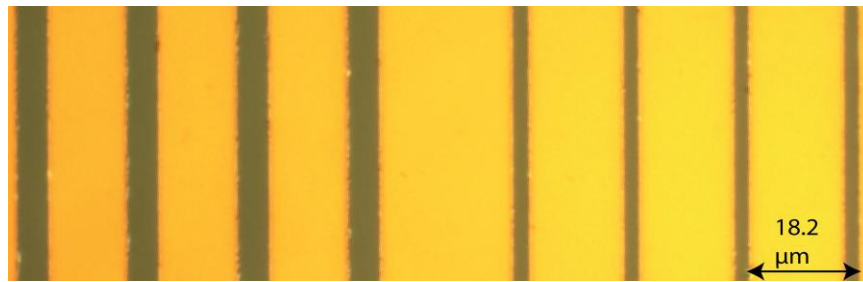
Figure 3.2: Microscopic images of the fabricated mask with two different duty ratios.

b. *Photolithographic printing*

The photolithographic domain patterning of periodic and aperiodic gratings is done in class-100 clean-room facilities of microfabrication laboratory at Polytechnique Montreal. Schematic of photolithography are shown in Figure 3.3, which is done in following six steps: cleaning, spin-coating, soft baking, mask exposure, development and hard baking. All these steps take one day for lithium niobate to proceed. We use quarters of full 3-inch LN wafers, purchased from Crystal Technology; because our designed gratings have a maximum 2 cm length. A dicing machine with diamond grit blades is used to cut the wafers into four equal pieces. In cutting process, we cover the positive side of lithium niobate by a Teflon tape to prevent minuscule particles coming from dicing from sticking on the photolithographic side of the sample. The $+c$ side can be determined by heating the crystal and monitoring the deflection of a multi-meter to check the electric charge on the wafer surface as it was explained in the last section.

Step1: Cleaning the Wafer

The important initial step in the photolithography process is cleaning the sample. Any dirt or particles on the sample leads to having unevenness in spin coating and emerging comets on the surface. The comets can cause large errors in the final fabricated sample. In addition, the particles on photoresist layer can disturb the distribution of electric field during the poling process and eventually cause the break of the sample. Series of solvents such as Acetone and Isopropanol are used in order to remove the grease, dirt or any other particles. We first wipe up the samples with a special napkin wetted by Acetone and isopropanol to remove all dust and stains. After that, we soak the sample in beakers containing the Acetone and shaking it for 5 minutes to clean all small particles. Then we repeat the step with isopropanol, which is the solvent of Acetone to remove the residue of acetone. Finally, we use deionized (DI) water to clean the isopropanol. The sample is quickly dried by blowing dry N_2 to avoid any stain from water. We always keep the $+z$ of the sample with no contact with napkins or any surface. A hot plate is not used for dehydration as it is used in a normal photolithography process due to the high sensitivity of LN to abrupt temperature changes.
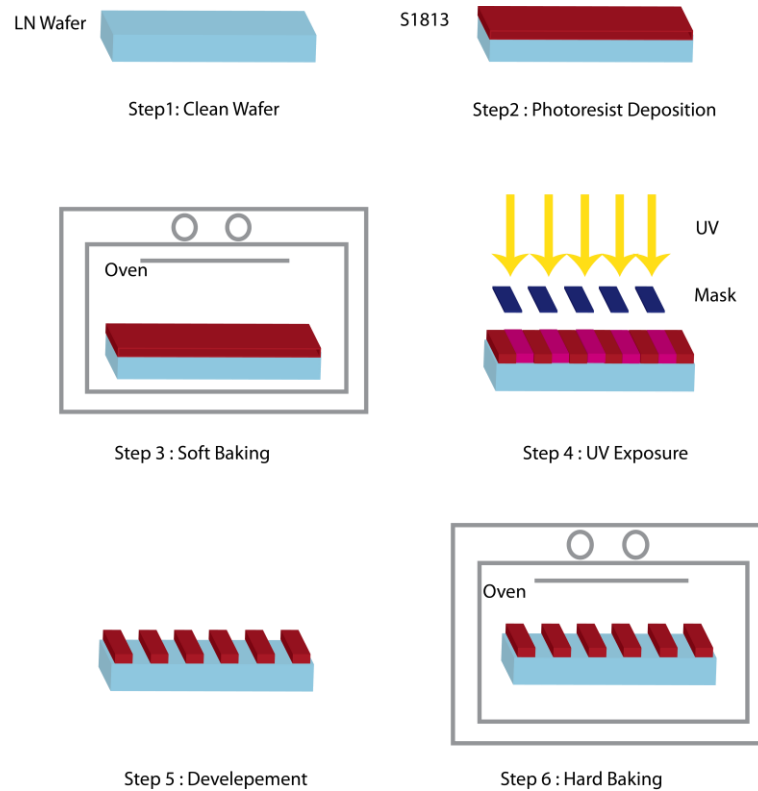
Figure 3.3: Schematic of photolithography process of LN.

Step2: Spin-coating

The $+z$ face of the sample should be coated by a positive resist. After cleaning, without any delay, the sample is placed on the spin mount and is stuck to the mount by vacuuming the air between the mount and the sample. In order to increase cohesion between the photoresist and lithium niobate, adhesive assistant HMDS is spin coated before photoresist. We use photoresist S1813 for the spin coating. The thickness of the photoresist depends on the speed and spinning time. Therefore, the sample is spin coated with the speed of 4000 rpm for 30 seconds to obtain 1.5-micron thickness. The thickness of 1.5 µm is selected to optimize fabrication in both photolithography and poling processes as decreasing the thickness of photoresist leads to increase of the accuracy in photolithography. However, the resist should be thick enough to be a good isolator in the high voltage electric field in the poling process.

Step 3: Soft baking

In soft backing, all the solvent should be removed from the photoresist coating. Soft-baking plays a very critical role in the photo-imaging. The photoresist coating becomes photosensitive, or

imageable, only after soft baking. We put the samples in an oven for 30 minutes in the temperature of 90 ºC. If the sample is over soft-baked at a higher temperature or longer duration, the photosensitivity of resists is degraded by either reducing the solubility of the developer or destroying part of the sensitizer. In contrast, under-soft-baking does not allow the light to reach the sensitizer and the exposure cannot be done completely. Therefore, the resist can be easily removed in both exposed and unexposed areas and it leads to ruining the desired pattern. Since LN is a pyroelectric and is highly sensitive to temperature variations, the charge can accumulate on the surface of the sample during the baking and break the sample. Thus, we place the sample in a cavity on to discharge the accumulated electricity the sample surface due to the temperature rising. An aluminum foil under the samples in a petri-dish and a metallic wire mesh on top are used to make a cavity. The mesh and foil are folded around the edges to be connected electronically. Then the sample is put in the oven while it is turned off and has the initial room temperature. Then the temperature gradually is increased by the rate of 2 ºC/min to reach 90 ºC. After half an hour, the oven is turned off and is left closed to reach the room temperature again.

Step 4: UV Exposure

Mask pattern is transferred to the sample in this step. As the domain growth in lithium niobate is along the *y*-axis, we align the channels in the *x*-direction of crystal to allow domains grow in *y*-axis. Once the mask has been precisely aligned with the pattern on the wafer's surface, the photoresist is exposed to the pattern on the mask with a high-intensity ultraviolet light at 314 nm. The exposure to light causes a chemical change that allows exposed positive photoresist to be removed by a developer. We use the Karl Suss MA4 photomask aligner, which works based on contact exposure. The wafer and assistant holding assembly rise to be in physical contact with the mask, which is grasped by a vacuum chuck. In contact exposure, usually, a high-resolution patterning is expected. The intensity of lamp light is around 3.5 mW/cm^2. Based on the lamp intensity, the required time is calculated to give the total 75 mJ to the sample in the duration of 20 seconds. The intensity of an old UV lamp decays over the time, so the exposure time is calculated each time after a trial exposure. If the exposure time is too low, the development time and thus the dark erosion increases. Too high exposure duration causes light scattering and diffraction in the resist film, which lessens the resolution.

Step 5: Development

After exposure, the substrate is immersed in a developer solution for 60 seconds while agitating. We have used developer MF319 for photoresist S1813. The solution dissolves away areas of the photoresist that were exposed to the light. After, the sample is soaked in water to stop developing the process in the sample. Then it is washed in running DI water and is dried with nitrogen gas. Develop time is critical, as putting in the developer more than the required time leads to opening the windows wider that desirable one and reduce the resolution. After drying, the sample is watched under a microscope to check the quality of the development. Sometimes longer develop time is required to reach sharp edges in the sample due to the reduction of lamp intensity. In Figure 3.4 part of the sample after development is shown under the microscope.
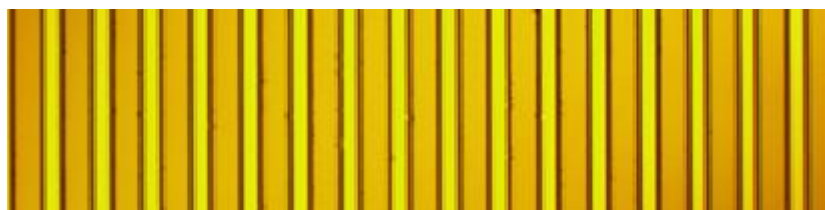
Figure 3.4: Photolithographic image under the microscope after development.
The period is 18.6 μm.

Step 6: Hard Baking

Hard baking is the final step in the photolithographic process. The hard bake solidifies the remaining photoresist. This step is similar to the soft backing. The only difference is time and temperature of baking samples in the oven. The sample is placed in the center of the oven for 40 minutes at the temperature of 120 °C to enhance the insulation and to harden the photoresist. In this stage, also, the cavity made by aluminum foil and wire mesh is used to surround the sample to prevent cracking the sample in temperature variable environment.

    c. Poling

In the poling step, the high voltage electric field is applied to $\pm z$ faces of patterned lithium niobate. Electrically conductive liquid electrode (Electrolyte) made of the saturated solution of

lithium chloride over the un-resist area on both sides of the sample is used to convey the electric field to the LN sample.
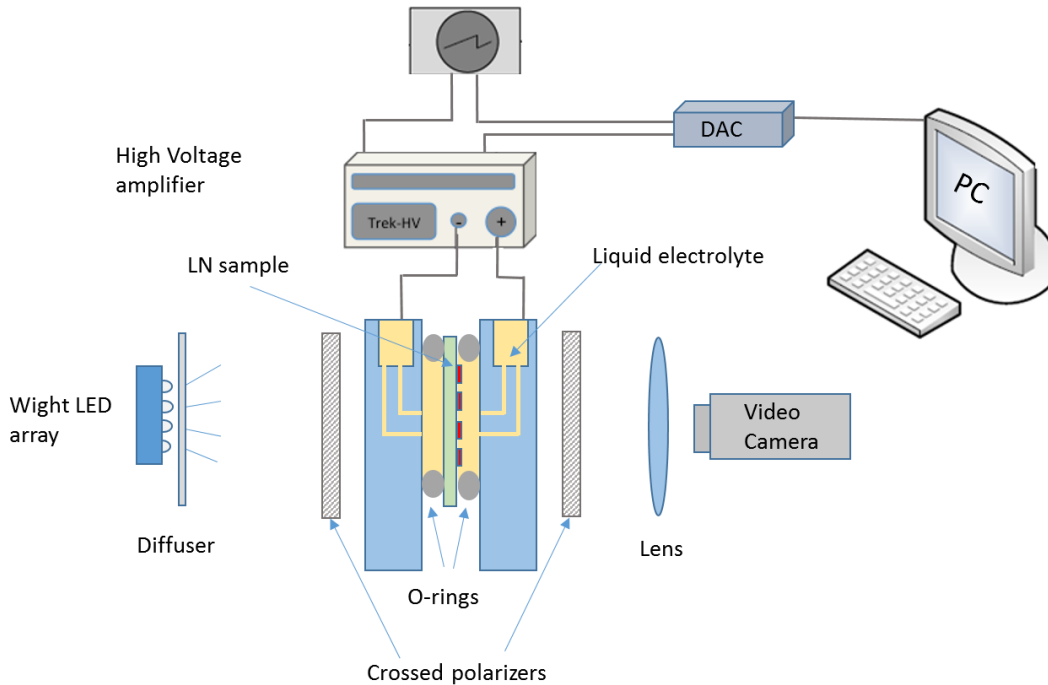
Figure 3.5: Schematic of poling experiment setup showing the high voltage set-up and in-situ optical monitoring using crossed polarizers, DAC: data acquisition card, PC: computer [79].

A transparent isolator sample holder made from plexiglass keeps the sample by sandwiching the sample between two plastic O-rings. The O-rings enclose the liquid electrolyte around the sample as demonstrated in Figure 3.5. In addition, other elements in the set-up are shown in this schematic. The sample holder is placed between two crossed polarizers and illuminated by white light source. A camera records the changes of the sample during poling for optical monitoring. A data acquisition card (DAQ) which is controlled by a LabVIEW program generates the required pulse for poling. A Trek-20 high voltage (HV) amplifier intensifies the input voltage pulse 2000 times to generate the high electric field required for domain inversion in LN. An oscilloscope measures the input voltage and current. The generated pulse by DAQ card in the poling setup for a 0.5 mm LN sample is shown in Figure 3.6. Here the initial pulse generated from DAQ is 1/(2000) of the final pulse that is applied to the sample. The coercive field for lithium niobate is 21.5 kV/mm. Therefore, we have generated an electric pulse more than the coercive field (22

kV/mm) but lower than the breakdown field (~26 kV/mm) which is responsible for the domain growth. Shape, pulse duration and duty cycle of applied pulse are critical for controlling poling and preventing breakdown. All factors are optimized by researching previous studies and experiments. Duration of this pulse is 0.5 ms that is shown in the middle of the larger pulse. The initial stage is applied to warm up the sample and prevents breaking the sample due to receiving abrupt voltage. The final stage prevents the back switching in which the partial or total poled crystal de-poles after turning off the electric field. After amplification, the positive end of the HV output is connected to the $+z$ side of the crystal while the ground wire is connected to the initial $-z$ side of the crystal by inserting the wires on the electrolyte. The electrolyte is directly connected to the sample through the capillaries on two blocks of the sample holder and acts as liquid electrodes. Before fixing the patterned lithium niobate in the sample holder, all around the sample edge are covered by insulation tape. The insulation tape avoids charge leaking from the edges of the sample due to surface conduction, which can cause an electrical breakdown.
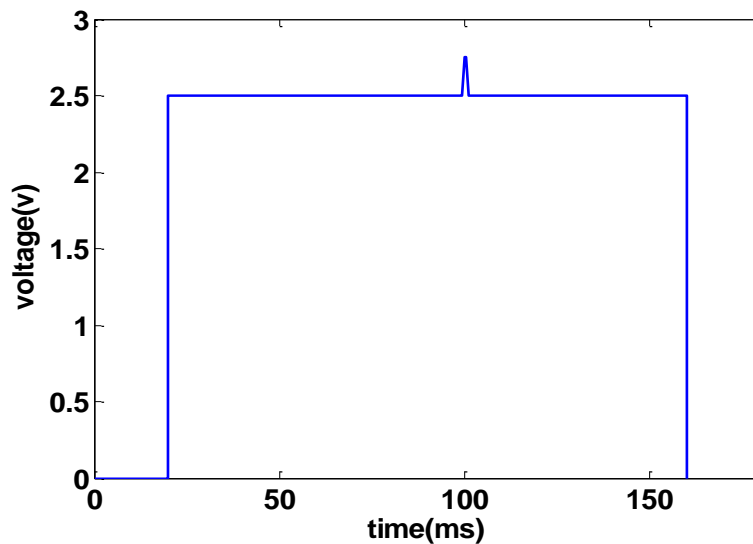
Figure 3.6: Applied voltage during the poling process.

The number of pulses that is needed for poling a uniform grating can be determined by calculation of required charge for entire domain reversal by the following equation:

$$Q = \int I dt = n(I_p \times t_p)$$

$$n = Q / I_p \times t_p \qquad\qquad 3.4$$

I and *t* present the current and the duration time of pulse.

The surface charge is given by $Q = 2P_s \times A$, where *A* is the area of the samples to be poled and P_s is the spontaneous polarization [31]. For lithium niobate at room temperature, spontaneous polarization is $P_s \sim 78$ C/cm^2 [80]. For uniform grating, the duty ratio is 50:50 and the half of channels need to be poled. The current can be read from the DAQ card which is recorded during poling process. The calculation of the number of pulses is more complicated for chirped and apodization gratings. Therefore, this equation just provides an approximation for the number of pulses. The reason is that the open areas are not homogeneous in the length of channels. In order to monitor poling process, we use optical monitoring which is shown in Figure 3.5. In-situ optical monitoring utilizes observing the contrast of two polarization state between two crossed polarizer [81], [82]. The light is scattered due to birefringence associated with oppositely oriented adjacent domains. Figure 3.7 presents pictures taken by a camera during the poling process from starting point to ending point. Before sending the pulses, the stripes on the photolithographic pattern are observed like (a) in the figure. Pictures (b) and (c) show domain inversion during the poling. After few pulses, the domain inversion starts randomly in the channels and grow around the initial random area. The final point is depicted in the picture (d) in which all areas are poled. Sometimes poling does not start from everywhere in channels and leads to over poling and merging periods in some parts and under poling in other places.
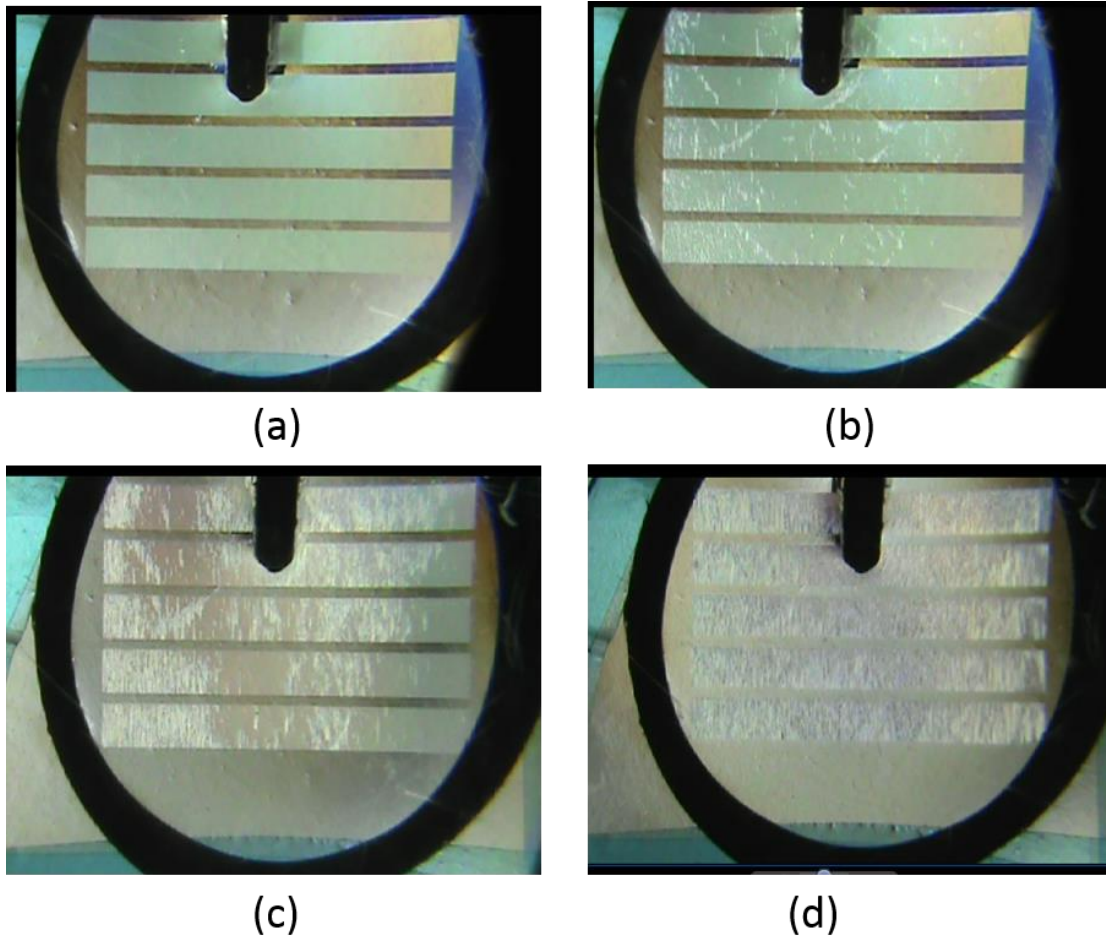
Figure 3.7: Images of samples under poling process in optical monitoring. a) Before sending the pulse. b) After starting several pulses. c) After receiving more pulses than b. d) After completion of domain reversal area.

d. Chemical etching

Chemical etching is a corrosive diagnostic method on the surface of the ferroelectric material to reveal the inverted pattern after poling [83]. Usually, acids are used for chemical etching. The method is based on the different etch rates for the positive and negative ends of ferroelectric dipoles. In the negative face, absorption of the proton with a positive charge is easier than positive face and it accelerates the rate of etching. Also the etch rate rises by increasing the concentration of acidic protons [84]. The mechanism is shown in Figure 3.8. For observation of etched patterns, an optical microscope can be used. Also, imaging of the etched structures with a

scanning electron microscope or topographic imaging with a scanning force microscope are other alternatives [85].

After poling, the photoresist is washed out with acetone and IPA. The original positive side of lithium niobate is covered by Teflon tape to prevent etching on one side. The HF (hydrofluoric) acid with a concentration of 49% is used for etching. The sample is dipped into the acid for 5 minutes, washed with deionized water, and then dried by N_2. The inverted domain pattern is observed using an optical microscope. One well-poled sample after etching can be observed in Figure 3.9.
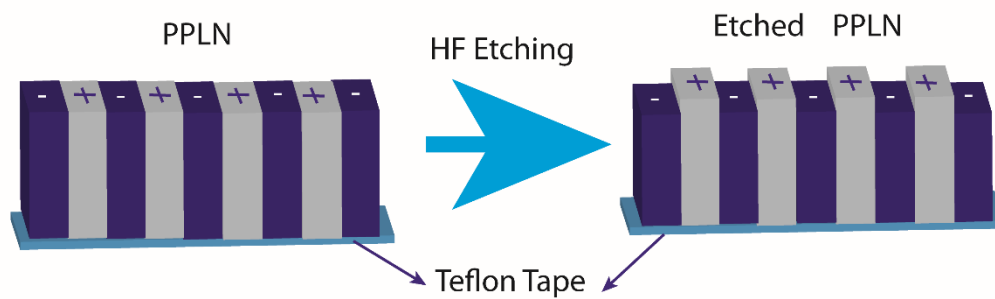
Figure 3.8: Schematic of revealing poled features in LN using HF etchant.

Figure 3.9: Inverted domain pattern in lithium niobate after etching under the microscope.
The period is around 18.5 µm.

e.   Cut and polish

In order to prepare a sample for characterization set-up, it is cut from the edge of poled channel perpendicular to channels by a diamond dicing saw. Then the input and output light interaction

faces are polished using a polishing machine and grain sheets. Four sizes of grain sheets as 30 μm, 6 μm, 1 μm, and 0.1 μm are used in polishing machine. Polishing is done for each grain size at the spin rate of 30 rpm in two directions of clockwise and anticlockwise approximately 10 minutes. The sample is sandwiched between two rectangular lithium niobate pieces and is placed in the holder of polishing machine to prevent breaking sample during polishing. The polishing reduces the scattering losses due to the coarseness of the surface to fresnel reflection (~14% on each surface).

CHAPTER 4   ARTICLE 1: ENGINEERING OF EFFECTIVE SECOND-ORDER NONLINEARITY IN UNIFORM AND CHIRPED GRATINGS

Ameneh Bostani,[1,*] Amirhossein Tehranchi,[2] and Raman Kashyap[1,2]

[1]Department of Engineering Physics, Ecole Polytechnique de Montreal, Montreal, QC, Canada, H3C 3A7

[2]Department of Electrical Engineering, Ecole Polytechnique de Montreal, Montreal, QC, Canada

[*]Corresponding author: bostani.ameneh@polymtl.ca

Overview

This paper demonstrates for the first time, how a mathematical apodization function can be implemented exactly in a nonlinear quasi-phase-matched grating. Previously for applying an apodization on a nonlinear grating, the change of duty cycle (ratio of poled to un-poled region) had been suggested. However, here in this article, we show that the position of poled regions within the pitches can affect the SHG response in addition to duty ratio, through influencing of the phase of the generated SH electric field. The phase study of the SHG leads to proposing the proper design which improves the tolerance to fabrication errors. All results in this paper come from the theoretical calculations and numerical simulations. Experimental demonstration of this article is explained in Chapter 6 by fabrication of the apodized step-chirped grating. The result of this paper was also presented at nonlinear photonic conference 2012, in Colorado Spring.

The complete reference to the article:

A. Bostani, A. Tehranchi, and R. Kashyap, "Engineering of effective second-order nonlinearity in uniform and chirped gratings," *J. Opt. Soc. Am. B*, vol. 29, no. 10, pp. 2929–2934, Oct. 2012.

4.1   Abstract

The dependence of second harmonic generation (SHG) conversion efficiency resulting from the position of poled regions of the second-order nonlinearity in uniform and chirped gratings in

ferroelectric materials has been studied analytically and numerically. The displacement of the poled region's position from a specific location in second order nonlinear materials can introduce a wavelength shift in a uniform grating's second harmonic intensity peak and strongly influences the bandwidth and ripple in the harmonic conversion response of chirped gratings. We propose that the poled regions should be located at specific positions within the single period to minimize the ripples and achieve a desired nonlinearity function, also for significantly improving tolerance to fabrication errors.

4.2   Introduction

Quasi-phase-matched (QPM) gratings in the form of periodically poled ferroelectric crystals have been widely used for frequency conversion [65], [86]–[97]. Chirped QPM gratings have been utilized to achieve broadband conversion, e.g. in aperiodically poled lithium niobate (APPLN), for example in broadband second harmonic generation (SHG) [5], [98]–[101], however the conversion efficiency response suffers from ripples. These ripples cause the output of SH power to vary with wavelength and the use of optical equalizer for chirped PPLN is thus required [102]. The ripples on the SHG response have been shown to be reduced by applying apodization in periodically poled structures [7]. For applying apodization to gratings, a change of the effective nonlinear coefficient is required as a function of length. An apodization function is used to bring the effective second-order nonlinear coefficient to zero at the edges of the grating, thereby diminishing the side-lobes of a sinc-type response function in unchirped [103] as well as the ripples in chirped gratings [60]. In order to change the effective nonlinear coefficient along the grating, the duty cycle, i.e. the length ratio of positive and negative polarity region needs to be varied throughout the structure [59], [60]. In practice the apodized chirped structure has been used as a wavelength converter [59].However the experimental results still exhibit ripples that do not exist in theoretical simulation. The source of the ripple may be caused by errors in the fabrication [104] or in the engineering of apodized chirped grating. Indeed, these could be minimized by choosing a design of grating which is less sensitive to fabrication errors. For realizing and minimizing errors in SH broadband intensity response, effective factors in apodization should be examined.

In this paper, we examine the dependence of SH intensity response, resulting from the effective second-order nonlinearity, on the physical location of the poled regions within each period of the

chirped gratings. Chirped gratings can be considered as an array of short uniform gratings each with a slightly different period. Thus, the study of short uniform gratings is also necessary to realize the impact of the position of the poled space on its transfer function. In the following sections, first, three different schemes are assumed and analyzed to determine how as a moving frame, the poled region in a pitch, affects the SH intensity in a generalized periodically poled material. Three structures based on the arrangement of several pitches (or cells) obeying the proposed schemes are studied analytically. Second, the simulation results of the SHG intensity response for uniform and chirped gratings with assumed structures in lithium niobate are presented. Altering the location of the poled (mark) space from a specific position leads to a frequency shift in a uniform grating depending on the symmetry of the function. In a chirped grating, changing the place of mark space strongly influences the profile of SH intensity versus wavelength. Finally, we propose a proper grating design to obtain an exact SH response for a desired nonlinearity function.

4.3 Theory

The coupled wave equations for SHG in a crystal can be written for a grating by introducing *d(z)* as:

$$
\frac{dA_1}{dz} = \frac{2j\omega_1^2 d(z)}{n_1 c} A_2 A_1^* e^{-j\Delta kz}
$$

$$
\frac{dA_2}{dz} = \frac{2j\omega_2^2 d(z)}{n_2 c} A_1^2 e^{j\Delta kz}.
$$

4.1

where A_1 and A_2 are the fields of fundamental harmonic (FH) and second harmonic (SH), and $\Delta k = k_{2\omega} - 2k_\omega$ represents the wave vector mismatch between the SH and FH. c is the speed of light, $\omega_{1,2}$ and $n_{1,2}$ are the angular frequency and refractive index of FH and SH field. $d(z) = d_a(z) f_{ap}(z)$ is the nonlinearity function in the length of grating where d_a is the modulation of nonlinearity which can possess only the positive and negative states of a constant nonlinear coefficient in ferroelectrics, and f_{ap} is the desired apodization function. In order to examine the dependence of the SH intensity on the position of the poled region, one cell of grating is

considered which includes just one positive and one negative poled region with the total length of $\Lambda = 2\pi/(k_{2\omega} - 2k_{\omega})$, which is also the period for the 1-st order quasi-phase matching.

For a non-depleted pump, the SH field is calculated by integrating over the length of Λ in the second equation of Eq.4.1. The duty cycle in one cell is considered as a parameter in Eq.4.1 to find the required duty cycle for getting the desired nonlinearity in SHG. Integrating over one cell, putting $\dfrac{2j\omega_2^2 d_a}{n_2 c} A_1^2 = D$ and considering the duty cycle as a variable, the SH electric field can be written as $A_2/D = \displaystyle\int_0^{C-a\Lambda/2} e^{-i\Delta kz}dz - \int_{C-a\Lambda/2}^{C+a\Lambda/2} e^{-i\Delta kz}dz + \int_{C+a\Lambda/2}^{\Lambda} e^{-i\Delta kz}dz$. C represents the poled region center, which can move from $a\Lambda/2$ to $\Lambda - a\Lambda/2$ by considering the poled region as a frame, and moving from right to the left of the cell. The SH intensity in frequency of 2ω is proportional to $\sin(\pi a)^2$ for all allowed values of C and the duty cycle can be obtained by $a = \arcsin(d)/\pi$, but the phase in the SH electric field varies from $-i\Delta ka\Lambda/2$ to $i\Delta ka\Lambda/2$ linearly with changing of C from right to the left and it is eliminated when it is placed in the middle of the cell. To apply the desired apodization function f_{ap}, the duty cycle should change as $a(z)$, however the position of poled region should also be determined.

In order to examine how the moving of the mark space frame can influence the SH output, three positions are assumed as shown in Figure 4.1. They are named cell Scheme I, II and III if the poled regions are placed in the right (maximum negative phase), center (zero phase) and left (maximum positive phase) of the cell, respectively. Based on Schemes I, II and III incorporating several cells with specific poled positions, the three considered structures are called Structure I, II and III.
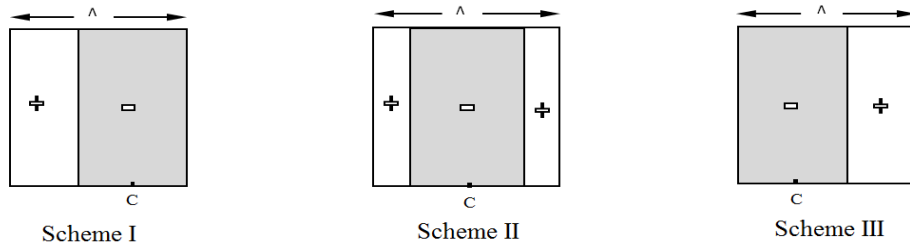
Figure 4.1. Three supposed schemes when the poled region is in the right (Scheme I), middle (Scheme II) and left (Scheme III) of a cell. C is the center of space region.

The second harmonic electric field produced by apodized Structure I for the function f_{ap} can be written as:

$$A_2 / D = \frac{1}{\Delta k}\left(\sum_{i=0}^{N-1} 4\sin(\Delta k a_i L / 2)e^{-i\Delta k L(i+a_i/2)}\right) - \frac{2}{\Delta k}\sin(\Delta k L / 2)e^{-i\Delta k L/2}) \qquad 4.2$$

where L is twice the coherence length for the phase matched wavelength and a_i is the duty cycle. N is the number of cells. For apodized Structure III, the phase in the first term of Eq.4.2 changes to $\exp(-i\Delta k \Lambda(i+1-a_i/2))$. However for Structure II the SH electric field for the apodized device is calculated by:

$$A_2 / D = \frac{1}{\Delta k}\left(\sum_{i=0}^{N-1} 4\sin(\Delta k L(1-a_i)/2)e^{-i\Delta k L(i+1/2)}\right) - \frac{2}{\Delta k}\sin(\Delta k NL / 2)e^{-i\Delta k NL/2}) \qquad 4.3$$

The phase of electric field in Structure II is independent of the duty cycle a_i and its amplitude just for the specific frequency of ω which satisfies the phase matching condition $(\Delta k L = 0)$ is the same as other structures.

In chirped gratings, the length of nth period changes as $\Lambda_n = \Lambda + (n-1)\delta$ where the δ is the length difference for the neighboring cell. Therefore, the phase of the electric field, similar to the uniform grating for Structure I and III remain dependent and for Structure II it is independent of the duty cycle. The SH electric field in the chirped gratings for Structure II varies as:

$$A_2 / D = \frac{1}{\Delta k}(\sum_{n} 4\sin(\Delta k(L - a_{n-1}(L+n-1)\delta)/2)e^{-i\Delta k[(n-1)(L+\delta)+L/2)]} \qquad 4.4$$
$$-2\sin(\Delta k NL/2)e^{-i\Delta k(LN+(N-1)\delta/2} + 4\sin(\Delta k L(1-a_0)/2)e^{-i\Delta k L/2})$$

where L is first pitch length. Positive and negative values of δ give increasing and decreasing period for chirped gratings, respectively.

The intensity, which includes multiples of each two terms of the electric field, is dependent on the duty-cycle difference for Structure I and III unlike Structure II. The dependence of SH intensity on duty cycle difference in various structures influences the SHG intensity response. In

the two next sections, the effect of this dependence in the three proposed structures is studied for uniform gratings with a small number of cells and chirped gratings.

4.4 The case of apodized uniform gratings

If in the uniform grating with a period of Λ, the mark space frame moves from left to the right in all cells, it results in a maximum intensity at different wavelengths. The wavelength shift of SH intensity from the phase matched wavelength (λ_0) for the period of Λ, is shown in terms of a relative wavelength shift in Figure 4.2(a) for different number of cells.

(a)   (b)
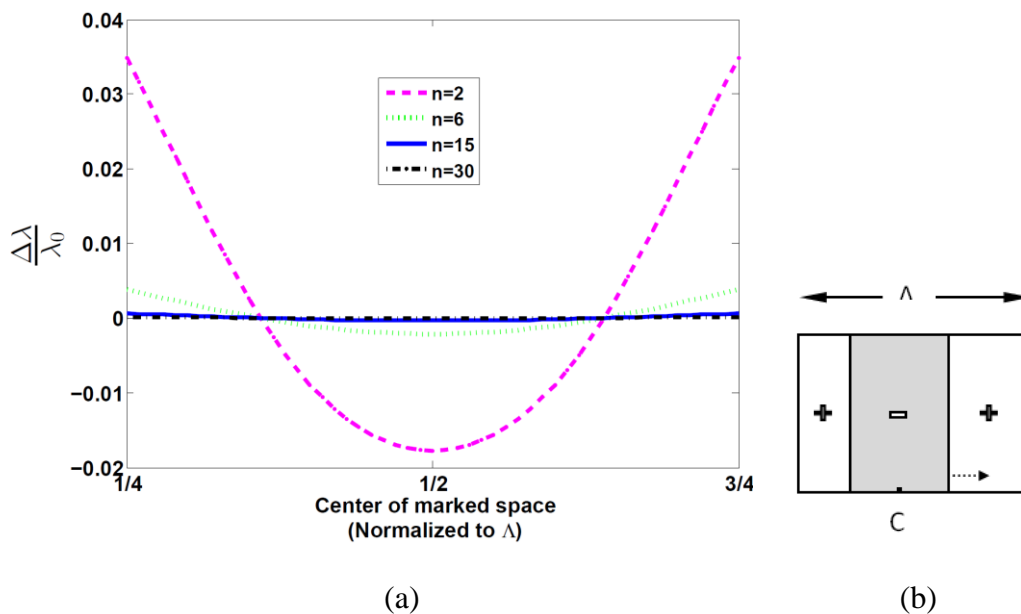
Figure 4.2 a) Effect of moving poled mark space with a duty cycle of 1/2 on the wavelength shift from left to the right side according to b) in which, C, the central poled region changes from Λ/4 to 3Λ/4.

Based on Figure 4.2(a) for a small number of cells, the maximum intensity deviates from the phase matched wavelength (λ_0) due to a movement of the poled mark space. However for a large number of cells (>30) it is not affected significantly. Since the duty cycle is constant throughout the crystal, the movement of the poled region just changes the first and last cell in the structures.

Therefore, by increasing the number of cells it has almost no impact on SHG intensity. If the duty cycle and consequently the effective nonlinearity changes, depending on the function of the nonlinearity (f_{ap}), a shift in the peak intensity can be observed.

The relative wavelength shifts for the intensity peak vs. cell numbers are shown in Figure 4.3 for the three introduced Structures in the previous section. The nonlinearity changes as the functions are shown in the insets of the figures. Figure 4.3(a) shows the wavelength shift of the intensity peak for an applied asymmetric nonlinearity function of 1/4 cycle of a sine function, which changes from zero to a maximum. This shift is reduced by increasing the number of cells and becomes constant for a large number of cells. The maximum intensity shifts to longer wavelengths in Structure I and to shorter wavelengths in Structure III relative to the primary phase matching wavelength (λ_0). The minimum wavelength shift occurs when Structure II is used.
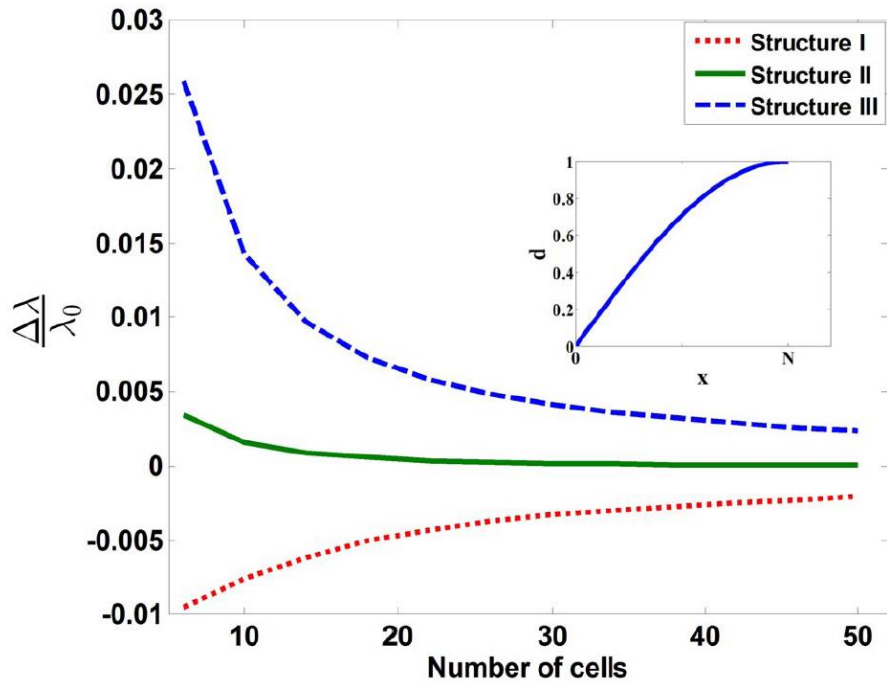
(a)
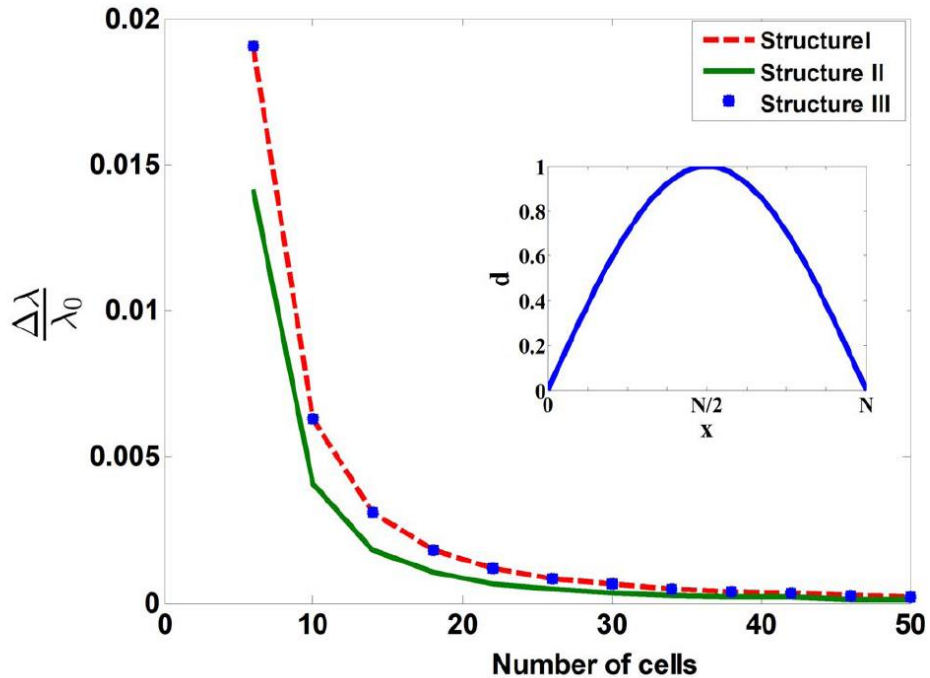
(b)

Figure 4.3. Relative wavelength shift for the three supposed structures in uniform grating according to inset functions for change of nonlinearity as (a) asymmetric (b) symmetric.

In Figure 4.3(b) the relative wavelength shifts are shown for the ½ cycle sine function, which is symmetric. In this case, the wavelength shift disappears with increasing number of cells. The reason is that the shift produced in the first half of the crystal, is compensated in the second half. The responses of the Structures I and III are exactly the same but it is different compared to Structure II as a result of a different amplitude value in the electric field (Eq.4. 2 and Eq. 4.3). The deviation from a constant value for small numbers of cells (<20 cell in the plot) is due to the jump of the value of the duty cycle and the reduction of precision in the applied apodization function.

The observed wavelength shifts in Figure 4.3(a) are caused by an accumulation of different electric field phases from every cell. The intensity includes multiples of every pair terms of the electric fields in the summation shown in Eqs. 4.2 and 4.3. In these multiplications, the phase difference of every pair appears in terms of cosines. These phases do not depend on duty cycle in Structures II unlike Structure I and III, in which the duty cycles are variable in the crystal length

due to the change of nonlinearity. In Structure II the phase is just a function of $\Delta k\Lambda$, therefore there is no phase accumulation reliant on the duty cycle differences in this structure.

If a symmetric apodization function is applied to a uniform grating, there is no difference in the transfer function of SHG for the location of the mark space. However, according to our results, for an asymmetric function, the position of mark space can introduce a wavelength shift in the intensity output. On the contrary, in chirped gratings another variable, the pitch length, is a contributing factor, which may lead to a different result. The change of SH intensity by applying an apodizing nonlinearity function in chirped gratings is examined in the next section.

4.5   The case of apodized chirped gratings

In this section, the SH intensity in apodized chirped gratings of different lengths are simulated considering the three previous structures, which represent the movement of the mark space frame. In Figure 4.4(a) the normalized SH intensity versus (FH) wavelengths centered at 1535 nm is plotted for unapodized and apodized linearly chirped grating (LCG) using the three proposed structures with applied apodized sine functions shown in the inset. The lengths of the first and last pitches are 18.97 μm and 18.22 μm, respectively to achieve a bandwidth of 25 nm in an approximately 1-cm-long poled lithium niobate crystal with 500 cells. The intensity is normalized to the maximum intensity for the unapodized grating. Apodized linearly chirped grating's (LCG's) plot represents the SH intensity for a desired sine function applied mathematically to an unapodized LCG, which results in an almost ripple-free response. The SH intensity responses for Structures I and III differ from that for the mathematically apodized LCG. There is lower (higher) intensity at the edges of the response and higher (lower) in the middle for Structure I (III) in comparison with the SH intensity for the apodized LCG and Structure II. Normalized ripples and bandwidths for different grating lengths are plotted in Figure 4.4(b). These plots are normalized to the mathematically apodized LCG. The ripple and bandwidth are almost the same for structure II and the apodized LCG, however, the ripple for Structures I and III increases considerably depending on the grating length. The bandwidth for Structure III is reduced by ~20% and increases ~10% for Structure I compared to that of the structures with apodized LCGs.
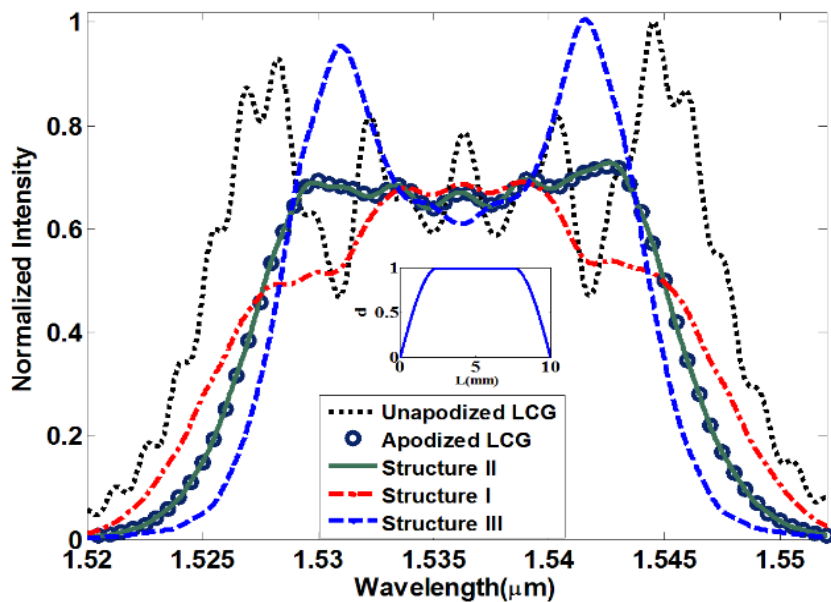
(a)
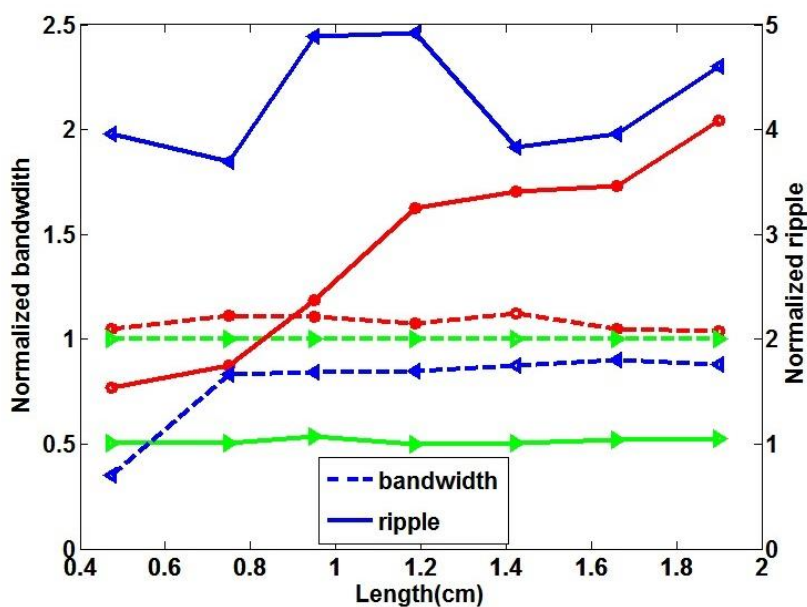
(b)

Figure 4.4. a) Normalized SH intensity response for 10-mm-long chirped APPLN crystal with different structure. b) Normalized bandwidth and ripple for structure I (red O), II (green>) and III (blue<).

Figure 4.4 demonstrates that positioning the poled region in the center of cells proposed by Structure II provides the best response for the required apodization function. This occurs because the position of the poled region within a period affects the overall SH intensity as both amplitude and phase of SH electric field change differently for the three proposed structures. The amplitude and phase can thus be controlled by the duty cycle, and the position of poled region, respectively. This explanation and result are not only applicable for the sine function and linear duty cycle changes, but also to other apodizing functions. For example, the intensity of the hyperbolic tangent apodized function is plotted in Figure 4.5(a). The "best" structure for the applied apodized function is related to structure II and its schematic is shown in Figure 4.5(b).

The positioning of poling in the center of cells eliminates the electric field phase dependence on the duty cycle as it is symmetric. Whatever position is chosen, except in Structure II, introduces a phase dependence on the duty cycle, when the effective nonlinearity is a function of position. The structure I and III can convert to each other by switching the direction of laser launch as the poled region changes from the right to the left side. Chirped gratings can be considered as many uniform gratings, each with a short length, with the period varying in each section. The wavelength shifts of the intensity peaks, arising from each uniform period short grating, interfere with each other and lead to a digression from the response of the mathematically applied function. Therefore, analytically and numerically it is concluded that using Structure II for apodization is the most desirable structure and gives the best match to the mathematically applied function to engineer the effective nonlinearity, and to achieve the flattest response. Furthermore, the simulation of similar structures in linear multilayer devices with modulated refractive indexes indicates that their reflection responses are sensitive to the positioning of the layers as well.
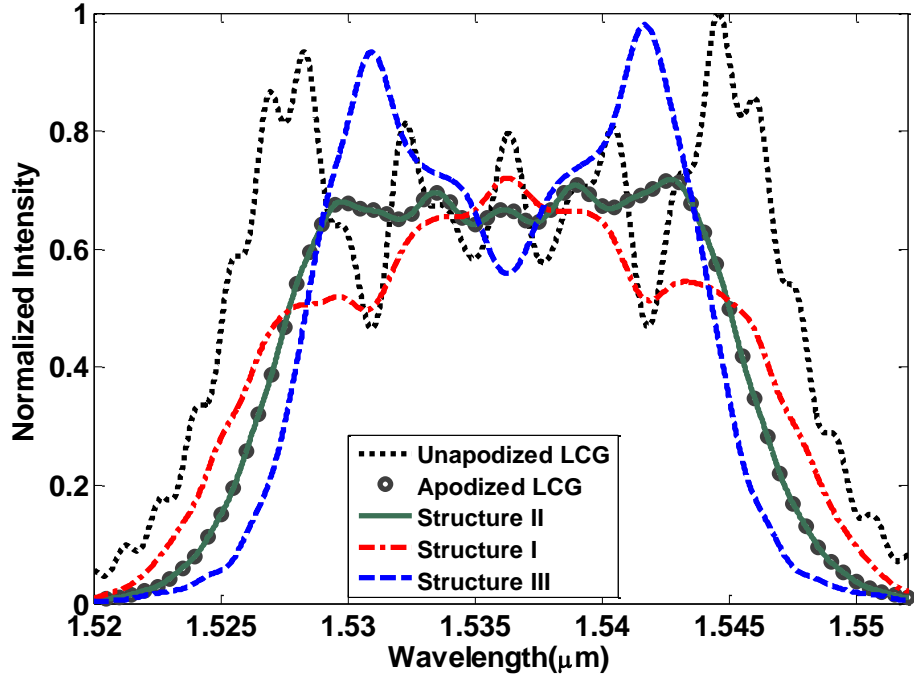
(a)
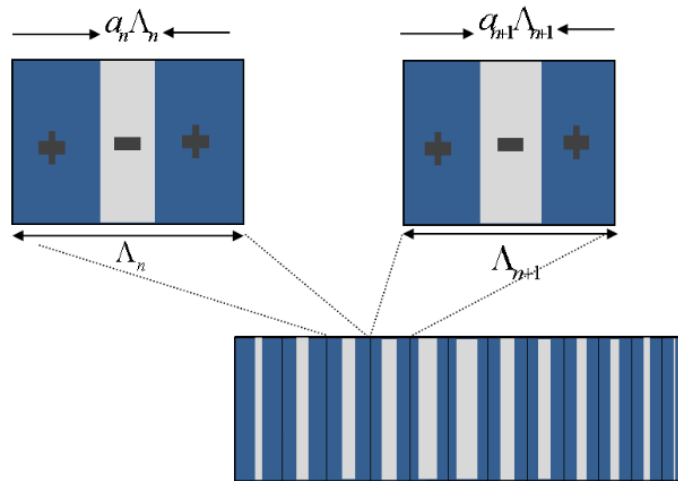
(b)

Figure 4.5.a) Normalized SH intensity versus the FH using hyperbolic tangent apodized function. b) Schematic of the proposed apodized chirped grating structures in APPLN composed of several cells. The middle un-poled (dark) space between nth and (n+1)th period changes as

$$(\Lambda + n\delta)(1 - \frac{a_n + a_{n+1}}{2}) + \frac{\delta}{2}(1 - a_{n+1})$$
.

4.6 Effect of domain error in proposed apodized chirped structure

In practice, the fabricated device may deviate from the designed device in the poling process or in the preparation of the mask. The errors degrade the intensity and flatness of SHG intensity response. Common errors such as broadening of poled regions or displacement of poled regions from the intended positions [105] is investigated for the best-proposed structure (Structure II). Figure 4.6 a) shows the effect of different errors. In certain cases, the domain boundary can shift from the ideal position without any change in the size of the periods or duty ratio. For this situation, with a 2-µm domain shift from the center of every cell to one side, the normalized SH intensity versus FH wavelength is plotted in Figure 4.6 (a) and is called error A. For Error A, since all poled regions shift together by 2 microns from the center in one direction to around 10% of the period, they never overlap. Normalization is kept the same as Figure 4.5 (a) for the SH response of unapodized LCG. The size of ripple with error A does not change significantly in Structure II. Furthermore, the width of poled regions may increase in the poling process. This broadening is considered in two cases of linear and random 12% broadening of poled region that can occur in the poling process [106]. For a 12 percent mark space broadening in each cell (Error B) and randomly varying between zero and 12% of the mark space ratio in poled regions (Error C), the ripples increase (0.35% of its average of minimum and maximum ripples) and the intensity shrinks while the shape of output still follows the response of ideal Structure II. For comparison with two other supposed structures, an error of 12 percent broadening in the duty ratio (Error B) is plotted in Figure 4.6 (b). This error introduces much larger ripples in Structure III and decreases the ripples in Structure I in comparison to its ideal structure. However, the errors in Structure I shrink the intensity significantly (around 30%) and the size of ripples increases to 52% of its average of ripples that is still more than Structure II. Even by considering the errors in fabrication, Structure II still results in a better SHG intensity response compared to the other two structures.
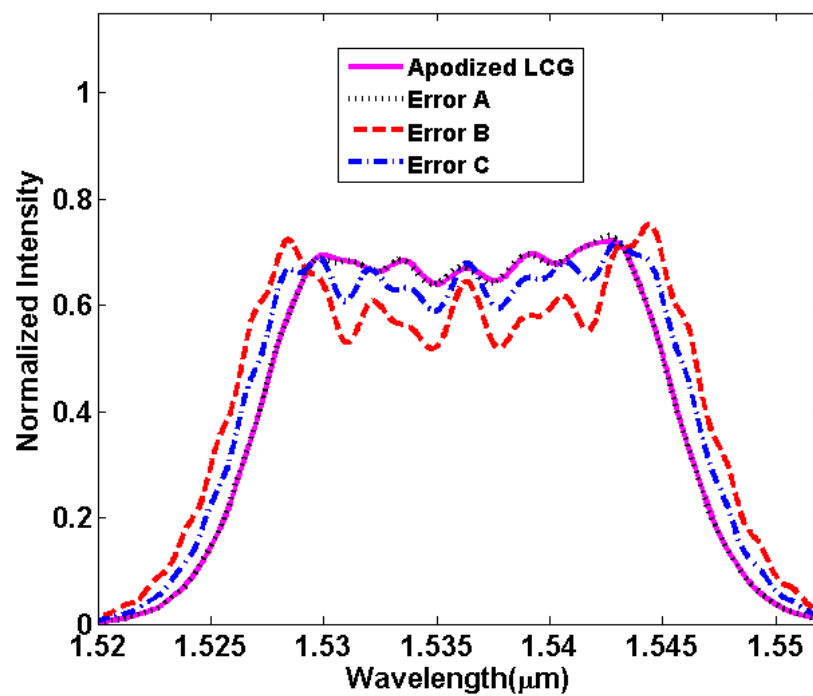
(a)
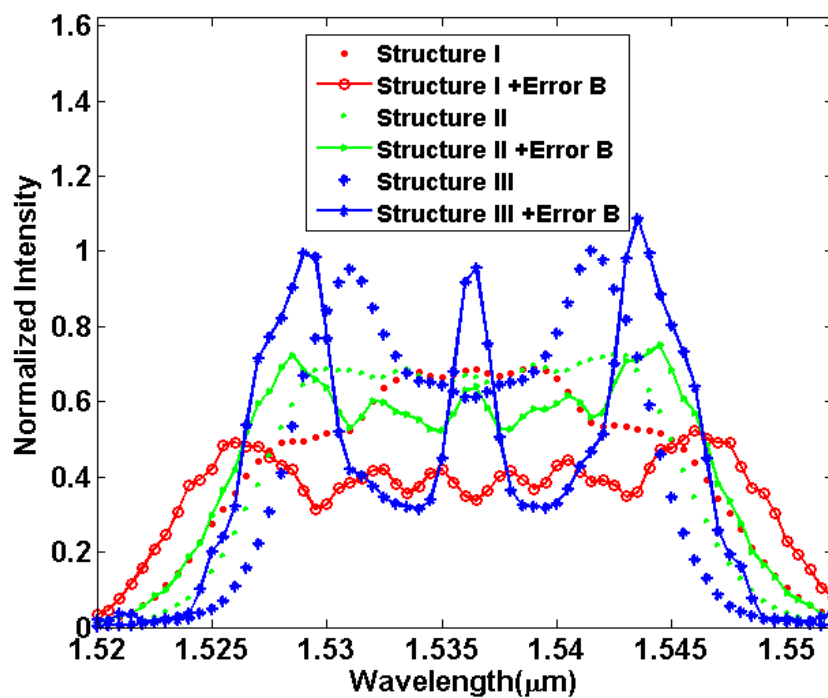
(b)

Figure 4.6. a) Influence of different types of errors in Structure II. b) Constant broadening errors in 3 different structures.

4.7   Conclusion

The dependence of the SH intensity on the location of poled regions in periodically and aperiodically poled crystals was theoretically analyzed to achieve the best structure for a desired nonlinearity function, we believe for the first time. It was shown that the SH response is dependent on the location of the poled region within the pitch, as the amplitude and phase of the SH electric field is controlled by the duty cycles and position of the poled regions, respectively. The simultaneous displacement of the poled regions (as a moving frame) from the center in all cells can lead to a wavelength shift in the intensity peak depending on the applied function and structures. In uniform gratings, the displacement of the poled mark space frame from the center of cells can lead to a wavelength shift for asymmetrical functions but it is insignificant for symmetric ones. In aperiodic gratings, this movement leads to increased ripples in the SH intensity response as a function of wavelength, especially at the bandwidth edges. For a required nonlinear function, Structure II, based on locating the poled region in the center of cells, is recommended since it has the closest response to the desired theoretical function. Simulations show that other structures diverge from the desired mathematical function. These results show that in periodically poled devices, positioning the poling region appropriately within the pitch can dramatically improve the SH transfer function of the structure, and should lead to better device performance, significantly increasing tolerance to fabrication errors. This result is applicable (extendable) to periodic linear refractive index or phase modulated structures and their reflection response as well.

CHAPTER 5   ARTICLE 2: TAILORING AND TUNING OF THE BROADBAND SPECTRUM OF A STEP-CHIRPED GRATING BASED FREQUENCY DOUBLER USING TIGHTLY-FOCUSED GAUSSIAN BEAMS

Ameneh Bostani,[1*] Meenu Ahlawat,[1] Amirhossein Tehranchi,[2,3] Roberto Morandotti [3] and Raman Kashyap[1,2]

[1] Dept. of Engineering Physics, Ecole Polytechnique de Montreal, Montreal, QC, H3C 3A7, Canada

[2]Dept. of Electrical Engineering, Ecole Polytechnique de Montreal, Montreal, QC, H3C 3A7, Canada

[3]INRS-EMT, 1650 Boulevard Lionel Boulet, Varennes, QC, J3X 1S2, Canada

Overview

In the previous chapter, we demonstrated applying apodization on a device using a proper design. Here in this chapter, we propose a different method for apodization. We suggest apodization by applying a shaped input beam such as tightly-focused beam into an un-apodized chirped device. In this case, the SH response of the un-apodized chirped grating can be controlled by changing the focusing condition in the set-up instead of fabricating an apodized chirped grating. We experimentally prove our proposal including the characterization of the SH response of the step-chirped grating, fabricated in our laboratory, using different degrees of beam focusing. The results of the work was also presented in CLEO 2013, San Jose, USA; and Nonlinear Optics 2013, Hawaii, USA.

The complete reference to the article:

A. Bostani, M. Ahlawat, A. Tehranchi, R. Morandotti, and R. Kashyap, "Tailoring and tuning of the broadband spectrum of a step-chirped grating based frequency doubler using tightly-focused Gaussian beams," *Opt. Express*, vol. 21, no. 24, pp. 29847–29853, 2013.

5.1   Abstract

We demonstrate theoretically and experimentally, that the non-uniform spectra of second harmonic generation (SHG) from an unapodized step-chirped periodically poled nonlinear optical grating can be apodized utilizing tightly-focused Gaussian beams to suppress the ripple in its wideband response. In our example, by increasing focusing, a ripple-free response is progressively achieved over a 6-dB bandwidth of >5nm, with a beam waist of 20 µm. With this tight focusing arrangement, a continuous tuning of 11-nm is also demonstrated by simply changing the focal point by 5.8 mm within the step-chirped grating based APPLN.

5.2   Introduction

Ultrafast optical signal processing based on cascaded second-order nonlinearities requires a broadband frequency doubler to perform waveband wavelength conversion [102], [107]–[111]. A good candidate for this purpose is quasi-phase matched second-harmonic generation (SHG) in poled crystals [65], [89] . As a uniform, periodically poled material has a narrow bandwidth, chirped gratings [5] and step-chirped gratings [7], [101]in the form of aperiodically poled material on the other hand, have been proposed to realize a broad bandwidth for SHG. However the SH response of these devices suffers from a highly non-uniform spectral response. Therefore, apodization techniques are applied during fabrication to minimize the ripples in the SH spectrum [7], [101], [112]. These methods are based on altering the effective nonlinearity to zero progressively by decreasing the duty cycle, i.e., the length ratio of positively and negatively poled regions, at the edges of chirped device [7], [112], [113]. Applying this kind of apodization with the fabrication of extremely fine-poled regions requires very precise and advanced equipment. To reduce the ripples, we suggest a new scheme for introducing some apodization, by launching tightly focused light into a step-chirped (SC) aperiodically poled material such as lithium niobate and controlling the wavelength range of the spectrum by moving its focal point inside the device.

The role of a focused light beam for frequency mixing for SHG in a nonlinear crystal [17], [18], [114] and in periodic structures, in particular PPLN, has been investigated theoretically and experimentally to determine the optimum focusing conditions [45], [46], [115]. Using a tighter focus in a periodic structure induces a Gouy phase shift [115], which reduces the maximum efficiency in comparison with a plane wave. Also a new design has been suggested to correct this

phase in the periodic structure [45]. The effect of adding chirp and Gouy phase shift compensator to a periodic structure has been studied using local phase mismatch in chirped and uniform structures for a Gaussian beam in order to find an optimum chirp rate to maximize efficiency [48]. The dependence of SHG on the focusing position has also been investigated in non periodically poled nonlinear crystals indicating that the maximum power is not generally yielded in the central focal point [20]. However, the effect of focusing and the focal position in the crystal have not been investigated to the best of our knowledge, in a chirped structure for frequency doubling. Of course, this applies to the generalized case of frequency mixing as well.

In this paper, in section 2, we discuss the theory of Gaussian beams for engineering the SHG response, which is used in our simulations. In section 3, the special design and fabrication of a wideband frequency doubler in the form of an unapodized step-chirped (SC) aperiodically poled lithium niobate (APPLN) are described. In section 4 we demonstrate the possibility of control over the SH efficiency of an unapodized SC-APPLN for different fundamental harmonic (FH) wavelengths obtained by focusing the FH pump to different beam waists. This allows us to engineer the conversion efficiency profile. In section 5 we examine the influence of shifting the focal point within the SC-APPLN to tune the spectrum of the SHG response. The experimental results are also compared with the theoretical simulations.

5.3   Theory

The coupled wave equations for SHG in chirped gratings can be written as [5]

$$\frac{dA_1}{dz} = \frac{2j\omega_1^2 d(z)}{n_1 c} A_2 A_1^* e^{-j\Delta kz}$$

$$\frac{dA_2}{dz} = \frac{2j\omega_2^2 d(z)}{n_2 c} A_1^2 e^{j\Delta kz}$$

5.1

where A_1 and A_2 are the fields of FH and second harmonic (SH) which are perpendicular to propagation direction (z), $\Delta k = k_{2\omega} - 2k_{\omega}$ is the phase mismatch between the SH and FH. c is the speed of light, $\omega_{1,2}$, $n_{1,2}$ and $k_{1,2}$ are the angular frequencies, refractive indexes and wave numbers of FH and SH field. $d(z) = f_{ap}(z)d_{chirped}$ is the nonlinearity of structure composed of two terms of apodization (f_{ap}) and chirping (dchirped). An apodization function is used to bring the effective second order nonlinear coefficient to zero at the edges of the grating, thereby diminishing the side

lobes of a sinc-type response function in unchirped gratings as well as the ripples in chirped gratings [7], [101]. Chirped structures have a monotonically variable period to cover all required periods for broadband SHG. The step-chirped grating consists sections, each of uniform gratings with different periods. The period in the i'th section changes as

$$\Lambda_i = \Lambda_1 + (i-1)\Delta,$$

5.2

Where Λ_1 is the period of first section and Δ represents the period difference between two successive sections.

When a laser beam is focused in the crystal, the electric field contribution using a first order approximation of electric field component results in [116]

$$E_{1y}(z) = \frac{E_0}{1+i\zeta} \exp(-\frac{x^2+y^2}{\omega_0^2(1+i\zeta)})e^{(ikz)},$$

5.3

where $\zeta = 2(z-f)/b$ where f is the focal position and $b = 2\pi\omega_0^2 n_1 / \lambda_1$ is the confocal parameter. ω_0, λ_1 and E_0 are beam waist and FH wavelength and initial electric field ($|E(0)|$), respectively. Considering the variation in the non-depleted case, the total SH field contribution at the observation point (r', z') outside the crystal can be written as

$$E_2(r', z') = \frac{ik_2 E_0}{4n_2} \exp(-\frac{2(x^2+y^2)}{\omega_0^2(1+i\zeta')}) \int \left[\frac{d(z)}{1+i\zeta(z)}\right] \exp(i\Delta kz)dz$$

5.4

where x, y, z are considered to be the coordinates of the source [17] . The first term in brackets can be considered as the total nonlinearity.

5.4   Design and fabrication

In order to design a wideband frequency doubler based on chirped gratings in PPLN with an SH efficiency centered at the FH wavelength of 1550 nm and possessing a bandwidth of 30 nm at a temperature of 125°C, the period of the device should change from 18.209 μm to 19.019 μm. The device covers SHG between 1535 nm and 1565 nm. However, achieving the resolution below

100 nm makes the mask fabrication for the photolithography process difficult and expensive. Therefore we designed an unapodized SC-APPLN considering this limitation and its schematic is shown in Figure 5.1(a). The total grating length (L) is divided into 10 equal sections with a varying periodic pattern. Using Eq. 2 with $\Lambda_1 = 18.2$ µm and $\Delta = 0.1$ µm, the last period is $\Lambda_{10} = 19.1$ µm. The device efficiency is then the power ratio of the output SH to input FH at any wavelength. The total length is engineered to be 20 mm, a compromise between the efficiency and the ripples. The uniform, 2-mm-long sections possess a 5-nm bandwidth which are short enough to produce a continuous 30-nm bandwidth with $< \sim 6$ dB peak-to-peak ripple.

Fabrication of the SC-APPLN is based on electric field poling at room temperature, a common technique used for the fabrication of QPM devices, especially for LN [106] . The $+z$ face of an undoped, 0.5-mm-thick, z-cut, optical grade lithium niobate crystals were used for the fabrication. The LN wafers were then coated with a 1.5 µm layer of positive photo-resist S1813 and exposed to 314 nm UV radiations through a specially designed SC grating pattern on the mask. After lithographic printing, the sample was mounted on a holder contacting both surfaces with saturated lithium chloride (LiCl) solutions as the electrolyte. A dc-electric field (22 kV/mm), higher than the coercive field strength of LN in the shape of pulses with duration of 0.5 ms were applied to the liquid electrode pattern until domain inversion is achieved in all grating regions. The in-situ monitoring of the poling process was made using a video camera through a crossed polarizer setup, observing the induced birefringence change between the poled and un-poled regions. The duty cycle and period of APPLN were examined under microscope after cleaning and etching in hydrofluoric acid (HF 49%). A microscope image of a section of the fabricated device is shown in Figure 5.1(b).

The domain broadening as a fabrication error in an SC-APPLN, unlike in uniform grating for which it reduces the efficiency, may change the shape of the spectrum and ripple heights if the broadening does not occur exactly the same in all sections. The response even could be better than perfectly fabricated one as the overall response comes from the phase accumulation of the SH electric field of every section. Our simulations indicate that if there is a random broadening in order of 20% of period, it does not influence the ripple height significantly.
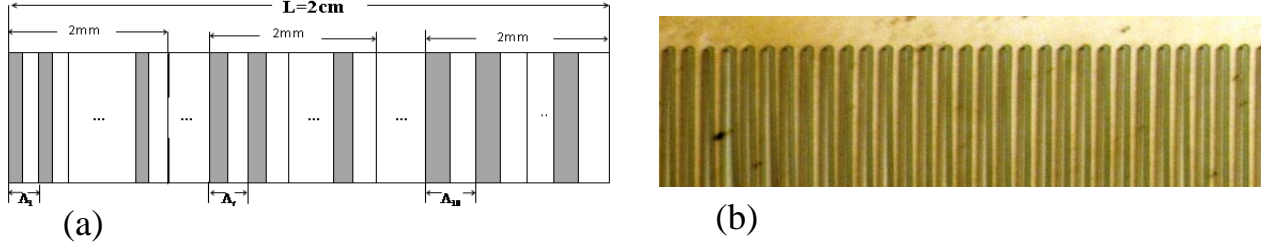
Figure 5.1.(a). Schematic of the designed SC-APPLN. (b) Part of the fabricated sample viewed under the microscope after etching.

5.5   SH Spectrum tailoring by focusing with different beam waists

In order to examine the effect of focusing on the wideband SH response of a step-chirped grating device, we simulated SHG with a Gaussian beam of different beam waists in the specially-designed SC-APPLN, and verified it experimentally.

In our theoretical simulations, the output power is calculated by integrating a Gaussian beam over the cross section as it changes along the length of a crystal. In the step-chirped gratings $d(z) = d_{chirped}(z)$ with focusing, part of the electric field variation can be translated to a change of the effective second-order nonlinearity and thus considered as an apodization term in the poled crystals as $f_{ap}(z) = 1/(1+i\zeta)$. This function is shown in Figure 5.2(a) for different beam waists (ω_0) of the focused light versus the length of crystal. In this plot, the focal position is considered to be in the middle of crystal; however, by changing this position the maximum in each graph changes to the point of the focus.

In the experimental setup, three different lenses (f = 5 cm, 7 cm, 12.5 cm) were used to achieve a focused beam waist of 20, 30 and 50 microns, respectively, in the center of the SC-APPLN. A JDSU tunable laser was used as the pump in the C-band, amplified by a Pritel high-power EDFA and passed through a polarization controller before being focused into the center of the SC-APPLN. The SC-APPLN sample was placed in a temperature-controlled oven at a fixed temperature of 125° C to avoid thermal damage. The output FH and SH waves were evaluated using an optical spectrum analyzer and a power meter. For an input pump power, P_p = 0.66 W, the experimentally observed peak power is ~0.21 mW which is in good agreement with the theoretical calculation P_{SHG} = 0.22 mW, resulting in an efficiency of −34.78 dB. The normalized

SHG efficiency versus FH wavelength is plotted in Figure 5.2(b-d) and compared with the simulation of a perfect SC-APPLN structure. We found, somewhat surprisingly, that the efficiency profiles for various beam waists change dramatically due to the apodization resulting from focusing. The ripple on the 6-dB bandwidth of the response reduces significantly with a decreasing beam waist or with an increasing degree of focusing in both the simulation and the experiment. A 6-dB bandwidth in an SC-APPLN for beam waists of 50, 30 and 20 µm, according to the theory are 14 nm, 8 nm and 7 nm, compared to the experimental data which are 25 nm, 7.5 nm and 5 nm, respectively, in reasonably good agreement with the simulations. The bandwidth difference in loose focusing is due to the existence of large ripples in the theoretical SHG efficiency which decreases in practice by random phase accumulation in imperfect devices. Further, there is a ripple-free response (for both theory and experiment) using a tightly-focused beam ($\omega 0 = 20\mu m$) within the 6-dB bandwidth. Thus, the use of focused light as a novel apodization technique can increase the tolerance in fabrication for apodized SC-APPLN.
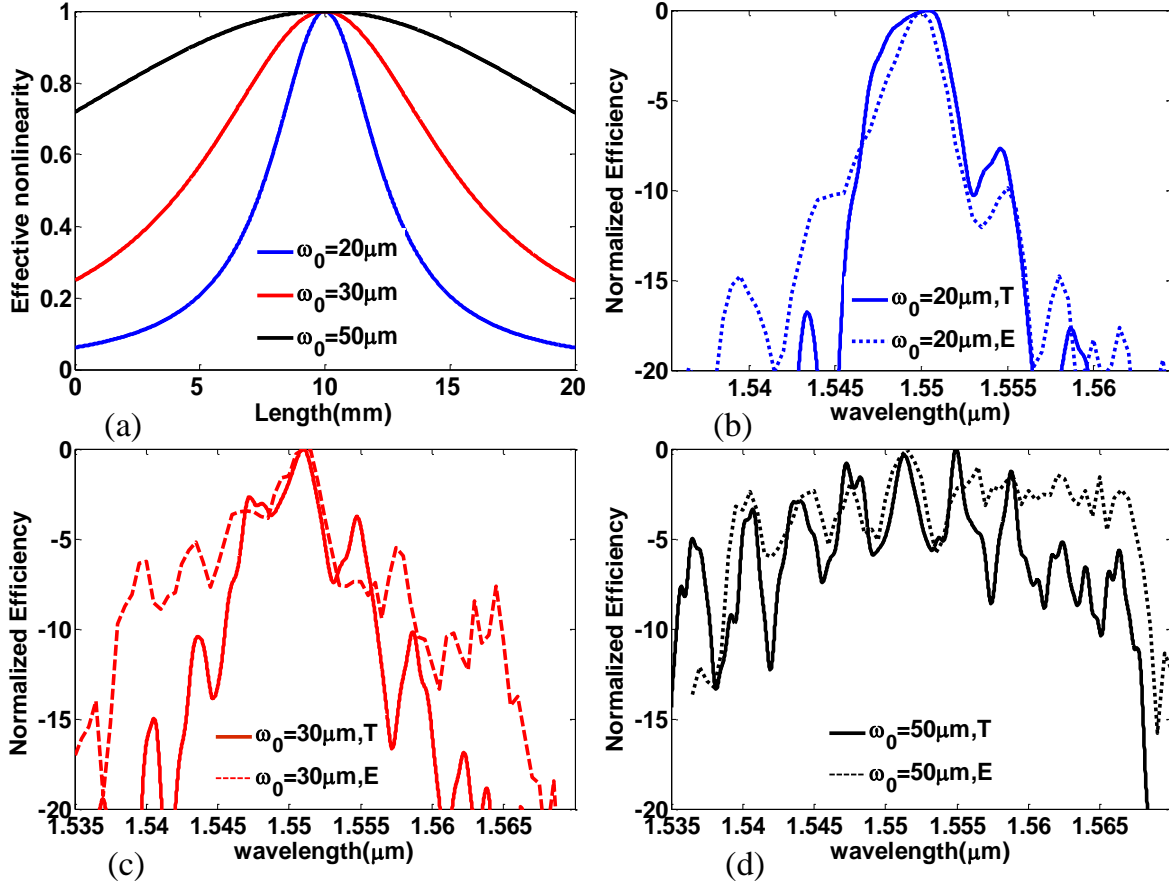
Figure 5.2. a) Normalized effective second-order nonlinearity vs. grating length as a function of focused beam waist and b-d) Normalized measured and simulated SHG efficiency vs. FH wavelength, for a focused light with different beam waists. In the legend "T" and "E" represent theoretical and experimental result, respectively.

5.6   SH spectrum tuning by changing the focal point in the grating

When the light is focused in a specific point in the SC-APPLN with a particular period, the intensity in its Rayleigh range is increased significantly and raises the efficiency in that regime by a factor of 2 [5]. The confocal parameter is 1.62 mm for a beam waist of 20 microns and less than the length of one section of the fixed period grating section. Therefore, it is expected that the efficiency will be improved within the bandwidth; however, as the intensity decreases rapidly out of the Rayleigh range for a tight focusing, the bandwidth is also reduced with respect to the bandwidth of full chirped grating. To convert other wavelengths available within the bandwidth of the SC-APPLN, one can simply change the focal point in the device. Here we swept the focal

point from ¼ to almost the middle of the crystal length using a translation stage and a fixed lens with a 5-cm focal length. The normalized measured and simulated SHG efficiency versus FH wavelengths are shown in Fig. 3 (a-d) for four different focusing positions. By varying the focal point by ~5.8 mm along the length of the broadband device, the spectrum and its peak wavelength can be tuned by ~11 nm. Therefore, 1 nm tuning is possible by a 0.52 mm position displacement. The tiny changes in the shape of SHG responses in Figure 5.3 (a-d) are due to the intrinsic non-smooth behavior of the fabricated SC-APPLN. This specially designed and fabricated device has the capacity to operate over its entire designed bandwidth. Again, the experimental results are in reasonable agreement with the experimental results. Note that the spectra remains essentially unchanged as the focal point is moved in the grating, evident fromFigure 5.3 (a)-(d), indicating that the apodization scheme by focusing works well even with tuning of the central SHG wavelength.
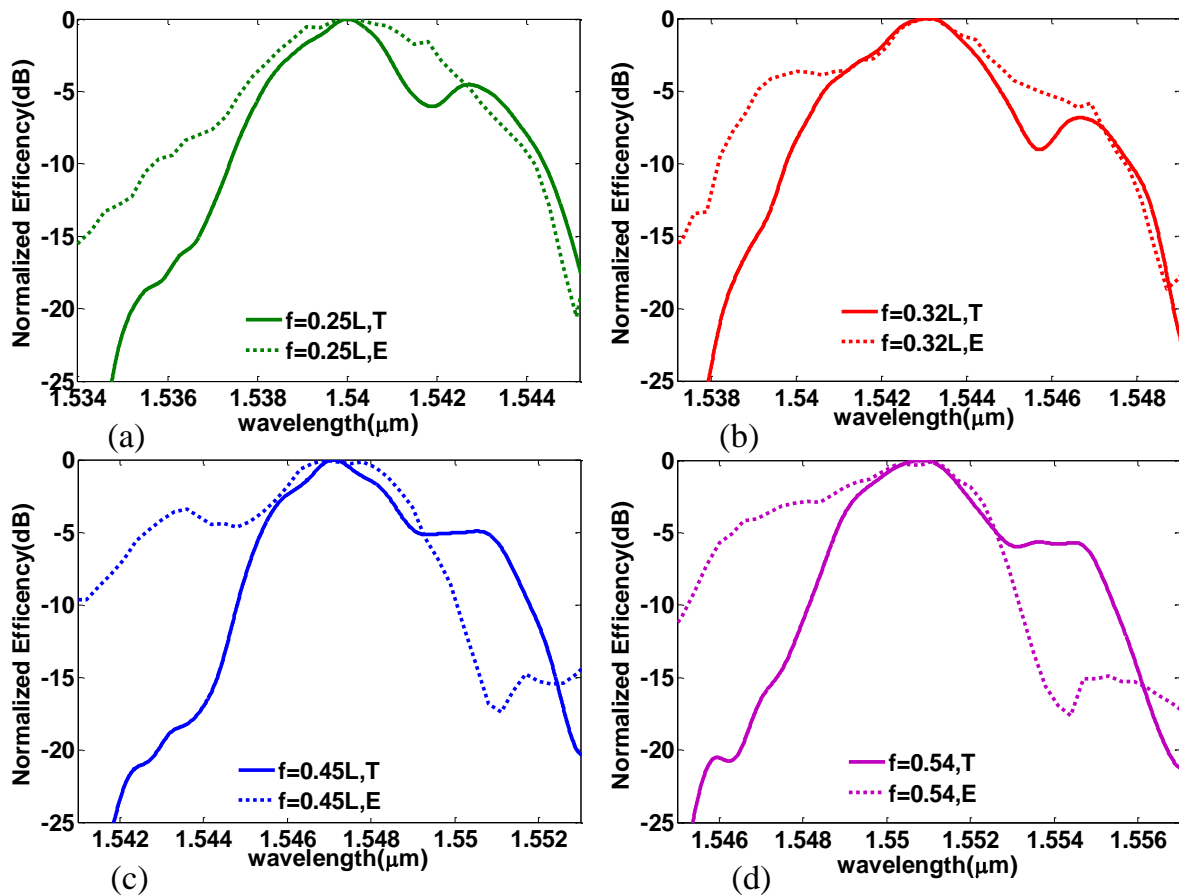
Figure 5.3. Normalized measured and simulated SHG efficiency vs. FH wavelength for focused light with a beam waist of 20 µm for four different focusing positions *f*, within the SC-APPLN device. In the legend "T" and "E" are theoretical and experimental data, respectively.

5.7   Conclusion

In summary, a broadband unapodized SC-APPLN was designed and carefully fabricated using a liquid-electrode poling scheme to obtain a maximum of 30-nm SHG bandwidth. The device efficiency was characterized using focused light with different beam waists. The tightly-focused Gaussian beam significantly affected the efficiency profile and suppressed the ripple in the wideband SHG response of the SC-APPLN. By increasing the degree of focusing, a ripple-free response is obtained, e.g., for a 6-dB bandwidth. For a tightly-focused beam with a beam waist of around 20 microns, the bandwidth in the unapodized SC-APPLN is >5 nm for both simulation and measurement. Furthermore, tuning the SHG spectrum over the entire SC-APPLN bandwidth is possible by displacing the focal point of the input beam inside the device. Tuning of the spectrum by 1 nm per 0.52 mm change of focal point was obtained using simulations and verified experimentally. Changing the point of focus in the crystal led to the realization of a temperature-independent tunable broadband frequency doubler, which can be used in agile multicasting of a signal via cascaded SHG and difference frequency generation (DFG) for the construction of flexible all-optical networks [108], or in the frequency doubling of high power tunable lasers, amongst other applications.

CHAPTER 6   ARTICLE 3: DESIGN, FABRICATION AND CHARACTERIZATION OF A SPECIALLY APODIZED CHIRPED GRATING FOR RECIPROCAL SECOND HARMONIC GENERATION

Ameneh Bostani,[1*] Meenu Ahlawat,[1] Amirhossein Tehranchi,[2,3] Roberto Morandotti,[3] and Raman Kashyap[1,2]

[1]Department of Engineering Physics, Ecole Polytechnique de Montreal, Montreal, QC, Canada, H3T1J4

[2]Department of Electrical Engineering, Ecole Polytechnique de Montreal, Montreal, QC, Canada, H3T1J4

[3]INRS-EMT, 1650 Boulevard Lionel Boulet, Varennes, QC, Canada, J3X 1S2

[*]Corresponding author: bostani.ameneh@polymtl.ca

Overview

This chapter presents the experimental demonstration of the proposed design in Chapter 4 for apodized chirped grating based on locating the poled regions in the center of pitches. In Chapter 4, the analysis and numerical simulation were done for a continuously chirped grating. Here, the device design is based on step-chirped grating which is feasible for fabrication. We experimentally realize the reciprocity of the SH response in the newly-proposed device.

This work was also presented in the OSA conference, Nonlinear Photonics 2014 in Barcelona, Spain.

The complete reference to the article:

A. Bostani, M. Ahlawat, A. Tehranchi, R. Morandotti, and R. Kashyap, "Design, fabrication and characterization of a specially apodized chirped grating for a reciprocal second harmonic generation," *Opt. Express*, vol. 23, no. 4, pp. 5183–5189, 2015.

6.1   Abstract

A specially-designed apodized chirped PPLN based on particular positioning of poled regions within the periods has been realized theoretically and experimentally to demonstrate the reciprocal response in the SHG spectra over a 30-nm bandwidth, for up-chirp and down-chirp directions. The simulation results are compared with another apodized chirped PPLN for which the placement of poled regions is deviated from optimum positions. The average power difference is less than 0.75 dB and the standard deviations of extrema on second harmonic power responses are 1.34 dB and 1.64 dB for two up-chirp and down-chirp directions respectively.

6.2   Introduction

All optical networks and ultrafast optical signal processing require broadband optical wavelength conversion which can be provided with engineered periodically poled nonlinear materials, using quasi phase-matching (QPM), due to their several advantages [102], [107], [108], [111], [117]–[124]. QPM has been widely used in uniform gratings such as periodically poled lithium niobate (PPLN) for narrowband frequency doubling [86], [91], [125], and in the form of chirped and step-chirped gratings for broadband frequency doubling using variation of period within the device continuously or in steps or nonlinearly [5], [126]. However, the chirped-one is available at a cost of lowered SH intensity compared to a uniform grating [5], [101], [126]. Apodized chirped grating devices have also been suggested [7], [59], [113], [127], [128] to reduce the conversion ripples in the spectral response of chirped devices employing a second-order nonlinearity profile that approaches zero at both ends of the grating. The apodized one also may further reduce the generated SH power of the chirped PPLN device. In order to compensate the loss of SH power, pump resonant devices may be used [101]which demand the use of a device with a reciprocal SH response, resulting in an identical spectral SH response as for a single-pass propagation of input pump in both directions in the apodized chirped PPLN (AC-PPLN). As the period changes in a linear chirped PPLN device, the two different directions of input pump propagation in the device can be defined as the up-chirp (period getting bigger with distance) and down-chirp (period getting smaller with distance) directions.

 In our recent work, we theoretically proposed a particular structure for the fabrication of an apodized chirped grating based on a desired apodization function on continuously chirped

gratings ignoring group-velocity mismatch between fundamental and second harmonic wave and considering un-depleted pump condition [128]. Since the second-order nonlinearity has just two polarization states, positive and negative, in practice, apodization in chirped PPLN can be achieved by changing the duty ratio, i.e. the length ratio of the positively and negatively poled regions within the pitch of the grating [59], [128]. In our proposed structure, the position of the poled region within the pitch should be in the center of each cell to arrive at a better performance, as it increases the tolerance to fabrication errors. Here, for convenience we call this proposed device "center-poled structure (CPS)". In practice due to fabrication limitation, the step-wise apodized chirped grating is suggested for which period and duty ratio change in sections and subsections instead of in every period. AC-PPLN based on CPS design which is still symmetric in each subsection can possess the reciprocity property in terms of having the same SH intensity response when the input light passes through both up-chirp and down-chirp directions. However, for "off-center-poled structure (OCPS)" the poled regions are placed in one side of cells. As OCPS is not symmetric in each subsection it can introduce extra phase in SH amplitude and present two different SH responses for up-chirp and down-chirp direction [128].

In this paper, we present the design, fabrication and characterization of our home-made AC-PPLN device (using CPS model) based on our proposal in the earlier work [128] for both the up-chirp and down-chirp directions in the same grating and experimentally demonstrate its reciprocity in its SH power response profile.

6.3   Theory and design

The coupled wave equations for second harmonic generation (SHG) in an apodized chirped grating can be written for a grating by introducing $d(z)$ as

$$\frac{dA_1}{dz} = \frac{2i\omega_1^2 d(z)}{n_1 c} A_2 A_1^* e^{-i\Delta kz}$$

$$\frac{dA_2}{dz} = \frac{2i\omega_2^2 d(z)}{n_2 c} A_1^2 e^{i\Delta kz},$$

6.1

where, A_1 and A_2 are the fields of fundamental harmonic (FH) and second harmonic (SH), and $\Delta k = k_{2\omega} - 2k_{\omega}$ represents the wave vector mismatch between the SH and FH. c is the speed of light, $\omega_{1,2}$ and $n_{1,2}$ are the angular frequency and refractive index of FH and SH field. is the nonlinearity function $d(z) = f_{ap}(z)d_{eff}M_{chirp}(z)$ in the length of grating where M_{chirp} is the modulation of nonlinearity which can possess only the positive and negative states of unit and d_{eff} is the effective nonlinear coefficient in ferroelectrics, and f_{ap} is the desired apodization function.

In order to introduce the importance of the position of the poled region in the apodized chirped grating we consider a unit cell with a length of Λ and the poled region of $a\Lambda$ where a is the duty ratio. For one cell, in non-depleted pump case, the SH field is calculated by integrating over the length of Λ in the second equation of Eq.6.1. Integrating over one cell, putting $\dfrac{2i\omega_2^2 d_{eff}}{n_2 c} A_1^2 = D$ and considering the duty cycle as a variable, the SH electric field can be written as

$$A_2 = D\left[\int_{0}^{C-a\Lambda/2} e^{i\Delta kz}dz - \int_{C-a\Lambda/2}^{C+a\Lambda/2} e^{i\Delta kz}dz + \int_{C+a\Lambda/2}^{\Lambda} e^{i\Delta kz}dz \right],$$ 6.2

where C represents the poled region center, which can move from $a\Lambda/2$ to $\Lambda - a\Lambda/2$ by considering the poled region as a frame, and moving from right to the left of the cell. The SH intensity in frequency of 2ω is proportional to $\sin(\pi a)^2$ for all allowed values of C and the duty cycle can be obtained in a structure by $a = \arcsin(f_{ap})/\pi$, but the phase of the SH electric field varies from $-i\Delta ka\Lambda/2$ to $+i\Delta ka\Lambda/2$ by changing C from the right to left and it is eliminated when it is placed in the middle of the cell as it remains symmetric. Therefore, the AC grating design based on laying several symmetrically apodized cells in each section, ie., CPS, does not introduce any additional phase in the SH electric field unlike any asymmetrically apodized sections using the off center positioning, ie., OCPS.

To design the grating mask which can be feasible for fabrication, we use a step-wise AC design including 10 sections for which the period changes in each section. The 3 sections at the beginning and at the end of the grating have 3 subsections with variable step-wise duty ratios. To observe how the displacement of poled region can affect the SH response theoretically, we

simulate two AC-PPLN devices, with CPS and OCPS. The periods change from 18.2 μm to 19.1 μm in steps of 0.1 μm to cover a 30-nm bandwidth. Considering $f_{ap}(z) = \sin(z)$ the duty ratio should change linearly. In our design, we applied the step-wise apodization function on half of the device. Therefore, the duty ratio is changed step-wise in first three and last three sections. Due to fabrication limitation, the duty ratio begins at 0.18 in the first subsection and increases to 0.5 in 9 steps in the last subsection of the 3rd section. It is reversed symmetrically for last 9 subsections at the end of the grating as well. The schematic of our design is shown in Figure 6.1. While the period Λ remains constant in each section, the duty ratio may change in each subsection. The difference between the CPS and OCPS model, is the placement of poled regions in each apodized subsections.

In CPS design, as there is no additional phase from sections we expect reciprocal property. However, in OCPS model depending on the placement of poled regions different phases can add up. Phase interference from these 18 subsections (9 in beginning and 9 at the end) of OCPS influences the SH response and make it different for up-chirp and down-chirp resulting in a non-reciprocal device. This difference can be smaller compared with that of the continuous apodized chirped grating with many cells [128] due to fewer numbers of sections. Reciprocity of this device can be investigated theoretically by changing the periods for the up-chirp to down-chirp gratings and mirroring the poled region location with regard to the center of each cell and experimentally, by reversing the direction of input FH light.
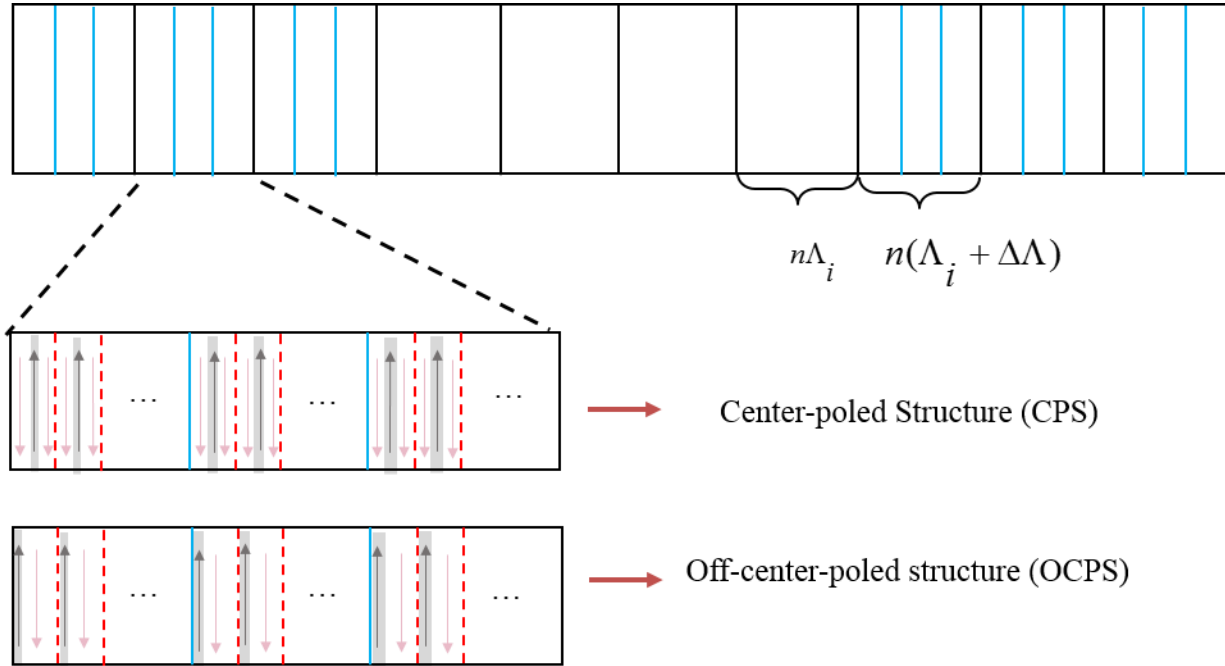
Figure 6.1. Schematic of apodized step-chirped grating, using CPS & OCPS design. The 10 sections and 18 subsections are divided by black and blue line, respectively. n is the number of periods in each section. Periods are separated by red dash line. Gray area with black arrow shows the domain-inverted region within each period while the white area with pink arrow shows the region with natural domain.

6.4   Fabrication and characterization

We have fabricated a 15-mm-long CPS-AC-PPLN based on electric field poling at room temperature, a common technique used for the fabrication of QPM devices, especially for LN [106], [129]. The +z faces of undoped, 0.5-mm-thick, z-cut, optical grade lithium niobate crystals were used. The LN wafers are then coated with 1.5 μm layer of positive photoresist S1813 and exposed to 314 nm UV radiation through the specially designed AC grating pattern on the mask. After lithographic printing, the sample was mounted on a holder contacting both surfaces with saturated lithium chloride (LiCl) solution as the electrolyte. A dc electric field (22 kV/mm) higher than coercive field strength of LN in the shape of pulses with duration of 0.5 ms were applied to the liquid electrode pattern until the domain inversion is achieved in all grating regions

In order to characterize the SH intensity response of our AC-PPLN device for two up-chirp and down-chirp directions while the beam passes the same path in the grating channel, we used a

symmetric set-up as shown in Figure 6.2. A JDSU tunable laser was used as a pump signal in the C band. It was amplified using a high-power EDFA connected to a polarization controller, the light from the fiber is collimated with a spherical lens and is then focused into the center of the AC-PPLN. A lens with the focal length of 12.5 cm is used to make a roughly parallel beam through the device which is placed in a temperature-controlled oven at a fixed temperature of 125 °C. The SH power is evaluated using a power meter and spectrum analyzer after collimation and coupling into the fiber.

(a)

(b)   (c)
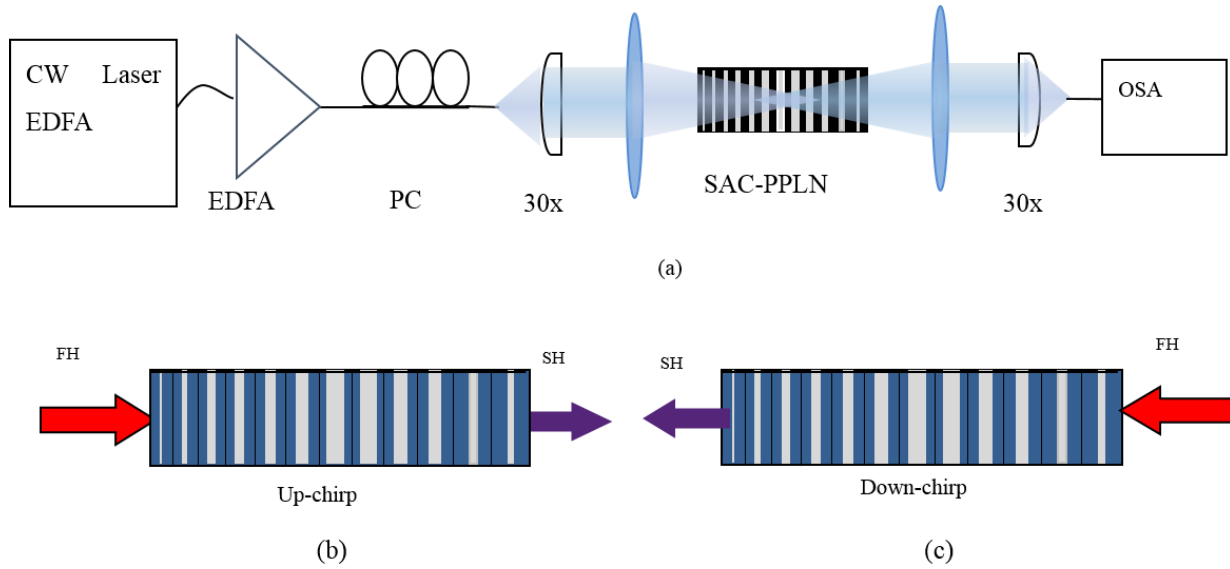
Figure 6.2.a) Experimental setup to evaluate SH response reciprocity with a CW pump laser, EDFA: Erbium-doped fiber amplifier, PC: Polarization Controller and OSA: Optical Spectrum Analyzer. An AC-PPLN device is mounted on a temperature-controlled oven. b) up-chirp and (c) down-chirp configurations, when the input and output fiber is interchanged.

The maximum SH power generated for each section of an *m*-section SC-PPLN with the length *l*, in the plane wave approximation can be calculated using

$$P_{SHG} = \frac{8\pi d_{eff}^2 P_p^2}{\varepsilon_0 c n_p^2 n_{SH} \lambda_p^2 \omega_f^2} (\frac{l^2}{m^2}),$$

6.3

where λ_P is the pump wavelength. The effective nonlinear coefficient of each section is $d_{eff} = 2d_{33}/\pi = 15$ pm / V, the free space permittivity (ε_0) is 8.85×10^{-12} F/m, the speed of light in vacuum (c) is 3×10^8 m / s, the confocal beam waist ω_f is 50 μm, and n_p and n_{SH} are the refractive indices of LN at the pump and SH wavelength, respectively. For an input pump power, $P_p = 0.55$ W we used in the experiments, the calculation gives a maximum SH power, $P_{SHG} = 0.0129$ mW which is reduced to 70% with apodization over half of the structure [130]. Therefore we expect the SHG power of 0.009 mW or -20.45 dBm. What we measured in practice is around -23 dBm. Considering ~-3dB loss in our setup including the coupling loss of light from free space to the fiber, the reflection loss from lenses and fiber connector loss, it is in fairly good agreement with the theory. We ignore back reflection effect in bulk AC-PPLN. The SH power is measured as a function of the FH wavelength and for each wavelength the polarization is adjusted to reach maximum SH power. After the SH power characterization for one direction, the input and output fiber are interchanged. The measurement for the second direction is completed immediately after the first to ensure the same conditions for the laser and amplifier to minimize the effects of drift.

6.5   Results and discussion

Considering two CPS and OCPS model, the simulated normalized SH intensities versus the FH wavelengths are plotted for two different up-chirp and down-chirp directions in Figure 6.3(a) and 3(b), respectively. Due to fabrication limitation we have deliberately used fewer sections than what are required to give a smooth response, so that the difference may be highlighted. In the CPS model, the SH responses overlap for the two, up-chirp and down-chirp directions as there is no phase variation contributing to spectrum shape change. On the contrary, in the OCPS model the phase accumulation from 18 subsection borders (9 on left side and 9 on right side of the grating) is different in two directions as it can have positive phase in one and negative in another due to the fact that the place of poled region can move from one side to another as mentioned in section 2. The theoretical simulation shows that not only should we expect a difference between the bandwidth in two directions but also in extrema (maxima and minima) points in the spectrum. Note the wildly different response for the OCPS scheme [Figure 6.3(b).]
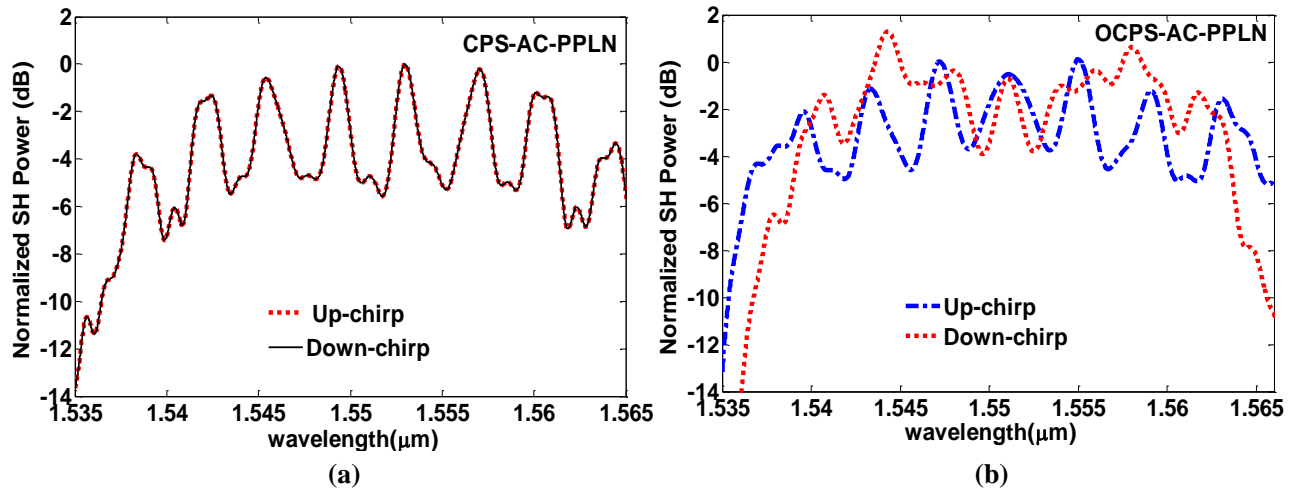
Figure 6.3. Normalized simulated SH power versus FH wavelength for up-chirp and down-chirp configurations using AC-PPLN with a) CPS and b) OCPS design.

Results for fabricated CPS AC-PPLN in the two, up-chirp and down-chirp directions are shown in Figure 6.4. In order to compare the results and examine reciprocity in two directions, we have considered two criteria; the bandwidth and the extrema points in the SH spectra. As it can be seen in Figure 6.4 the bandwidth for CPS design is almost the same for both up-chirp and down-chirp as we expect from the theoretical simulation. In addition, the extrema in spectra of CPS design for up-chirp and down-chirp follow each other reasonably well. The only difference is in the amount of the extrema which can come from measurement errors due to adjusting the polarization controller at each measurement wavelength. The average power difference in two directions in less than 0.75 dB and the standard deviation of extrema are 1.34 dB and 1.64 dB for up-chip and down-chirp respectively. We believe that the main issue in making this comparison is in the precise control of the input polarization for each wavelength in the two directions, as it is difficult to maintain linear polarization for each of the wavelengths used in the measurements due to the imperfection of the polarization controller, and would have to be better controlled to take full advantage of the CPS scheme. Nevertheless, the closeness of the spectra in the two directions is clearly visible. The measured bandwidth is limited by the erbium amplifier used in the experiments.
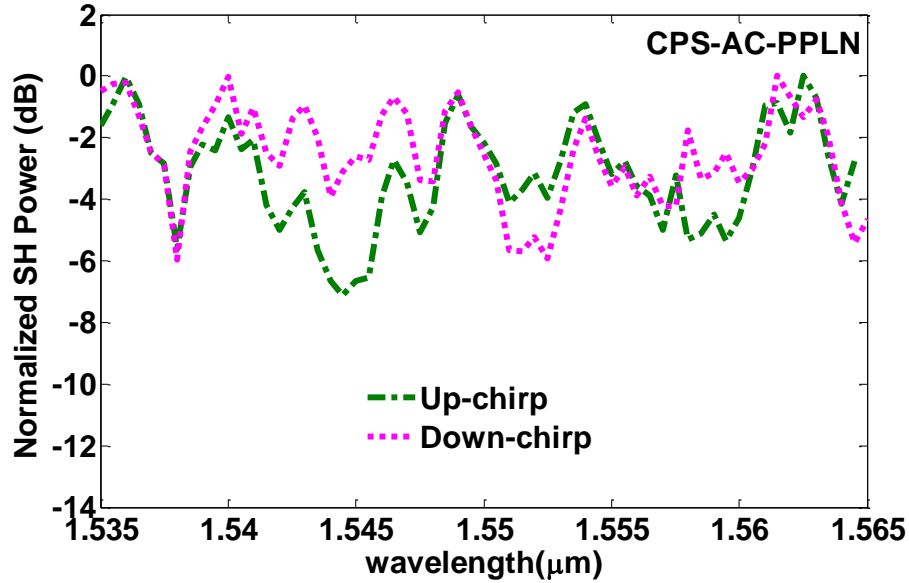
Figure 6.4. Normalized measured SH power versus FH wavelength for up-chirp and down-chirp configurations using AC-PPLN based on CPS.

6.6   Conclusion

In summary, the effect of displacement of poled regions within periods on SH spectral response of apodized chirped gratings was evaluated theoretically. An AC-PPLN devices based on center poled structures was designed and fabricated using electric field poling method in room temperature. It was shown theoretically that for the device composed of symmetric cells called CPS, the SH response is the identical for up-chirp and down-chirp directions and thus the AC-PPLN device is reciprocal for SHG. Experimental results on the CPS scheme have indeed shown the benefit in terms of preserving the bandwidth and also the similarity in structure in the conversion response. The reciprocal device based on CPS, can have application in resonant cavities and multi-pass configuration to improve SHG performance.

CHAPTER 7   ARTICLE 4: SUPER-TUNABLE, BROADBAND UP-CONVERSION OF A HIGH-POWER CW LASER BASED ON X[(2)] PROCESSES IN AN ENGINEERED NONLINEAR PHOTONIC CRYSTAL

Ameneh Bostani,[1]* Amirhossein Tehranchi,[2] Raman Kashyap,[1,2]

[1]*Department of Engineering Physics, Montreal Polytechnique ,Montreal, QC, Canada, H3T 1J4*

[2]*Department of Electrical Engineering, Montreal Polytechnique, Montreal,QC, Canada, H3T1J4*

Corresponding author: bostani.ameneh@polymtl.ca

Submitted to Optica in May 2016

7.1   Overview

In two previous chapters, the characterization of the fabricated grating has been done by tuning a narrowband laser in the communication band. In this paper, we use a high power fiber laser as a source for frequency conversion in an SC-PPLN at room temperature without using temperature controller. The CW high power fiber laser has a much broader bandwidth than the tunable laser and suffers from some drift in central wavelength and bandwidth broadening. Here, we show several important features of step-chirped grating such as insensitivity to the laser frequency drift and bandwidth broadening of the fiber laser and also its functionality in a wide range of temperatures. Also, the effect of focusing is considered in the development of the theory and characterization. The design of the device has been described in details. We realize a tunable broadband laser (centered around 775 nm) with the help of an amplified tunable narrowband laser as a control signal and a high power fiber laser as the pump (both centered around 1550 nm) based on SFG. Also, SHG of the entire spectrum of the fiber laser has been obtained and the result is discussed.

This paper was presented at different international conferences such as Optical Society of America (Nonlinear Optic 2015) in Hawaii, the USA, and SPIE Photonic west 2016 in San Francisco, USA.

7.2 Abstract

A specially-designed chirped periodically poled lithium niobate nonlinear photonic crystal was fabricated with a phase-matching bandwidth as large as 50 nm for sum frequency generation to operate at room and higher temperatures. This device also benefits from insensitivity to laser frequency drift and fine alignment. The loosely-focused beam position of a high-power CW laser at around 1550 nm is optimized within the grating for maximum up-conversion efficiency, to realize a super-tunable source in the range of 770-778 nm by tuning a narrowband control signal over 30 nm in the communication band. This device is demonstrated to be fully phased-matched simultaneously for both second-order nonlinear up-conversion processes, namely second harmonic generation (SHG) and sum frequency generation (SFG). The measurement of the generated SF power versus wavelength agrees well with the theory. Also, a quadratic SH power with respect to the pump power is realized.

7.3 Introduction

There is increasing demand for tunable CW sources at shorter wavelengths due to many applications in biomedicine and spectroscopy [131], [132]. Due to the lack of suitable sources, a feasible approach is by the up-conversion of available fiber lasers in nonlinear materials. However, high-power fiber lasers in the form of continuous wave generally possess a bandwidth (BW) in the order of hundreds of GHz proportional to the laser output power due to the use of fiber Bragg gratings [133] or four-wave mixing (FWM) between the different longitudinal modes [134], [135]. Further, these high-power fiber lasers are only available in limited wavelength ranges. In addition, they experience a drift in their central wavelength when the output power varies [136], [137]. Nevertheless, in order to realize tunable CW sources at the desired higher frequencies, up-conversion based on second-order nonlinearities using engineered quasi-phase-matching (QPM) in nonlinear photonic crystals can be exploited with several advantages [107],

[138]. There are many works on second harmonic generation (SHG) and sum frequency generation (SFG) in uniform gratings in the form of periodically poled crystals [138]–[142]. However, uniform gratings limit the BW of up-conversion process as it is inversely proportional to the length of a grating. Since the up-conversion efficiency (assuming an undepleted pump) is also increased by the length squared, using a long grating leads to a reduction in the up-converted BW of a few-nm-wide pump and consequently results in a waste of power whilst a short grating up-converts the whole BW with a very low efficiency. Also, at higher pump powers, the use of a short grating may lead to the crystal damage. Moreover, as the effective period of uniform grating changes by angular rotation and temperature, fine alignment and a controlled temperature are required to obtain maximum efficiency for the central wavelength of a pump. Also, accurate temperature control is necessary for uniform gratings to tune the up-conversion wavelength [143]. Thus, to convert the entire BW of a pump laser, broadband converters in the form of engineered chirped and step-chirped periodically poled lithium niobate (PPLN) [7], [102] with an efficiency almost linear proportional to the grating length have been proposed to provide higher efficiency compared to very short uniform gratings to achieve the same BW. Although for the same length the conversion efficiency of a chirped grating with wide BW is less compared to that of a uniform grating with narrow BW, using a high-power source, the efficiency is not of significant concern, as power can be traded for BW. Hence one can benefit from temperature- and fine-alignment-insensitivity of chirped grating and obtain a large conversion BW. Recently, temperature independent broadband up-conversion (i.e., SHG and SFG) as well as cascaded with DFG in step-chirped PPLN (SC-PPLN) were demonstrated for tunable monochromatic CW lasers [108], [144] and the effect of tight focusing on broadband output spectra of such converters was reported [129]. In this letter, we demonstrate super-tunable broadband frequency up-conversion of a high-power CW laser for the first time to the best of our knowledge, in a specially-designed nonlinear photonic crystal namely SC-PPLN, demonstrating wideband SFG where the tuning is achieved using a tunable monochromatic laser as a signal source. The loosely-focused beam position of the high-power CW laser is optimized within the grating for maximum up-conversion efficiency. A tunable source at shorter wavelengths is thus

realized in which the central frequency is controlled by tuning the control signal laser without concern of the frequency drift of the high-power CW laser pump.

7.4   Theory and Design

Under the undepleted pump regime and plane wave approximation, the SFG electric field envelope in the frequency domain is given by the product of the transfer function, $\hat{D}(\omega)$ and the convolution of the pump and signal electric field envelopes [145]

$$A_3(\omega-\omega_3) = \hat{D}(\omega).[A_1(\omega-\omega_1) * A_2(\omega-\omega_2)]$$ 7.1

where A_i and ω_i are the electric field envelope in the frequency domain and angular frequency. The star sign denotes a convolution. i = 1, 2 and 3 denotes the pump, signal, and SF waves, respectively. $\hat{D}(\omega)$ is proportional to the Fourier transform of the nonlinear modulation function, $d(z)$ in a quasi-phase-matched structure which is engineered [17]. In addition, the effect of focusing can be added to the transfer function integral as follows [129]

$$\hat{D}(\omega) = -j\gamma \int_{-\infty}^{+\infty} \frac{d(z)}{1 + j\zeta(z)} \exp(j\Delta kz) dz$$ 7.2

where $\Delta k = k1 + k2 - k3$ and ki is the wave vector. $\zeta = 2(z-f)/b$ where f and z are the focal position and propagation axis, respectively. $b \simeq 2\pi w2n1/\lambda1$ is the confocal parameter where w and n1 are the beam waist, and refractive index, respectively, at the pump wavelength, λ_1. $\gamma = 8\pi\omega_3^2\gamma_0 / k_3c^2$ where c is the speed of light in vacuum and   is considered to be a constant from the Boyd-Kleinman calculation for a focused Gaussian beam in a parametric interaction [22].

For the input pump, we suppose a Gaussian function with a peak amplitude of a_1 centered at ω_1, a BW of σ_1 as $A_1 = a_1 \exp[-(\omega-\omega_1)^2 / \sigma_1]$ and for the monochromic signal, we consider a Dirac delta function as $A_2 = \delta(\omega-\omega_2)$ at ω_2. Therefore, the SFG wave can be calculated as

$$A_3(\omega - \omega_3) = \hat{D}(\omega)\,a_1 \exp[-(\omega - (\omega_1 + \omega_2))^2 / \sigma_1]$$
<div align="right">7.3</div>

which can have the same BW as the pump if the transfer function is broad enough to accommodate the Gaussian function. Therefore, with the engineering of a proper transfer function, the entire BW of a pump laser can be converted to an SF wave. However, in the case of pump SHG, the spectra of A_2 is replaced with A_1 in Eq.7.1 and the amplitude of the SH wave can be calculated using an auto-convolution as

$$A_{SH}(\omega - \omega_{SH}) = (1/2)\hat{D}(\omega)\,a_1^2 \exp[-(\omega - 2\omega_1)^2 / \sqrt{2}\sigma_1]$$
<div align="right">7.4</div>

which shows a spectral broadening of the SH amplitude in the order of the square root of two, compared to that of the input pump BW, assuming a broad enough transfer function. Thus, we expect full BW conversion of the pump in SFG and broadening of the SHG BW compared to the pump BW only if the transfer function is wide enough to accommodate both processes. The nonlinear modulation function in the spatial domain can be presented by $d(z)$ as

$$d(z) = rect(z/L) \times \sum_{m=-\infty}^{+\infty} (2/m\pi)d_{33}\sin(\pi m/2)\,e^{i2\pi m/\Lambda(z)}$$
<div align="right">7.5</div>

where d_{33} is the nonlinear coefficient of the crystal and $\Lambda(z)$ is the period of the grating at different spatial positions, z.

In order to design an SC-PPLN with a wideband transfer function for SFG with a pump laser centered at 1550 nm and a swept control signal in the 30-nm C-band (1530 nm to 1560 nm), the device should work at room and possible higher temperatures to reduce possible photothermal damage [23]. Two pairs of minimum and maximum periods for SC-PPLNs at 25 $^\circ$C and an elevated temperature, i.e., 115°C can be calculated from the phase matching condition for SFG resulting in $\Lambda = 2\pi c / (\omega_3 n_3 - \omega_2 n_2 - \omega_1 n_1)$, where $\omega_3 = \omega_1 + \omega_2$ and the refractive indices are dependent on temperature through the Sellmeier equation. The minimum period at the higher temperature and the maximum period at the lower temperature are then chosen. Therefore, the SC-PPLN period change from 18.38 µm to 19.11 µm results in a 50-nm BW fully covering the

C-band for temperatures from 25 ℃ to 115 ℃. Given that our fabrication facility allows a minimum variation in the period of 100 nm (chirp step), the SC-PPLN device has to be designed in 8 sections. The length (L) of the device is then determined by a compromise between the higher efficiency and smaller ripple height. The normalized transfer function for different lengths of the SC-PPLN at room temperature is plotted in Figure 7.1. The length of 13 mm is then selected for fabrication to reduce the ripples to ±2 dB. Longer SC-PPLNs lead to peak-to-peak ripples greater than 4 dB reaching as high as 6 dB for a length of 18 mm. Shorter SC-PPLNs reduce the efficiency without a remarkable reduction in ripples. Our device works like a 2D photonic crystal as it has a very large acceptance angle. The device tolerates ±11.4° yaw to obtain a half BW which is almost 2 times greater than is possible for a short uniform PPLN with one section length in addition to benefiting from higher efficiency as large as 5dB.
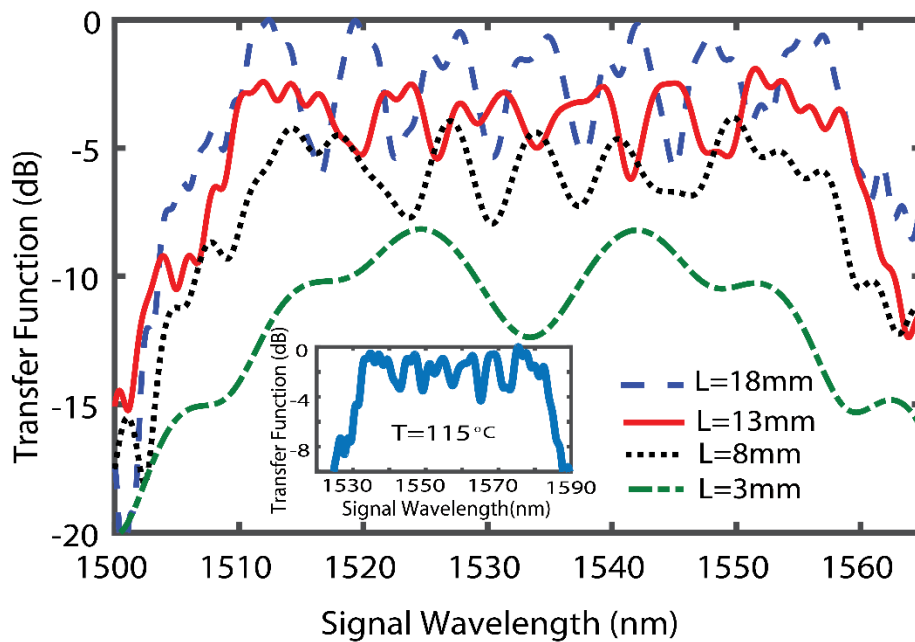
Figure 7.1. Normalized transfer functions for different lengths of SC-PPLN at 25 ℃, considering input pump (plane wave) at a wavelength of 1550 nm and a sweeping control signal. The inset shows the transfer function of the 13-mm-long SC-PPLN at $T = 115$ ℃.
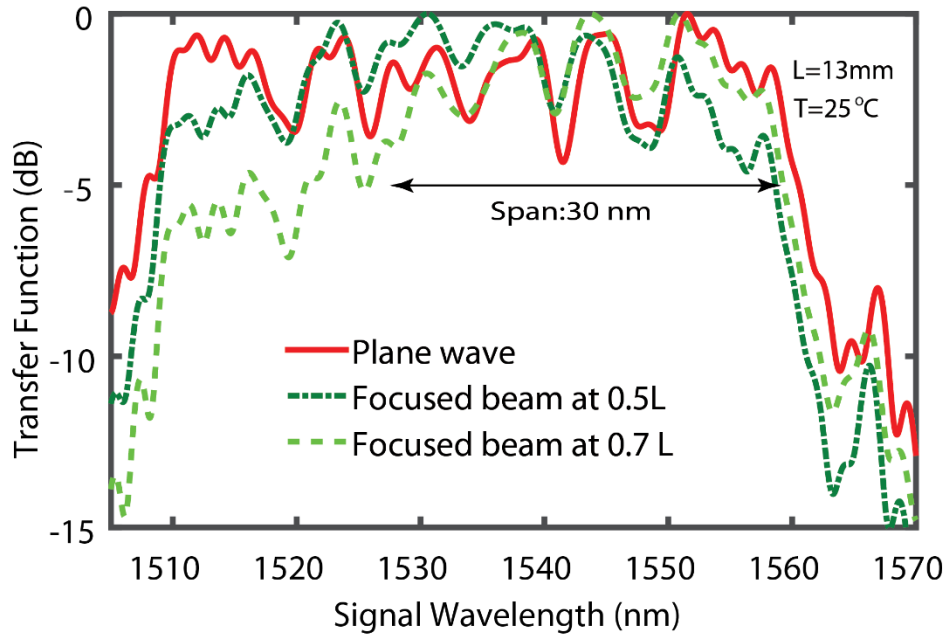
Figure 7.2. Normalized transfer functions of the SC-PPLN considering un-focused beam (plane wave) and focused beams at two different places along the gratings.

In addition, we can simulate the role of focusing on the transfer function, to approach the real experimental conditions. The effect of different degrees of focusing and the position of the focus within the grating were already examined in Ref. 129. Focusing can suppress the sidelobes in the transfer function of the SC-PPLN far from the phase-matching wavelength of the grating in the focusing point. In Figure 7.2, the transfer functions for a loosely focused light beam with a waist of 70 µm located at $0.5 \times L$ and $0.7 \times L$ are plotted for a 13-mm-long SC-PPLN at room temperature, using a fixed pump at 1550 nm and a swept signal. For comparison, the transfer function of the ideal plane wave is also shown in Figure 7.2. In the case of focused beams, the focal point is optimized to be at $0.7 \times L$ within the grating to achieve the maximum up-conversion power for 1550 nm, and to maintain the required 30-nm working BW. The transfer function is suppressed in the range of 1510 nm to 1530 nm, but this is not a concern as it is outside the designed working range.

7.5   Experiment and Results

A mask based on our design was fabricated by photolithography before electric field poling at room temperature, which is a common technique to fabricate PPLN [129]. After cutting the sample, it was polished and placed in the up-conversion setup as shown in Figure 7.3.
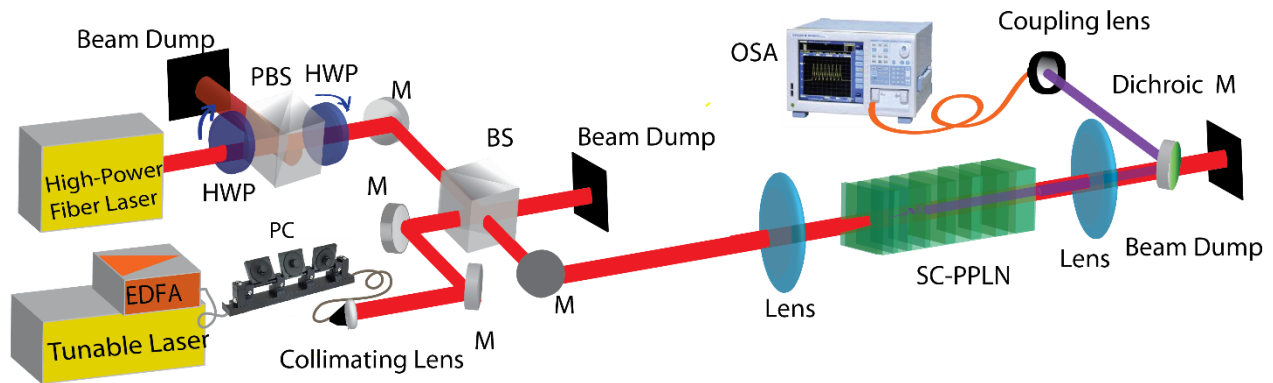
Figure 7.3. Experimental setup to evaluate SFG and SHG in an SC-PPLN with a high-power fiber laser as a pump and a tunable laser as a control signal, EDFA: erbium doped fiber amplifier, PC: polarization controller, M: mirror, BS: beam splitter, PBS: polarization beam splitter, HWP: half-wave plate and OSA: optical spectrum analyzer.

An erbium fiber laser (ELR-75-1550) from IPG photonics with a central emission wavelength around 1550 nm is used as a high-power fundamental harmonic (FH) pump. A combination of a half-wave plate and a polarization beam splitter (PBS) cube in front of the pump beam is placed to adjust the power. After the PBS, another half-wave-plate is located to fix the light polarization before entering into the SC-PPLN. The pump beam is combined in a beam splitter with the control signal source from another device: a C-band EDFA amplified JDSU tunable laser after a fiber-based polarization controller. The signal beam from the fiber, collimated by a spherical lens enters the beam splitter cube. The two combined beams (the pump and signal) are loosely focused into the SC-PPLN by a lens with a focal length of 12.5 cm (at around 1550 nm). The

output SF and SH waves were separated from the pump by a dichroic mirror, then collimated and coupled into the output fiber and analyzed using an optical spectrum analyzer and power meter.
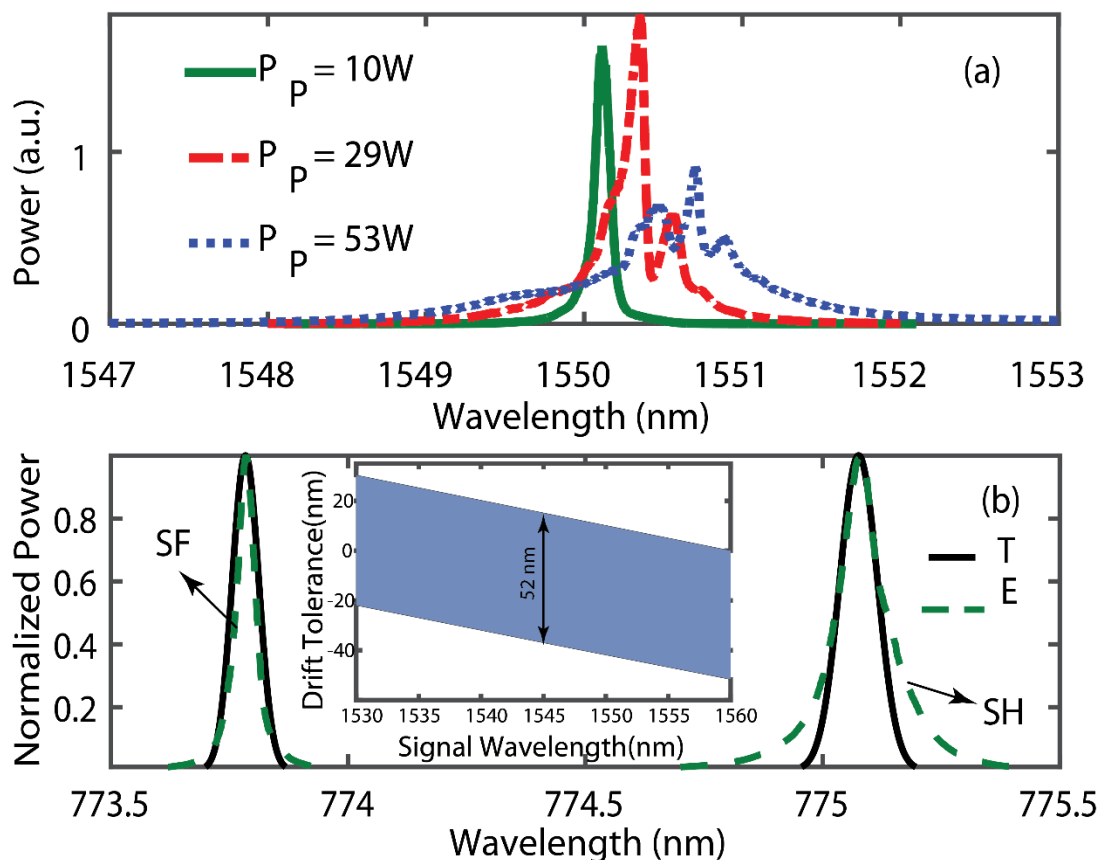
Figure 7.4. a) Pump spectra for different integrated powers. b) Theoretical (T) and experimental (E) results of simultaneous SFG and SHG when the pump and control signal are at 1550.16 nm and 1545 nm, respectively. The inset shows the region of tolerable drift in the pump central wavelength at 1550 nm for different signal wavelengths.

The spectra of the CW pump laser at three output powers are shown in Figure 7.4(a). The FWHM of the pump laser increases from ~0.1 nm at 10 W to ~1 nm at 53 W due to the FWM within the fiber laser. In addition, it shows a spectral-shift (with a peak wavelength drift < 0.75 nm) toward longer wavelengths as apparent in Figure 7.4 (a). The experimental spectra of simultaneous SFG and SHG for the high-power laser centered around 1550 nm and the signal at 1545 nm are shown in Figure 7.4 (b). The results are compared with the computed spectra for

SFG and SHG simulated by the real pump spectrum and a monochromatic wavelength at 1545 nm as the inputs to the SC-PPLN. The SF wave, centered around 773.78 nm, has a spectrum corresponding to the pump BW as expected from the theory. The SH BW centered at 775.08 is ~1.4 times broader compared to the SF as it is proportional to the auto-convolution of the FH beam in the agreement with the theory presented earlier in this letter. Also, both $\chi(2)$ processes tolerate the drift easily in the central wavelength of the pump. Based on the up-conversion simulation, the pump central wavelength (at 1550 nm) can undergo -37 nm to +15 nm drift for the signal at a wavelength of 1545 nm as shown in the inset of Figure 7.4(b).

Next, the control signal is tuned when the pump wavelength is fixed at 1550 nm and simultaneous SH spectra of the pump and signal and associated SF spectrum are observed. In Figure 7.5, four overlaying spectra of SH and SF for four different control signals centered at 1532 nm, 1536 nm, 1560 nm, and 1561 nm are shown. Each SF wave has a broader and narrower BW than that of the corresponding signal SH wave and pump SH wave, respectively, as predicted by Eqs. 3 and 4. The maximum power of SF waves alters for different signal wavelengths as expected from the ripply transfer function of the SC-PPLN, shown in Figure 7.2
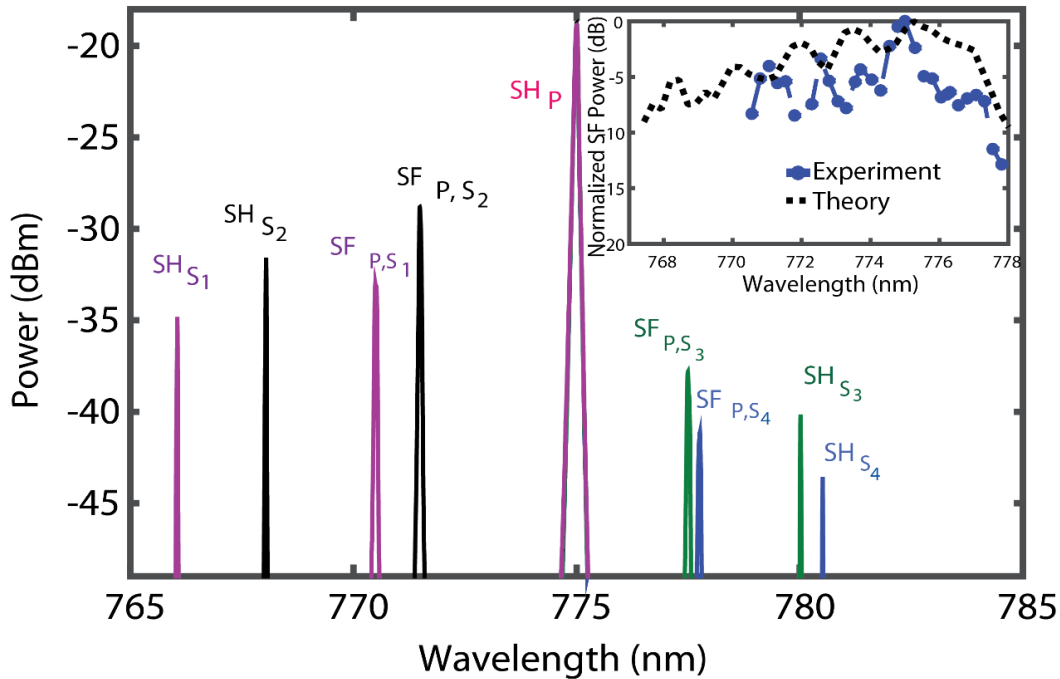
Figure 7.5. Overlaying of four experimentally observed spectra including SH of a pump (SH$_P$) at λ_1=1550 nm and SH of four tuned signals at λ_{S1}=1532 nm, λ_{S2}=1536 nm, λ_{S3}=1560 nm and λ_{S4}=1561 nm named as SH$_{S1}$, SH$_{S2}$, SH$_{S3}$ and SH$_{S4}$ and SF of the pump and signals presented by SF$_{P,S1}$, SF$_{P,S2}$, SF$_{P,S3}$ and SF$_{P,S4}$. The inset shows theoretical and experimental results for normalized SF power versus the wavelength.

The simulated and experimental results (at 25 ^{o}C) for normalized maximum SF power versus wavelength is plotted in the inset of Figure 7.5 for a pump at 1550 nm and a swept control signal. The measured SF central wavelength is successively tuned from ~770 nm to 778 nm by tuning the control signal from 1530 nm to 1560 nm, confirming an experimentally tunable BW of ~8 nm for the SF whilst for an equivalent-length, uniform PPLN, it is only 0.41 nm, demonstrating the super-tunability of our SC-PPLN. However, the difference between experimental and simulated results comes from accumulated phase differences in the fabrication and errors involved in the poling process. The simulated response in the inset is shown in a wider range than the experimental one as the SC-PPLN is designed to work also at higher temperatures. Theoretical calculation for the SF power using Eq.7.1 and assuming Gaussian functions with the

integrated powers and bandwidths of (P_1, σ_1) and (P_2, σ_2) for the pump and signal, respectively leads to $P_{SF} \propto P_1 P_2 \sigma_1 \sigma_2 / (\sigma_1^2 + \sigma_2^2)^{1/2}$ which results in a small SF power where $\sigma_1 \gg \sigma_2$ even if P_1 is comparable to P_2. For instance, considering a typical 1-W signal power at 1542 nm and a 3-W integrated power of the pump, the maximum integrated power in the generated SF power at 773.2 nm is measured to be around 75 µW.

In a special case, by turning the control signal off, an SH proportional to the auto-convolution of the high-power pump is generated. The SH spectra for three pump powers (already illustrated in Figure 7.4 (a) are shown in Fig. 6. It is obvious that the SC-PPLN performs well for full-BW frequency-doubling of the FH wave, and is also able to handle the pump spectral-shift. The generated SH power is measured and plotted versus the input power in the inset of Figure 7.6.
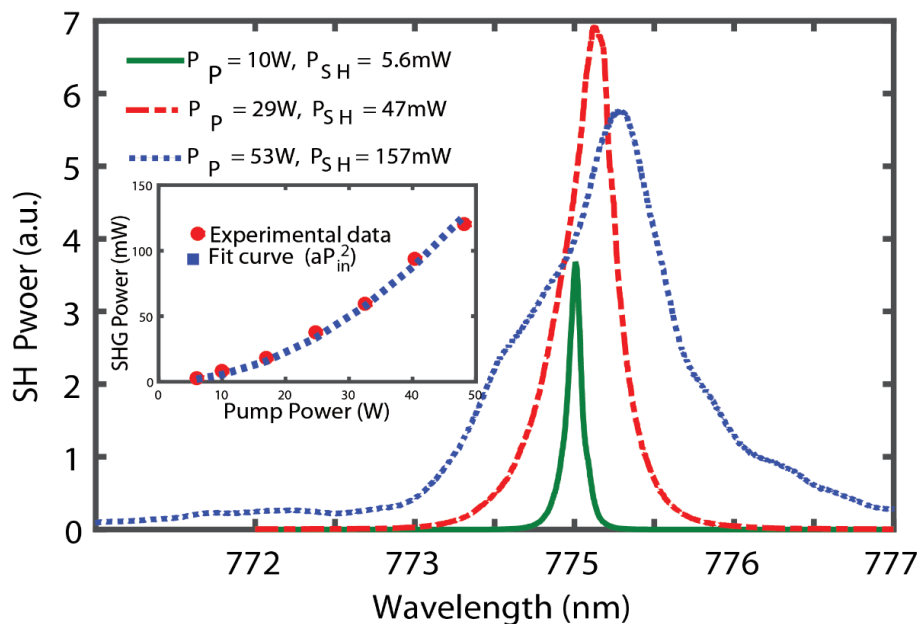
Figure 7.6. SH spectra for 3 pump powers shown in Figure 7.4 (a). The inset shows output SH power versus input FH pump power.

The SH power changes quadratically with the FH power as is expected from the un-depleted pump theory. The quadratic fit curve to the experimental data is shown in the inset and the estimated quadratic coefficient, a is 0.056/W, which is comparable with the theoretical

calculation using the following equation $a = P_{SH}/P_P^2 = 8\pi/\lambda_1^2 c\varepsilon_0 n_1 n_{SH}^2 w_0^2 \left[\int_0^L d(z)e^{i\Delta kz}dz\right]^2$ for an SC-PPLN, where d_{33} is 21 pm/V, the free space permittivity, ε_0 is 8.85 × 10−12 F/m, c is 3 × 108 m/s, w is 70 μm, and n_{SH} is the refractive index of LN at the SH wavelength, respectively. The calculation gives the coefficient, a in the range of 0.048/W to 0.12/W which depends on the chirp step, SC-PPLN length, working wavelength and temperature. No photorefractive damage was seen at 25 ℃ for different FH powers, however, we increased the temperature from room temperature to 115 ℃. The change in the SH power is less than 3 dB over a 90 ℃ temperature-tuning BW and thus, the device does not require a temperature controller. It is worth noting that the similar BW for an equivalent-length uniform PPLN is calculated to be only around 4 ℃.

7.6   Conclusion

In conclusion, it was demonstrated both experimentally and theoretically that by engineering the chirped grating in a nonlinear photonic crystals and designing the transfer function larger than the signal tuning span, all spectral components of a few-nm-wide pump and a tunable CW signal can be phase-matched over the transfer function's bandwidth to generate an SF wave with a corresponding bandwidth as the pump wave. For the SC-PPLN, a 50-nm wide transfer function was obtained to cover the C-band at room temperature and higher temperatures (up to 115 ℃). In this device, SFG phase-matching of the control signal swept over 30-nm in the C-band with a high-power CW pump at 1550 nm resulted in the generation of a super-tunable SF wave over ~8 nm around 775 nm. Also, the loosely-focused beam position along the grating is moved to maximize the up-conversion efficiency around 1550 nm in the transfer function. The focusing position has been found to be optimized at 0.7 × L of the grating. The measured generated SF power versus wavelength is in a good agreement with the theory. Although the SF response has ripple due to the transfer function profile, apodization of the SC-PPLN grating can remove the ripples [7], [128]. In a special case of turning the signal off and obtaining frequency doubling of the pump alone, the SH wave with a broader bandwidth than that of the pump was achieved which is the consequence of the auto-convolution of the pump wave distribution function in the frequency domain [145]. Quadratic SH power with respect to the pump power was realized and the quadratic coefficient was measured to be ~0.056/W. The device is insensitive to pump-

spectrum drift and does not need a temperature controller and also can tolerate $\pm 11.4^{\circ}$ yaw, i.e. an input acceptance angle. The current engineering technique can also be applied to other wavelength ranges and materials as long as the phase-matching conditions are met.

CHAPTER 8   GENERAL DISCUSSION

Aperiodically poled lithium niobate (APPLN) in the two forms of chirped and apodized chirped gratings in bulk crystals were investigated in this work to increase the bandwidth and thermal acceptance of frequency converters compared to uniform PPLNs. Using high power lasers and controlling the focus of input beam are available in bulk APPLNs compared to waveguides APPLNs. In chirped gratings the period of device changes linearly while in apodized chirped gratings, the duty ratio is also a variable. Apodized chirped gratings were suggested to improve the output response of chirped grating and to reduce its fluctuations. There are several parameters which should be determined for the design of APPLNs such as pump and control signal wavelengths, its bandwidth or tunability, and required thermal tolerance. In designing these devices, fabrication limits and the growth of poled regions under the electrodes should also be considered. Fabrication limits are related to the mask fabrication for APPLNs including the minimum period variations in chirped grating and minimum open windows for apodization. Step-chirped scheme is used in the design and fabrication of chirped grating as the fabrication of continuously chirp grating with the present fabrication facilities is impossible due to the smallness of variations in periods. For fabrication of these gratings, familiar liquid electrode poling method was used. The 0.5 mm thick z-cut lithium niobate wafer is patterned by coating positive photoresist S1813 and expositing UV through the mask. A dc electric field (22 kV/mm) higher than coercive field strength of LN in the shape of pulses with a duration of 0.5 ms is applied to the patterned LN to invert the domain polarization. During sending the pulses, poling process is monitored by two crossed polarizer placed on the two sides of the substrate. Domain inversion is initiated by nucleation sites under the electrodes. However, it does not occur homogeneously in different parts of the grating, due to the presence of an internal field in the crystal which trigger the nucleation [146]. This internal field originates from defects in lattice structures such as missing ions or unregulated packing of atoms into a place (nonstoichiometry) [147]. When the nucleation does not start in different parts of the grating simultaneously, it leads to over-poling near the starting point or under-poling far from the starting point. Sometimes the over-poling causes merging the domains and reduce the efficiency. The poled pattern after

receiving the pulses can be revealed by etching in HF. The fabricated sample then is cut, polished to reduce the scattered light in the characterization set-up.

Chirped gratings possess many ripples in order of 5 dB or larger in their SH efficiency responses depending on the device length, chirp steps and initial and final periods. Apodization can help to reduce the ripples of chirped gratings.

Based on this thesis, there are two ways for apodization to decrease the ripples in the SH efficiency response. The first way is relied on the fabrication of the converter by increasing the duty ratio from a minimum to a maximum and decreasing it smoothly at the end of the device. Generated harmonic field amplitude can be controlled by changing the duty ratio in the grating. The size of the duty ratio is determined by apodization function and fabrication limits. The place of poled regions should be centered within the pitch to control the phase of generated electric field. The reason for this accurate positioning extensively was explained in Chapter 4 by the theory and numerical simulation. When the poled regions are not placed in the center, in each period, generated harmonics gain an extra phase compared to the center positioning. Accumulation of this phase can lead to increased ripples in the generated SH intensity in the spectral response and its deviation from the response of the desired mathematical apodization function. Thus in designing the apodized chirped periodically poled material, positioning the poling regions in the center of pitch can improve the generated SH transfer function and results in better device performance, by increasing tolerance to fabrication errors.

However, fabrication of these devices is difficult because of two reasons. The first one is related to difficulty in making small windows in the mask fabrication and photolithography process. The second problem appears in poling process during sending the electrical pulses. Bigger windows require a larger amount of electric charge compared to small windows on both sides of the substrate while sending the pulse provides equal electric charge everywhere, which leads to leakage of the electric field under the electrodes in areas with small windows as trying to pole regions with bigger areas. The second approach for apodization was proposed in Chapter 5. This technique is based on shaping the pump beam by different degrees of focusing and displacing the focusing center within the converter. In fact, part of the pump electric field profile can be translated to the change of the effective second-order nonlinearity and thus is considered as an

apodization term in the poled crystal. In this approach, the intensity of light is altered spatially within the grating by focusing the laser beam. The intensity is maximized in the focusing point and decreases slowly in two sides of that. The nonlinear interaction amplifies when the intensity increases, therefore it acts similar to the change of duty cycles when it maximized (=1/2) in the grating center. The shape of apodization function associated with the focusing can be controlled by the focal length of the lens which focuses the light inside the device. When the focal length decreases, the light is focused more, gives smaller spot size, and suppresses the height of ripples in SH response and it also reduces the bandwidth of the grating transfer function. However, tuning the SH response over the entire SC-APPLN bandwidth is possible by displacing the focal point of the input beam inside the device. The theoretical analysis and experimental results of the second approach on a fabricated step-chirped grating were presented in Chapter 5. The laser beam was focused with 3 degrees of focusing using 3 lenses and four different focusing places by changing the place of the sample regarding the lens. For a designed and fabricated step-chirped grating with 30-nm SHG bandwidth, focusing the light with a beam waist of around 20 microns, a ripple-free response can be obtained, e.g., for a 6-dB bandwidth while its bandwidth shrinks to 5 nm for both simulation and measurement. Using this method, we are able to tune the central working wavelength by moving the focal point in the experimental set-up without any need to change the temperature. For tuning the central wavelength by 1 nm, displacement of the focal point by 0.52 nm in the SC-PPLN is required.

In order to demonstrate our first approach, step-apodized chirped grating was fabricated based on placing centered pole region, which was proposed in Chapter 4. The reason is that the continuously chirped grating presented in Chapter 4 is not feasible for fabrication. Therefore, in Chapter 6, we have demonstrated the simulations, fabrication, and characterization of the apodized step-chirped grating for 30 nm SHG bandwidth. Based on our analysis in Chapters 4 and 6, the apodized chirped grating and consequently the step-apodized chirped grating should showed the reciprocal behavior in which the SH efficiency response should be identical for both directions of propagating light through the converter. Also it should possess the same bandwidth for both propagation directions. This feature provides the use of this kind of converter convenient in resonators. Experimental results of our fabricated chirped apodized grating which

was demonstrated in Chapter 6 showed reciprocal behavior in two up-chirp and down-chirp directions of the grating.

Another feature of designed and fabricated APPLNs were temperature- and frequency-drift insensitivity, which were demonstrated in Chapter 7. The experiment was done at the room temperature without using any temperature controller. The laser source, which is used in the frequency conversion experiment, is a CW high power fiber laser. The idea of using high power was proposed in order to compensate for the lower efficiency of APPLNs compared to PPLNs. The high power fiber lasers show wavelength drift and bandwidth broadening when their output power is increased. This characteristic makes the frequency conversion difficult for their whole bandwidth in PPLNs. However, it can be converted entirely using a properly-designed APPLN as we demonstrated in Chapter 7. The SHG of the high power laser was obtained for different powers and the quadratic SH power with respect to the pump power was obtained and the quadratic coefficient was measured to be ~0.056/W which is in a good agreement with the theory. The SH spectral response profile follows the spectral shape of the input high power fiber laser regardless of the bandwidth broadening and frequency drift. We observed a little broadening (1.4 times) in the SHG bandwidth compared to the pump bandwidth, which was the result of the auto-convolution of the pump electric field envelope. As the central wavelength of the high power CW laser is non-tunable around 1550 nm, it gives a SHG around 775 nm. Therefore we combined this laser beam with a tunable laser as a control signal working in the communication band to make a tunable broadband CW laser around 775 nm. The transfer function for the SFG, considering important elements in design and fabrication is described in Chapter 7. By tuning the control signal, we generate a super-tunable SF wave over ~8 nm around 775 nm using the SFG of these two lasers. We also considered the effect of the beam focusing, discussed in Chapter 5, to maximize the up-conversion efficiency around 775 nm and have a more realistic simulation result for the characterization experiment.

Our devices were designed and characterized for the wavelengths in the communication band; however, the idea is general and can be applied to other wavelengths as long as the phase-matching conditions are met.

CHAPTER 9   CONCLUSION AND RECOMMENDATIONS

In this thesis, broadband temperature-insensitive QPM frequency converters were investigated through design, fabrication, and characterization. Earlier, the design of step-chirped and step-apodized chirped QPM devices in waveguides were introduced by our group in 2008 to flatten broadband SHG response [7]. Apodization of chirped QPM devices was studied in more details in this work by simulating the SHG response with various apodization functions and different apodization ratios. It was theoretically proved that in designing apodized chirped grating, the positions of poled regions play an important role in the SH spectral response. The poled region should locate in the center of the cell to provide the best structure for a desired apodized function in a broadband converter.

We designed the APPLNs in the form of SC-PPLNs and proportional to our fabrication limits. The samples were patterned by photolithography and then were fabricated using the high voltage electric field poling at room temperature in the laboratories of Montreal Polytechnic. The devices were fabricated to cover 30-nm SHG bandwidths in the communication band.

Two methods for apodization and suppression of ripples for chirped gratings were proposed in this dissertation. One based on design and fabrication of apodized converters and the other one based on spectral shaping of focused laser beam. We used a focused laser beam to change the SH efficiency spectral profile and suppress its ripple. In addition, it was shown that tuning the SHG response over the entire SC-PPLN bandwidth is possible by displacing the focal point of the input beam inside the device. This technique was demonstrated using a homemade un-apodized chirped grating.

In addition, step-apodized PPLN based on locating the poled region in the cell center was designed and fabricated. It was shown that the SHG responses of these devices should be identical for up-chirp and down-chirp directions and thus the apodized SC-PPLN device is reciprocal for SHG. Also theoretically it was shown that the displacement of the poled regions within periods leads to a difference in SH spectral response (non-reciprocity) for two directions.

Finally, a broadband converter is designed to generate tunable sum frequency of a high power laser using a control signal in the C-band. It was shown that all spectral components of a few-

nm-wide pump can be converted to SF with a wide enough transfer function as long as phase matching conditions are met. Considering the effect of focusing on the response profile of the broadband converter, the place of focusing was optimized. Moreover, the SHG of high power laser was obtained for different input powers and it was shown that the device is insensitive to pump-spectrum drift and does not need a temperature controller. The current engineering technique can also be applied to other wavelength ranges and materials as long as the phase-matching conditions are met.

9.1   Direction for future work

For all-optical broadband wavelength conversion, we fabricated the step-chirped grating with a 100-nm step change in the periods of gratings that introduces large ripples in the spectral frequency conversion response. In addition, in the fabrication of apodized devices, windows cannot be made smaller than a minimum size in the mask and consequently in final devices. Therefore, future work is needed to improve the fabrication of these devices by using facilities that are more advanced or applying different techniques to decrease the step changes in grating periods and also windows width which leads to better performance of APPLNs. Also fabrication of step-chirped and apodized step-chirped grating can be applied to semiconductors such as GaAs for frequency conversion in mid-infrared

In addition, we developed a proper design for apodization and showed that it results in a reciprocal SHG response. However, the optimization algorithm can be used to optimize the design of the step-apodized chirped gratings considering different shape or ratio of apodization functions and various parameters, to supress the ripples as much as possible. Also, as these devices are reciprocal, they would provide the possibility of enhancing the conversion efficiency by a double-pass configuration or using these devices in resonators or OPOs. As these devices do not need any temperature controller can lead to realizing compact optical conversion devices. Another scope of research that can be opened using the proposed ideas in this thesis is related to frequency conversion of different lasers with broad bandwidth or tunable frequencies.

BIBLIOGRAPHY

[1] Z. Zheng, A. M. Weiner, K. R. Parameswaran, M.-H. Chou, and M. M. Fejer, "Femtosecond second-harmonic generation in periodically poled lithium niobate waveguides with simultaneous strong pump depletion and group-velocity walk-off," *J. Opt. Soc. Am. B*, vol. 19, no. 4, pp. 839–848, Apr. 2002.

[2] G. Imeshev, M. A. Arbore, M. M. Fejer, A. Galvanauskas, M. Fermann, and D. Harter, "Ultrashort-pulse second-harmonic generation with longitudinally nonuniform quasi-phase-matching gratings: pulse compression and shaping," *J. Opt. Soc. Am. B*, vol. 17, no. 2, pp. 304–318, Feb. 2000.

[3] A. Arie, G. Rosenman, V. Mahal, A. Skliar, M. Oron, M. Katz, and D. Eger, "Green and ultraviolet quasi-phase-matched second harmonic generation in bulk periodically-poled KTiOPO4," *Opt. Commun.*, vol. 142, no. 4–6, pp. 265–268, 1997.

[4] S. G. Grechin, V. G. Dmitriev, and Y. V Yur'ev, "Second-harmonic generation under conditions of simultaneous phase-matched and quasi-phase-matched interactions in nonlinear crystals with a regular domain structure," *Quantum Electron.*, vol. 29, no. 2, p. 155, 1999.

[5] T. Suhara and H. Nishihara, "Theoretical analysis of waveguide second-harmonic generation phase matched with uniform and chirped gratings," *Quantum Electron. IEEE J.*, vol. 26, no. 7, pp. 1265–1276, 1990.

[6] Y. L. Lee, Y.-C. Noh, C. Jung, T. Yu, D.-K. Ko, and J. Lee, "Broadening of the second-harmonic phase-matching bandwidth in a temperature-gradient-controlled periodically poled Ti:LiNbO3 channel waveguide," *Opt. Express*, vol. 11, no. 22, pp. 2813–2819, Nov. 2003.

[7] A. Tehranchi and R. Kashyap, "Design of Novel Unapodized and Apodized Step-Chirped Quasi-Phase Matched Gratings for Broadband Frequency Converters Based on Second-Harmonic Generation," *Light. Technol. J.*, vol. 26, no. 3, pp. 343–349, 2008.

[8] P. A. Franken, A. E. Hill, C. W. Peters, and G. Weinreich, "Generation of Optical Harmonics," *Phys. Rev. Lett.*, vol. 7, no. 4, pp. 118–119, Aug. 1961.

[9] J. A. Armstrong, N. Bloembergen, J. Ducuing, and P. S. Pershan, "Interactions between Light Waves in a Nonlinear Dielectric," *Phys. Rev.*, vol. 127, no. 6, pp. 1918–1939, Sep. 1962.

[10] J. A. Giordmaine, "Mixing of Light Beams in Crystals," *Phys. Rev. Lett.*, vol. 8, no. 1, pp. 19–20, Jan. 1962.

[11] P. D. Maker, R. W. Terhune, M. Nisenoff, and C. M. Savage, "Effects of Dispersion and Focusing on the Production of Optical Harmonics," *Phys. Rev. Lett.*, vol. 8, no. 1, pp. 21–22, Jan. 1962.

[12] J.-C. Baumert, P. Günter, and H. Melchior, "High efficiency second-harmonic generation in KNbO3 crystals," *Opt. Commun.*, vol. 48, no. 3, pp. 215–220, 1983.

[13] W. A. Majewski, "A tunable, single frequency UV source for high resolution spectroscopy in the 293–330 nm range," *Opt. Commun.*, vol. 45, no. 3, pp. 201–206, 1983.

[14] D. A. Kleinman, "Theory of Second Harmonic Generation of Light," *Phys. Rev.*, vol. 128, no. 4, pp. 1761–1775, Nov. 1962.

[15] T. B. Razumikhina, L. S. Telegin, A. I. Kholodnykh, and A. S. Chirkin, "Three-frequency interactions of high-intensity light waves in media with quadratic and cubic nonlinearities," *Sov. J. Quantum Electron.*, vol. 14, no. 10, p. 1358, 1984.

[16] A. Ashkin, G. D. Boyd, and J. M. Dziedzic, "Observation of Continuous Optical Harmonic Generation with Gas Masers," *Phys. Rev. Lett.*, vol. 11, no. 1, pp. 14–17, Jul. 1963.

[17] G. D. Boyd and D. A. Kleinman, "Parametric Interaction of Focused Gaussian Light Beams," *J. Appl. Phys.*, vol. 39, no. 8, pp. 3597–3639, 1968.

[18] G. D. Boyd, A. Ashkin, J. M. Dziedzic, and D. A. Kleinman, "Second-Harmonic Generation of Light with Double Refraction," *Phys. Rev.*, vol. 137, no. 4A, pp. A1305–A1320, Feb. 1965.

[19] D. A. Kleinman, A. Ashkin, and G. D. Boyd, "Second-Harmonic Generation of Light by Focused Laser Beams," *Phys. Rev.*, vol. 145, no. 1, pp. 338–379, May 1966.

[20] D. A. Kleinman and R. C. Miller, "Dependence of Second-Harmonic Generation on the Position of the Focus," *Phys. Rev.*, vol. 148, no. 1, pp. 302–312, Aug. 1966.

[21] S. Somekh and A. Yariv, "Phase-matchable nonlinear optical interactions in periodic thin films," *Appl. Phys. Lett.*, vol. 21, no. 4, pp. 140–141, 1972.

[22] D. E. Thompson, J. D. McMullen, and D. B. Anderson, "Second-harmonic generation in GaAs stack of plates'' using high-power CO[sub 2] laser radiation," *Appl. Phys. Lett.*, vol. 29, no. 2, pp. 113–115, 1976.

[23] K. Kishima, "Fabrication of periodically reversed domain structure for SHG in LiNbO$_3$, by direct electron beam lithography at room temperature," *Electron. Lett.*, vol. 27, no. 10, pp. 828–829(1), 1991.

[24] W. K. Burns, W. McElhanon, and L. Goldberg, "Second harmonic generation in field poled, quasi-phase-matched, bulk $LiNbO_3$," *Photonics Technol. Lett. IEEE*, vol. 6, no. 2, pp. 252–254, 1994.

[25] M. Houé and P. D. Townsend, "Thermal polarization reversal of lithium niobate," *Appl. Phys. Lett.*, vol. 66, no. 20, 1995.

[26] W. J. E.J. Lim , M.M. Fejer , R.L. Byer , and W.J. Kozlovsky , "Blue light generation by frequency doubling in periodically poled lithium niobate channel waveguide," *Electron. Lett.*, vol. 25, no. 11, pp. 731–732(1), 1989.

[27] C. J. van der Poel, J. D. Bierlein, J. B. Brown, and S. Colak, "Efficient type I blue second- harmonic generation in periodically segmented $KTiOPO_4$ waveguides," *Appl. Phys. Lett.*, vol. 57, no. 20, 1990.

[28] M. Sato, P. G. R. Smith, and D. C. Hanna, "Contact electrode method for bulk periodically poled $LiNbO_3$," in *Lasers and Electro-Optics Society Annual Meeting, 1997. LEOS '97 10th Annual Meeting. Conference Proceedings., IEEE*, 1997, vol. 1, pp. 178–179 vol.1.

[29] M. M. F. S. Matsumoto , E.J. Lim , H.M. Hertz, "Quasiphase-matched second harmonic generation of blue light in electrically periodically-poled lithium tantalate waveguides," *Electron. Lett.*, vol. 27, no. 22, pp. 2040–2042(2), 1991.

[30] M. Yamada, N. Nada, M. Saitoh, and K. Watanabe, "First order quasi phase matched LiNbO3 waveguide periodically poled by applying an external field for efficient blue second harmonic generation," *Applied Physics Letters*, vol. 62, no. 5. pp. 435–436, 1993.

[31] L. E. Myers, R. C. Eckardt, M. M. Fejer, R. L. Byer, W. R. Bosenberg, and J. W. Pierce, "Quasi-phase-matched optical parametric oscillators in bulk periodically poled LiNbO3," *J. Opt. Soc. Am. B*, vol. 12, no. 11, pp. 2102–2116, Nov. 1995.

[32] M. C. Wengler, M. Müller, E. Soergel, and K. Buse, "Poling dynamics of lithium niobate crystals," *Appl. Phys. B Lasers Opt.*, vol. 76, no. 4, pp. 393–396.

[33] F. Jermann, M. Simon, and E. Krätzig, "Photorefractive properties of congruent and stoichiometric lithium niobate at high light intensities," *J. Opt. Soc. Am. B*, vol. 12, no. 11, pp. 2066–2070, Nov. 1995.

[34] A. Ashkin, G. D. Boyd, J. M. Dziedzic, R. G. Smith, A. A. Ballman, J. J. Levinstein, and K. Nassau, "Optically-induced refractive index inhomogeneities in $LiNbO_3$ and $LiTaO_3$," *Appl. Phys. Lett.*, vol. 9, no. 1, 1966.

[35]   K. Buse, S. Breer, K. Peithmann, S. Kapphan, M. Gao, and E. Krätzig, "Origin of thermal fixing in photorefractive lithium niobate crystals," *Phys. Rev. B*, vol. 56, no. 3, pp. 1225–1235, 1997.

[36]   D. A. Bryan, R. Gerson, and H. E. Tomaschke, "Increased optical damage resistance in lithium niobate," *Appl. Phys. Lett.*, vol. 44, no. 9, 1984.

[37]   Y. Furukawa, K. Kitamura, S. Takekawa, K. Niwa, and H. Hatano, "Stoichiometric Mg:LiNbO$_3$ as an effective material for nonlinear optics," *Opt. Lett.*, vol. 23, no. 24, pp. 1892–1894, 1998.

[38]   Y. Furukawa, K. Kitamura, S. Takekawa, A. Miyamoto, M. Terao, and N. Suda, "Photorefraction in LiNbO3 as a function of [Li]/[Nb] and MgO concentrations," *Appl. Phys. Lett.*, vol. 77, no. 16, 2000.

[39]   K. Yamamoto, K. Mizuuchi, and T. Taniuchi, "Milliwatt-order blue-light generation in a periodically domain-inverted LiTaO$_3$ waveguide," *Opt. Lett.*, vol. 16, no. 15, pp. 1156–1158, 1991.

[40]   K. R. Parameswaran, R. K. Route, J. R. Kurz, R. V Roussev, M. M. Fejer, and M. Fujimura, "Highly efficient second-harmonic generation in buried waveguides formed by annealed and reverse proton exchange in periodically poled lithium niobate," *Opt. Lett.*, vol. 27, no. 3, pp. 179–181, 2002.

[41]   G. Schreiber, H. Suche, Y. L. Lee, W. Grundkötter, V. Quiring, R. Ricken, and W. Sohler, "Efficient cascaded difference frequency conversion in periodically poled Ti:LiNbO$_3$ waveguides using pulsed and cw pumping," *Appl. Phys. B*, vol. 73, no. 5–6, pp. 501–504, 2001.

[42]   J. Rams, A. Alcázar-de-Velasco, M. Carrascosa, J. M. Cabrera, and F. Agulló-López, "Optical damage inhibition and thresholding effects in lithium niobate above room temperature," *Opt. Commun.*, vol. 178, no. 1–3, pp. 211–216, 2000.

[43]   K. R. Parameswaran, J. R. Kurz, R. V Roussev, and M. M. Fejer, "Observation of 99% pump depletion in single-pass second-harmonic generation in a periodically poled lithium niobate waveguide," *Opt. Lett.*, vol. 27, no. 1, pp. 43–45, Jan. 2002.

[44]   Y. Nishida, H. Miyazawa, M. Asobe, O. Tadanaga, and H. Suzuki, "0-dB wavelength conversion using direct-bonded QPM-Zn : LiNbO$_3$ ridge waveguide," *Photonics Technology Letters, IEEE*, vol. 17, no. 5. pp. 1049–1051, 2005.

[45]   S. Feng* and H. G. Winful, "Physical origin of the Gouy phase shift," *Opt. Lett.*, vol. 26, no. 8, pp. 485–487, Apr. 2001.

[46] H. E. Major, C. B. E. Gawith, and P. G. R. Smith, "Gouy phase compensation in quasi-phase matching," *Opt. Commun.*, vol. 281, no. 19, pp. 5036–5040, 2008.

[47] H. E. Major, J. C. Gates, C. B. E. Gawith, and P. G. R. Smith, "Improved SHG phase matching response for focused Gaussian beams in Gouy compensated quasi-phase-matched structures," in *Lasers and Electro-Optics 2009 and the European Quantum Electronics Conference. CLEO Europe - EQEC 2009. European Conference on*, 2009, p. 1.

[48] R. Shiloh and A. Arie, "Poling pattern for efficient frequency doubling of Gaussian beams," *Appl. Phys. B*, vol. 109, no. 4, pp. 573–579, 2012.

[49] M. Brown, "Increased spectral bandwidths in nonlinear conversion processes by use of multicrystal designs," *Opt. Lett.*, vol. 23, no. 20, pp. 1591–1593, Oct. 1998.

[50] W. J. Alford and A. V Smith, "Frequency-doubling broadband light in multiple crystals," *J. Opt. Soc. Am. B*, vol. 18, no. 4, pp. 515–523, 2001.

[51] A. V Smith, D. J. Armstrong, and W. J. Alford, "Increased acceptance bandwidths in optical frequency conversion by use of multiple walk-off-compensating nonlinear crystals," *J. Opt. Soc. Am. B*, vol. 15, no. 1, pp. 122–141, Jan. 1998.

[52] O. E. Martinez, "Achromatic phase matching for second harmonic generation of femtosecond pulses," *Quantum Electronics, IEEE Journal of*, vol. 25, no. 12. pp. 2464–2468, 1989.

[53] B. A. Richman, S. E. Bisson, R. Trebino, E. Sidick, and A. Jacobson, "Efficient broadband second-harmonic generation by dispersive achromatic nonlinear conversion using only prisms," *Opt. Lett.*, vol. 23, no. 7, pp. 497–499, 1998.

[54] A. M. Schober, M. Charbonneau-Lefort, and M. M. Fejer, "Broadband quasi-phase-matched second-harmonic generation of ultrashort optical pulses with spectral angular dispersion," *J. Opt. Soc. Am. B*, vol. 22, no. 8, pp. 1699–1713, 2005.

[55] K. Mizuuchi, K. Yamamoto, M. Kato, and H. Sato, "Broadening of the phase-matching bandwidth in quasi-phase-matched second-harmonic generation," *Quantum Electronics, IEEE Journal of*, vol. 30, no. 7. pp. 1596–1604, 1994.

[56] R. A. Haas, "Influence of a constant temperature gradient on the spectral-bandwidth of second-harmonic generation in nonlinear crystals," *Opt. Commun.*, vol. 113, no. 4–6, pp. 523–529, 1995.

[57] K. Regelskis, J. Želudevičius, N. Gavrilin, and G. Račiukaitis, "Efficient second-harmonic generation of a broadband radiation by control of the temperature distribution along a nonlinear crystal," *Opt. Express*, vol. 20, no. 27, pp. 28544–28556, 2012.

[58] A. M. Schober, G. Imeshev, and M. M. Fejer, "Tunable-chirp pulse compression in quasi-phase-matched second-harmonic generation," *Opt. Lett.*, vol. 27, no. 13, pp. 1129–1131, 2002.

[59] T. Umeki, M. Asobe, Y. Nishida, O. Tadanaga, K. Magari, T. Yanagawa, and H. Suzuki, "Widely tunable 3.4 μm band difference frequency generation using apodized χ(2) grating," *Opt. Lett.*, vol. 32, no. 9, pp. 1129–1131, 2007.

[60] J. Huang, X. P. Xie, C. Langrock, R. V Roussev, D. S. Hum, and M. M. Fejer, "Amplitude modulation and apodization of quasi-phase-matched interactions," *Opt. Lett.*, vol. 31, no. 5, pp. 604–606, Mar. 2006.

[61] R. W. Boyd, *Nonlinear optics*. Academic Press, 2003.

[62] D. A. Kleinman, "Nonlinear Dielectric Polarization in Optical Media," *Phys. Rev.*, vol. 126, no. 6, pp. 1977–1979, 1962.

[63] W. P. Risk, T. R. Gosnell, A. V Nurmikko, and I. Ebrary, *Compact blue-green lasers*. Cambridge: Cambridge University Press, 2003.

[64] M. J. . de Dood, "Second harmonic generation," Huygens Laboratorium 909a, 2006. http://users.uj.edu.pl/~ufdzierz/PracFot/SHG_Dood.pdf

[65] M. Houe and P. D. Townsend, "An introduction to methods of periodic poling for second-harmonic generation," *J. Phys. D. Appl. Phys.*, vol. 28, no. 9, p. 1747, 1995.

[66] B. T. Matthias and J. P. Remeika, "Ferroelectricity in the Ilmenite Structure," *Phys. Rev.*, vol. 76, no. 12, pp. 1886–1887, 1949.

[67] A. A. BALLMAN, "Growth of Piezoelectric and Ferroelectric Materials by the CzochraIski Technique," *J. Am. Ceram. Soc.*, vol. 48, no. 2, pp. 112–113, 1965.

[68] K. Nassau, H. J. Levinstein, and G. M. Loiacono, "Ferroelectric lithium niobate. 1. Growth, domain structure, dislocations and etching," *J. Phys. Chem. Solids*, vol. 27, no. 6, pp. 983–988, 1966.

[69] K. Nassau, H. J. Levinstein, and G. M. Loiacono, "Ferroelectric lithium niobate. 2. Preparation of single domain crystals," *J. Phys. Chem. Solids*, vol. 27, no. 6–7, pp. 989–996, 1966.

[70] S. C. Abrahams, J. M. Reddy, and J. L. Bernstein, "Ferroelectric lithium niobate. 3. Single crystal X-ray diffraction study at 24°C," *J. Phys. Chem. Solids*, vol. 27, no. 6, pp. 997–1012, 1966.

[71] S. C. Abrahams, W. C. Hamilton, and J. M. Reddy, "Ferroelectric lithium niobate. 4. Single crystal neutron diffraction study at 24°C," *J. Phys. Chem. Solids*, vol. 27, no. 6–7, pp. 1013–1018, 1966.

[72] S. C. Abrahams, H. J. Levinstein, and J. M. Reddy, "Ferroelectric lithium niobate. 5. Polycrystal X-ray diffraction study between 24° and 1200°C," *J. Phys. Chem. Solids*, vol. 27, no. 6–7, pp. 1019–1026, 1966.

[73] V. L. I. Boris K. Vainshtein, Vladimir M. Fridkin, *Modern Crystallography 2: Structure of Crystals*. Springer Science, 2012.

[74] R. S. Weis and T. K. Gaylord, "Lithium niobate: Summary of physical properties and crystal structure," *Appl. Phys. A*, vol. 37, no. 4, pp. 191–203, 1985.

[75] I. P. Kaminow, E. H. Turner, R. L. Barns, and J. L. Bernstein, "Crystallographic and electro- optic properties of cleaved $LiNbO_3$," *J. Appl. Phys.*, vol. 51, no. 8, 1980.

[76] G. P. Agrawal, *Fiber-optic Communication Systems*. John Wiley & sons, Inc, 1992.

[77] D. H. Jundt, "Temperature-dependent Sellmeier equation for the index of refraction, ne, in congruent lithium niobate," *Opt. Lett.*, vol. 22, no. 20, pp. 1553–1555, Oct. 1997.

[78] K. Pandiyan, Y. S. Kang, H. H. Lim, B. J. Kim, and M. Cha, "Nondestructive quality evaluation of periodically poled lithium niobate crystals by diffraction," *Opt. Express*, vol. 17, no. 20, pp. 17862–17867, Sep. 2009.

[79] M. Kajal, "Design and Implementation of Novel Nonlinear Processes in Bulk and Waveguide Periodic Structures," Ph. D. dissertation,Polytechnique Montreal,2014.

[80] G. D. Miller, "Periodically Poled Lithium Niobate: Modeling, Fabrication, and Nonlinear-Optical Performances," Stanford university, 1998.

[81] M. Missey, S. Russell, V. Dominic, R. Batchko, and K. Schepler, "Real-time visualization of domain formation in periodically poled lithium niobate," *Opt. Express*, vol. 6, no. 10, pp. 186–195, 2000.

[82] V. Y. Shur, E. L. Rumyantsev, E. Nikolaeva, E. Shishkin, R. G. Batchko, G. D. Miller, M. M. Fejer, and R. L. Byer, "Micro- and nanoscale domain engineering in lithium niobate and lithium tantalate," *Proc. SPIE*, vol. 3992. pp. 143–154, 2000.

[83] I. E. Barry, G. W. Ross, P. G. R. Smith, R. W. Eason, and G. Cook, "Microstructuring of lithium niobate using differential etch-rate between inverted and non-inverted ferroelectric domains," *Mater. Lett.*, vol. 37, no. 4–5, pp. 246–254, 1998.

[84] C. L. Sones, S. Mailis, W. S. Brocklesby, R. W. Eason, and J. R. Owen, "Differential etch rates in z-cut $LiNbO_3$ for variable HF/HNO_3 concentrations," *J. Mater. Chem.*, vol. 12, no. 2, pp. 295–298, 2002.

[85] E. Soergel, "Visualization of ferroelectric domains in bulk single crystals," *Appl. Phys. B*, vol. 81, no. 6, pp. 729–751, 2005.

[86] L. E. Myers and W. R. Bosenberg, "Periodically poled lithium niobate and quasi-phase-matched optical parametric oscillators," *Quantum Electron. IEEE J.*, vol. 33, no. 10, pp. 1663–1672, 1997.

[87] X. Liu, H. Zhang, Y. Guo, and Y. Li, "Optimal design and applications for quasi-phase-matching three-wave mixing," *Quantum Electron. IEEE J.*, vol. 38, no. 9, pp. 1225–1233, 2002.

[88] G. K. Kitaeva, "Frequency conversion in aperiodic quasi-phase-matched structures," *Phys. Rev. A*, vol. 76, no. 4, p. 43841, Oct. 2007.

[89] J. Wang, J. Sun, X. Zhang, D. Huang, and M. M. Fejer, "Optical phase erasure and its application to format conversion through cascaded second-order processes in periodically poled lithium niobate," *Opt. Lett.*, vol. 33, no. 16, pp. 1804–1806, 2008.

[90] F. Ji, R. Lu, B. Li, B. Zhang, and J. Yao, "Mid-infrared tunable dual-wavelength generation based on a quasi-phase-matched optical parametric oscillator," *Opt. Commun.*, vol. 282, no. 1, pp. 126–128, Jan. 2009.

[91] M. Fujimura, T. Kodama, T. Suhara, and H. Nishihara, "Quasi-phase-matched self-frequency-doubling waveguide laser in $Nd:LiNbO_3$," *Photonics Technol. Lett. IEEE*, vol. 12, no. 11, pp. 1513–1515, 2000.

[92] M. Ahlawat, A. Tehranchi, C. Q. Xu, and R. Kashyap, "Ultrabroadband flattop wavelength conversion based on cascaded sum frequency generation and difference frequency generation using pump detuning in quasi-phase-matched lithium niobate waveguides," *Appl. Opt.*, vol. 50, no. 25, pp. E108–E111, Sep. 2011.

[93] J. Wang, J. Sun, X. Zhang, D. Huang, and M. M. Fejer, "All-Optical Format Conversions Using Periodically Poled Lithium Niobate Waveguides," *Quantum Electron. IEEE J.*, vol. 45, no. 2, pp. 195–205, 2009.

[94] G. W. Ross, M. Pollnau, P. G. R. Smith, W. A. Clarkson, P. E. Britton, and D. C. Hanna, "Generation of high-power blue light in periodically poled LiNbO$_3$," *Opt. Lett.*, vol. 23, no. 3, pp. 171–173, 1998.

[95] V. V Volkov and A. S. Chirkin, "Quasi-phase-matched parametric amplification of waves with low-frequency pumping," *Quantum Electron.*, vol. 28, no. 2, p. 95, 1998.

[96] K. Kintaka, M. Fujimura, T. Suhara, and H. Nishihara, "High-efficiency LiNbO$_3$ waveguide second-harmonic generation devices with ferroelectric-domain-inverted gratings fabricated by applying voltage," *Light. Technol. J.*, vol. 14, no. 3, pp. 462–468, 1996.

[97] X. Liu, H. Zhang, and Y. Guo, "Theoretical analyses and optimizations for wavelength conversion by quasi-phase-matching difference frequency generation," *Light. Technol. J.*, vol. 19, no. 11, pp. 1785–1792, 2001.

[98] S. Gao, C. Yang, and G. Jin, "Flat broad-band wavelength conversion based on sinusoidally chirped optical superlattices in lithium niobate," *Photonics Technol. Lett. IEEE*, vol. 16, no. 2, pp. 557–559, 2004.

[99] K. L. Baker, "Single-pass gain in a chirped quasi-phase-matched optical parametric oscillator," *Applied Physics Letters*, vol. 82, no. 22. pp. 3841–3843, 2003.

[100] K. A. Tillman and D. T. Reid, "Monolithic optical parametric oscillator using chirped quasi-phase matching," *Opt. Lett.*, vol. 32, no. 11, pp. 1548–1550, Jun. 2007.

[101] A. Tehranchi and R. Kashyap, "Novel Designs for Efficient Broadband Frequency Doublers Using Singly Pump-Resonant Waveguide and Engineered Chirped Gratings," *Quantum Electron. IEEE J.*, vol. 45, no. 2, pp. 187–194, 2009.

[102] G.-W. Lu, S. Shinada, H. Furukawa, N. Wada, T. Miyazaki, and H. Ito, "160-Gb/s all-optical phase-transparent wavelength conversion through cascaded SFG-DFG in a broadband linear-chirped PPLN waveguide," *Opt. Express*, vol. 18, no. 6, pp. 6064–6070, Mar. 2010.

[103] R. Kashyap, *Fiber Bragg gratings*. Academic Press, 1999.

[104] M. M. Fejer, G. A. Magel, D. H. Jundt, and R. L. Byer, "Quasi-phase-matched second harmonic generation: tuning and tolerances," *IEEE Journal of Quantum Electronics*, vol. 28, no. 11. pp. 2631–2654, 1992.

[105] T. Umeki, M. Asobe, T. Yanagawa, O. Tadanaga, Y. Nishida, K. Magari, and H. Suzuki, "Broadband wavelength conversion based on apodized $\chi(2)$ grating," *J. Opt. Soc. Am. B*, vol. 26, no. 12, pp. 2315–2322, 2009.

[106] K. Pandiyan, Y.-S. Kang, H.-H. Lim, B.-J. Kim, O. Prakash, and M.-S. Cha, "Poling Quality Evaluation of Periodically Poled Lithium Niobate Using Diffraction Method," *J. Opt. Soc. Korea*, vol. 12, no. 3, pp. 205–209, Sep. 2008.

[107] C. Langrock, S. Kumar, J. E. McGeehan, A. E. Willner, and M. M. Fejer, "All-Optical Signal Processing Using χ(2) Nonlinearities in Guided-Wave Devices," *J. Light. Technol.*, vol. 24, no. 7, p. 2579, 2006.

[108] M. Ahlawat, A. Bostani, A. Tehranchi, and R. Kashyap, "Agile multicasting based on cascaded $\chi^{(2)}$ nonlinearities in a step-chirped periodically poled lithium niobate," *Opt. Lett.*, vol. 38, no. 15, pp. 2760–2762, 2013.

[109] A. Bogoni, X. Wu, I. Fazal, and A. E. Willner, "Photonic processing of 320 Gbits/s based on sum-/difference-frequency generation and pump depletion in a single PPLN waveguide," *Opt. Lett.*, vol. 34, no. 12, pp. 1825–1827, 2009.

[110] M. H. Chou, K. R. Parameswaran, M. M. Fejer, and I. Brener, "Multiple-channel wavelength conversion by use of engineered quasi-phase-matching structures in LiNbO$_3$ waveguides," *Opt. Lett.*, vol. 24, no. 16, pp. 1157–1159, 1999.

[111] W. Dang, Y. Chen, and X. Chen, "Performance Enhancement for Ultrashort-Pulse Wavelength Conversion by Using an Aperiodic Domain-Inverted Optical Superlattice," *IEEE Photonics Technology Letters*, vol. 24, no. 5. pp. 347–349, 2012.

[112] A. Bostani, A. Tehranchi, and R. Kashyap, "Engineering of apodized chirped gratings based on desired second-order nonlinearity function," in *Advanced Photonics Congress*, 2012, p. JM5A.17.

[113] C. R. Phillips, C. Langrock, D. Chang, Y. W. Lin, L. Gallmann, and M. M. Fejer, "Apodization of chirped quasi-phasematching devices," *J. Opt. Soc. Am. B*, vol. 30, no. 6, pp. 1551–1568, 2013.

[114] S. Guha and J. Falk, "The effects of focusing in the three frequency parametric upconverter," *J. Appl. Phys.*, vol. 51, no. 1, 1980.

[115] N. Lastzka and R. Schnabel, "The Gouy phase shift in nonlinear interactions of waves," *Opt. Express*, vol. 15, no. 12, pp. 7211–7217, 2007.

[116] K. T. McDonald, "Second-order paraxial Gaussian beam,"princeton, 2009. http://www.physics.princeton.edu/~mcdonald/examples/davis_psi2.pdf

[117] M. Ahlawat, A. Bostani, A. Tehranchi, and R. Kashyap, "Tunable single-to-dual channel wavelength conversion in an ultra-wideband SC-PPLN," *Opt. Express*, vol. 21, no. 23, pp. 28809–28816, Nov. 2013.

[118] A. Bogoni, X. Wu, S. R. Nuccio, and A. E. Willner, "640 Gb/s All-Optical Regenerator Based on a Periodically Poled Lithium Niobate Waveguide," *Journal of Lightwave Technology*, vol. 30, no. 12. pp. 1829–1834, 2012.

[119] A. Malacarne, G. Meloni, G. Berrettini, N. Sambo, L. Poti, and A. Bogoni, "Optical Multicasting of 16QAM Signals in Periodically-Poled Lithium Niobate Waveguide," *Journal of Lightwave Technology*, vol. 31, no. 11. pp. 1797–1803, 2013.

[120] T. Richter, R. Nouroozi, H. Suche, W. Sohler, and C. Schubert, "PPLN-Waveguide Based Tunable Wavelength Conversion of QAM Data Within the C-Band," *IEEE Photonics Technology Letters*, vol. 25, no. 21. pp. 2085–2088, 2013.

[121] J. Wang, H. Fu, D. Geng, and A. E. Willner, "Single-PPLN-assisted wavelength-/time-selective switching/dropping/swapping for 100-GHz-spaced WDM signals," *Opt. Express*, vol. 21, no. 3, pp. 3756–3774, 2013.

[122] Y. Xia, "Broadcast wavelength conversion based on cascaded $\chi^{(2)}$ nonlinearity in MgO-doped periodically poled $LiNbO_3$," *Electron. Lett.*, vol. 43, no. 25, pp. 1446–1447(1), 2007.

[123] U. K. Sapaev and D. T. Reid, "General second-harmonic pulse shaping in grating-engineered quasi-phase-matched nonlinear crystals," *Opt. Express*, vol. 13, no. 9, pp. 3264–3276, 2005.

[124] M. Conforti, F. Baronio, and C. De Angelis, "From femtosecond infrared to picosecond visible pulses: temporal shaping with high-efficiency conversion," *Opt. Lett.*, vol. 32, no. 13, pp. 1779–1781, 2007.

[125] R. Schiek and T. Pertsch, "Absolute measurement of the quadratic nonlinear susceptibility of lithium niobate in waveguides," *Opt. Mater. Express*, vol. 2, no. 2, pp. 126–139, 2012.

[126] A. Leshem, R. Shiloh, and A. Arie, "Experimental realization of spectral shaping using nonlinear optical holograms," *Opt. Lett.*, vol. 39, no. 18, pp. 5370–5373, Sep. 2014.

[127] I. Tomita, T. Umeki, O. Tadanaga, H. Song, M. Asobe, and H. Takenouchi, "Properties of power dependence on low-crosstalk waveband conversion with an apodized multiperiod-QPM LiNbO3 device," *Opt. Express*, vol. 22, no. 12, pp. 15232–15244, 2014.

[128] A. Bostani, A. Tehranchi, and R. Kashyap, "Engineering of effective second-order nonlinearity in uniform and chirped gratings," *J. Opt. Soc. Am. B*, vol. 29, no. 10, pp. 2929–2934, Oct. 2012.

[129] A. Bostani, M. Ahlawat, A. Tehranchi, R. Morandotti, and R. Kashyap, "Tailoring and tuning of the broadband spectrum of a step-chirped grating based frequency doubler using tightly-focused Gaussian beams," *Opt. Express*, vol. 21, no. 24, pp. 29847–29853, 2013.

[130] A. Bostani, A. Tehranchi, and R. Kashyap, "Study of apodization of aperiodically poled lithium niobate (APPLN) for second harmonic generation (SHG)," in *Fibre and Optical Passive Components (WFOPC), 2011 7th Workshop on*, 2011, pp. 1–4.

[131] C.-F. Cheng, Y. R. Sun, H. Pan, Y. Lu, X.-F. Li, J. Wang, A.-W. Liu, and S.-M. Hu, "Cavity ring-down spectroscopy of Doppler-broadened absorption line with sub-MHz absolute frequency accuracy," *Opt. Express*, vol. 20, no. 9, pp. 9956–9961, 2012.

[132] C. Yang, A. Wax, M. S. Hahn, K. Badizadegan, R. R. Dasari, and M. S. Feld, "Phase-referenced interferometer with subwavelength and subhertz sensitivity applied to the study of cell membrane dynamics," *Opt. Lett.*, vol. 26, no. 16, pp. 1271–1273, 2001.

[133] S. I. Kablukov, E. A. Zlobina, E. V Podivilov, and S. A. Babin, "Output spectrum of Yb-doped fiber lasers," *Opt. Lett.*, vol. 37, no. 13, pp. 2508–2510, 2012.

[134] J. Nilsson and D. N. Payne, "High-Power Fiber Lasers," *Sci.* , vol. 332 , no. 6032 , pp. 921–922, May 2011.

[135] M.-A. Lapointe and M. Piché, "Linewidth of high-power fiber lasers," *Proc. SPIE*, vol. 7386. p. 73860S–73860S–8, 2009.

[136] S. D. Jackson, A. Sabella, A. Hemming, S. Bennetts, and D. G. Lancaster, "High-power 83 W holmium-doped silica fiber laser operating with high beam quality," *Opt. Lett.*, vol. 32, no. 3, pp. 241–243, 2007.

[137] M.-C. Chan, C.-H. Lien, J.-Y. Lu, and B.-H. Lyu, "High power NIR fiber-optic femtosecond Cherenkov radiation and its application on nonlinear light microscopy," *Opt. Express*, vol. 22, no. 8, pp. 9498–9507, 2014.

[138] B.-Q. Chen, M.-L. Ren, R.-J. Liu, C. Zhang, Y. Sheng, B.-Q. Ma, and Z.-Y. Li, "Simultaneous broadband generation of second and third harmonics from chirped nonlinear photonic crystals," *Light Sci Appl*, vol. 3, p. e189, Jul. 2014.

[139] X. P. Hu, P. Xu, and S. N. Zhu, "Engineered quasi-phase-matching for laser techniques \[Invited\]," *Photon. Res.*, vol. 1, no. 4, pp. 171–185, 2013.

[140] T. Umeki, T. Kazama, O. Tadanaga, K. Enbutsu, M. Asobe, Y. Miyamoto, and H. Takenouchi, "PDM Signal Amplification Using PPLN-Based Polarization-Independent Phase-Sensitive Amplifier," *J. Light. Technol.*, vol. 33, no. 7, pp. 1326–1332, 2015.

[141] A. A. C. Albuquerque, M. V Drummond, B. J. Puttnam, N. Wada, and R. N. Nogueira, "Investigation of PPLN-Based PSAs for High-Gain Optical Amplification," *Lightwave Technology, Journal of*, vol. 33, no. 13. pp. 2802–2810, 2015.

[142] S. Arahira and H. Murai, "Wavelength conversion of incoherent light by sum-frequency generation," *Opt. Express*, vol. 22, no. 11, pp. 12944–12961, 2014.

[143] M. Ahlawat, A. Tehranchi, K. Pandiyan, M. Cha, and R. Kashyap, "Tunable all-optical wavelength broadcasting in a PPLN with multiple QPM peaks," *Opt. Express*, vol. 20, no. 24, pp. 27425–27433, 2012.

[144] A. Bostani, M. Ahlawat, A. Tehranchi, R. Morandotti, and R. Kashyap, "Design, fabrication and characterization of a specially apodized chirped grating for reciprocal second harmonic generation," *Opt. Express*, vol. 23, no. 4, pp. 5183–5189, 2015.

[145] M. A. Arbore, "Generation and manipulation of infrared light using quasi phase matched devices: ultrashort-pulse, aperiodic-grating and guided-wave frequency conversion," Stanford University, 1998.

[146] R. Landauer, "Electrostatic Considerations in BaTiO3 Domain Formation during Polarization Reversal," *J. Appl. Phys.*, vol. 28, no. 2, 1957.

[147] V. Gopalan, T. E. Mitchell, Y. Furukawa, and K. Kitamura, "The role of nonstoichiometry in 180° domain switching of LiNbO3 crystals," *Appl. Phys. Lett.*, vol. 72, no. 16, 1998.

APPENDIX A – CONVOLUTION OF TWO GAUSSIAN BEAMS

The convolution of two Gaussian functions centered at frequency of ω_1 and ω_2 with bandwidth of σ_1 and σ_2

$$f(x) = a_1 \exp(-(\omega - \omega_1)^2 / \sigma_1^2)$$

$$g(x) = a_2 \exp(-(\omega - \omega_2)^2 / \sigma_2^2)$$

Can be written as :

$$f(x) * g(x) = a_1 a_2 \frac{\sigma_1 \sigma_2 \sqrt{\pi}}{\sqrt{\sigma_1^2 + \sigma_2^2}} \exp(-\frac{(\omega - (\omega_1 + \omega_2))^2}{\sigma_1^2 + \sigma_2^2})$$

Therefore, for SFG and SHG the amplitude of electric field can be written as

$$A_{SF} = a_1 a_2 D \frac{\sigma_1 \sigma_2 \sqrt{\pi}}{\sqrt{\sigma_1^2 + \sigma_2^2}} \exp(-\frac{(\omega - \omega_3)^2}{\sigma_1^2 + \sigma_2^2})$$

$$A_{SH} = a_1^2 \frac{D}{2} \frac{\sigma_1 \sqrt{\pi}}{\sqrt{2}} \exp(-\frac{(\omega - 2\omega_1)^2}{2\sigma_1^2})$$

We can calculate the power of SFG and SHG by integrating the squared electric field

$$P_{SF} = \int_{-\infty}^{+\infty} A_{SF}^2 = a_1^2 a_2^2 D^2 \frac{\sigma_1^2 \sigma_2^2 \pi}{\sigma_1^2 + \sigma_2^2} (\sqrt{\sigma_1^2 + \sigma_2^2} \sqrt{\pi/2}) = a_1^2 a_2^2 D^2 \frac{\sigma_1^2 \sigma_2^2 \pi}{\sqrt{\sigma_1^2 + \sigma_2^2}} (\sqrt{\pi/2})$$

$$P_{SH} = \int_{-\infty}^{+\infty} A_{SH}^2 = a_1^4 \frac{D^2}{4} \frac{\sigma_1^2 \pi}{2} (\sigma_1 \sqrt{\pi/2}) = a_1^4 D^2 \frac{\sigma_1^3 \pi}{8} (\sqrt{\pi/2})$$

The relative power of SFG to SHG can be obtained:

$$\frac{P_{SF}}{P_{SH}} = \frac{a_2^2 \dfrac{\sigma_2^2}{\sqrt{\sigma_1^2 + \sigma_2^2}}}{a_1^2 \dfrac{\sigma_1}{8}} = \frac{8 a_2^2 \sigma_2^2}{a_1^2 \sigma_1 \sqrt{\sigma_1^2 + \sigma_2^2}} = \frac{8 P_2}{P_1} \frac{\sigma_2}{\sqrt{\sigma_1^2 + \sigma_2^2}}$$